Chemical Vapor Deposition and Characterization of Poly(*p*-phenylene vinylene) Films

by

Cynthia Ann Gedelian

A Thesis Submitted to the Graduate

Faculty of Rensselaer Polytechnic Institute

in Partial Fulfillment of the

Requirements for the degree of

DOCTOR OF PHILOSOPHY

Major Subject: Physics

Approved by the
Examining Committee:

_____
Toh-Ming Lu, Thesis Adviser

_____
Gwo-Ching Wang, Member

_____
John Schroeder, Member

_____
Saroj Nayak, Member

_____
Hassaram Bakhru, Member

Rensselaer Polytechnic Institute
Troy, New York

May 2008

CONTENTS

LIST OF TABLES

LIST OF FIGURES

ACKNOWLEDGMENTS

"Everything starts somewhere, although many physicists disagree." –Terry Pratchett, *Hogfather*

First of all, thanks are due to my advisor, Prof. Toh-Ming Lu, without whom I would not be where I am now. He spent a lot of time and energy on my behalf, and I am grateful for it. Similar thanks are due to my committee members, Prof. Gwo-Ching Wang, Prof. John Schroeder, Prof. Hassaram Bakhru, and Prof. Saroj Nayak. Each contributed valuable pieces to my projects in their own way, from equipment to advice, and I am very grateful for their support throughout this process. Prof. Bakhru in particular as well as his student Lakshmanan Vanamurthy were a large help in providing RBS spectra and NRA spectra of my picky samples at the Ion Beam facilities at SUNY Albany. Additional thanks are due to Prof. Peter Persans, who provided large amounts of optical equipment, lab space, and multitudes of freely given advice. Further invaluable help was given by Visiting Scholar Dr. K. C. Rajanna from Osmania University in India, who spent his summer helping me apply chemistry principles to a physics project.

Three years of my research was funded by a Graduate Assistance in Areas of National Need (GAANN) Fellowship, provided by the Department of Education. I would like to thank them for supporting me and my fellow recipients, as well as Prof. Wang for bringing and administering this funding to our department.

RPI is a large community and there are many people there who provided me with instruction, information, advice, and company whenever I need it. I would especially like to thank my group members past and present for all their help and for sometimes allowing me to help them: Dr. Pei-I Wang, Dr. Tansel Karabacak, Dr. Dexian Ye, Dr. Jasbir Juneja, Dr. Gregory Ten Eyck, Thomas Parker, Ya Ou, and Ming He. Other students at RPI who have helped me out include Dr. Dmitry Veksler for FTIR spectra and Dr. Huafang Li for TEM data. A special shout out goes to my undergraduate minion, Brian Premerlani, who spent an entire summer saving me from sweaty lab work

and catering to my every whim. I'm sure his graduate career will be more successful than mine (especially after all that sage advice I constantly gave him).

I've met all sorts of wonderful and interesting people in grad school and I will never forget them. One in particular I'm sure saved my sanity a few times: Lauren O'Malley. Thanks for all those margaritas and nights away from work!

The biggest thanks in the world go out to my incredible family, who have stood by me every step of the way. My parents Tom and Anita and siblings Laura and Robert are all amazing people, and I am so lucky to have them with me!

I was fortunate enough to acquire a second family along the way, and I want to thank Carrie, Jurgen, Anja, and Matt for welcoming me into their family with open arms and providing sanctuary whenever I needed it.

First and last, always and forever, is my husband Damian, an amazing man and the best thing that ever happened to me! Without him, I would never have made it as far as I did. He has held me when I cried and cheered with me when I won, and I will love him forever.

Thanks so much to everyone!!

ABSTRACT

As a conducting, electroluminescent, and photoluminescent polymer, poly(*p*-phenylene vinylene) (PPV) is a material of much interest for electronic and optical applications. Although this polymer has traditionally been deposited using spin-on methods and soluble precursor polymers, the technique has several drawbacks including an increase in contamination and defects from the solvent, the need to convert the precursor into PPV without adding further impurities or damaging the film, and the processing restrictions when dealing with liquid depositions. Chemical vapor deposition (CVD), on the other hand, deposits the precursor polymer in the gas phase and therefore eliminates the need for a solvent and creates the capability for conformal deposition on many types of nanostructured substrates. However, PPV films deposited by CVD remain under-studied. This work aims to investigate properties of those films including the removal of bromine left from the CVD precursor, the behavior and structure of PPV after heat treatment at elevated temperatures (>450 °C), the usefulness of encapsulation materials for preventing photodegradation, and characteristics of films deposited on top of nano-size porous materials.

Bromine from the precursor polymer is removed during the first thirty minutes of heating. Films annealed at 300 °C in nitrogen gas consisted of 0.36 % bromine; however, photoluminescence spectra comparing films annealed at 150 and 300 °C showed more defects in the 300 °C film. Heat treatment of PPV beyond the initial anneal showed that the film degrades at 500 °C by emitting monomer fragments without crosslinking.

Photodegradation of PPV films due to incorporation of oxygen during light exposure can be reduced from 80 % to 30 % under UV light and nearly prevented under blue light when encapsulated with 10 nm aluminum oxide. Encapsulation with organic Parylene shows no significant improvement.

Use of the Stern-Volmer equation to examine self-quenching in films shows larger conformational change and increased restriction from change in electron density due to electron transition during excitation in bulk polymer films over 60 nm thick. PPV deposited into porous (~4 nm in diameter) nanostructured substrate shows a larger 0-0 than 0-1 transition peak intensity and decreased disorder in the films due to structure imposed by substrate matrix.

1. Introduction

Conducting polymers been developed in tremendous ways in the four decades since their discovery. The controllability of their electrical properties, the malleability of their form, the ease of their deposition, and the variability of their optical and mechanical properties all combine to make these polymers invaluable materials for the development of high tech devices. As the field evolves, more and more organic electronic and optical devices are becoming common in everyday life. In this chapter I will introduce the basic properties of conjugated polymers as well as more detailed properties for one in particular, poly(*p*-phenylene vinylene) (PPV). The luminescence properties are given special attention, as they are the focus of most of the interest in the PPV family. Finally, several methods for the deposition of PPV are compared.

1.1 Conjugated Polymers

Serendipity played a large role in the discovery and development of an exciting and relatively new class of materials: semiconducting and conducting polymers. Typically insulators, the discovery of the conducting capabilities of easily processable and variable plastics opened a variety of new possibilities for products of all kinds, from transparent, flexible electronics to organic computer and television displays. The first conducting polymer studied extensively was also the simplest: polyacetylene. Consisting purely of chains of carbon atoms attached together with alternating single and double bonds (Figure 1.1), this polymer has proven to be the gateway to the exciting field of organic electronics. The collaboration of Hideki Shirakawa with Alan Heeger and Alan MacDiarmid led to the discovery that polyacetylene could be doped with ions, and upon such doping the conductivity of the films could be increased to rival the conductivity of some metals. As the conjugated, conducting polymers have continued to be studied, their usefulness and applicability to modern products led to the awarding of the Nobel Prize in Chemistry to Shirakawa, Heeger, and MacDiarmid in the year 2000.

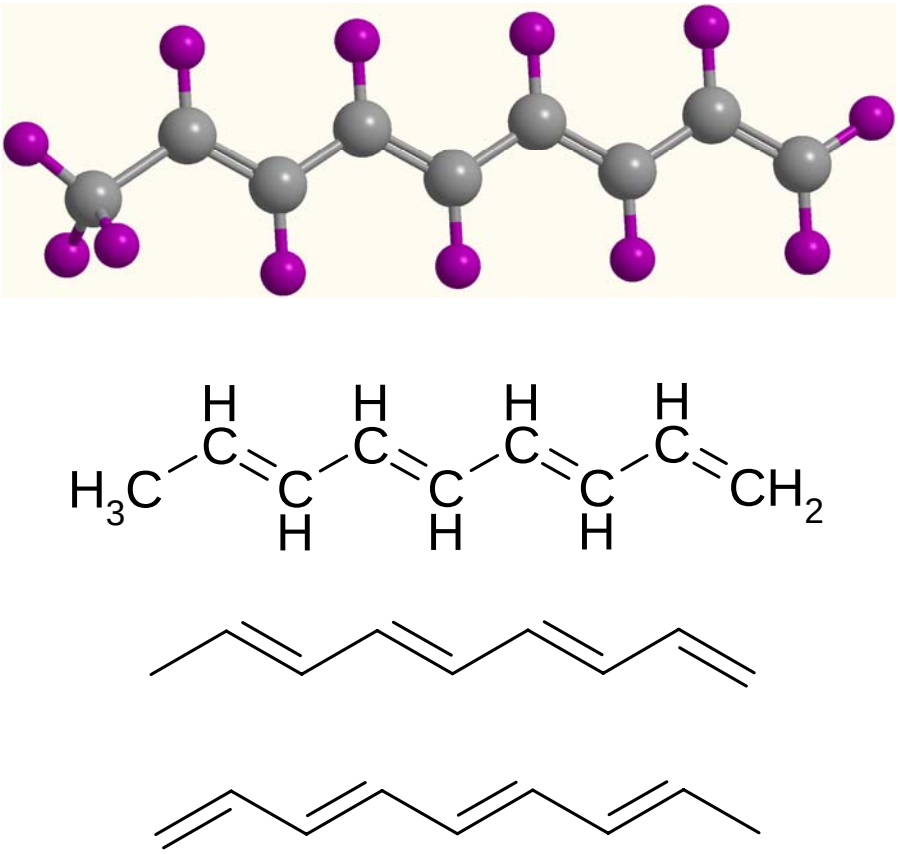

Figure 1.1: Alternate ways of drawing polyacetylene (9 carbon chain).

The key to the electronic properties of conducting polymers lies in the conjugated nature of their backbone structure. The alternating double and single bonds (or the "extra" electrons in certain other elements such as nitrogen in the backbone of polymers like polypyrrole) create an extended environment of delocalized π-electron bonding along the backbone of the polymer chain. Charge carriers are supported by the delocalized valence and conduction wavefunctions from the π (bonding) and π* (antibonding) orbitals [1]. Simple theories such as Hückel's theory predict that each bond in the conjugated series is equal, a hybrid of double and single bonds with the π electrons diffused over the entire system; however, because the polymer does not behave as an ideal model in this way it is clear that there is a difference in the bonds. Since the single and double bonds still have no given preference for their orientation, this alternating system be pictured as having a resonance structure, meaning the double and single bonds

can be "switched" from their positions and the polymer structure will not be altered, as demonstrated in Figure 1.1. This freedom of movement can be directed (such as through applying a voltage along the polymer chains) allowing the electrons in the bonds to "travel" along the chains instead of flipping back and forth. Doping with ions such as iodine can increase the conductivities exponetially. This mobility is what gives the conjugated polymers their high conductivities when properly doped. Figure 1.2 shows one example of the effect of dopants on the excitations in polyacetylene, where the dopant confines one soliton and attracts another mobile one enough that it causes an electron to jump between polymer chains.

There are several families of conjugated polymers and most of them have a multitude of applications for which they are suited. The main interest in using conjugated polymers in devices is the capability of combining the usefulness of metals and semiconductor with the ease of processing, tunable characteristics, flexibility, and low-cost manufacturing of plastics. Examples of some conjugated polymer families (Figure 1.3) and a sample of their uses include:

- Poly(pyrrole) – microwave-absorbing "stealth" (radar-invisible) screen coating (doped film) [2]; active layer of sensors (undoped film) [3]
- Poly(thiophene) – field effect transistors [4]
- Poly(dialkylfluorene) – emissive layer in full color video matrix displays [5]
- Polyaniline – electromagnetic shielding of devices [6] and corrosion inhibition [7]
- Poly(ethylenedioxythiophene) (PEDOT) – hole injecting material in polymer light emitting devices [8]
- Poly(phenylene vinylene) – active layer in electroluminescent displays [5, 9, 10] and solar cells [11]

It is with the last polymer, poly(*p*-phenylene vinylene), that this work is concerned.

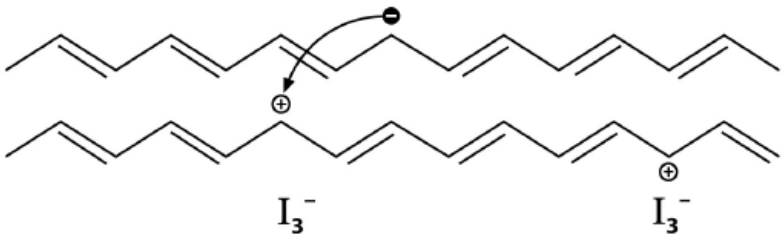

Figure 1.2: Example of dopant effect on polyacetylene: intersoliton hopping. Charged solitons on the bottom chain are trapped by dopant ions. When the freely moving uncharged soliton on the top chain nears the charged soliton, the electron can hop from one defect to the other [12].

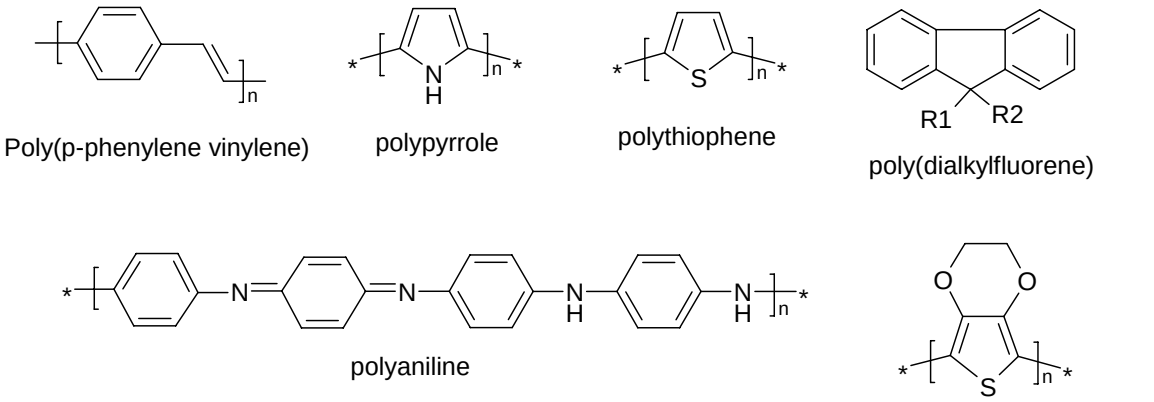

Figure 1.3: Conjugated polymers poly(*p*-phenylene vinylene), polypyrrole, polythiophene, poly(dialkylfluorene), polyaniline, and poly(3,4-ethylenedioxythiophene).

1.2 Role of PPV

The polymer structure of poly(*p*-phenylene vinylene) (PPV) contains benzene rings along the backbone joined by single-double-single (vinylene) bonds, preserving the conjugated structure and adding the strength of the benzene ring to the typical carbon chain. PPV and some examples of related polymers are shown in Figure 1.4. Although PPV has been known for many decades, it was not widely studied until 1990, when

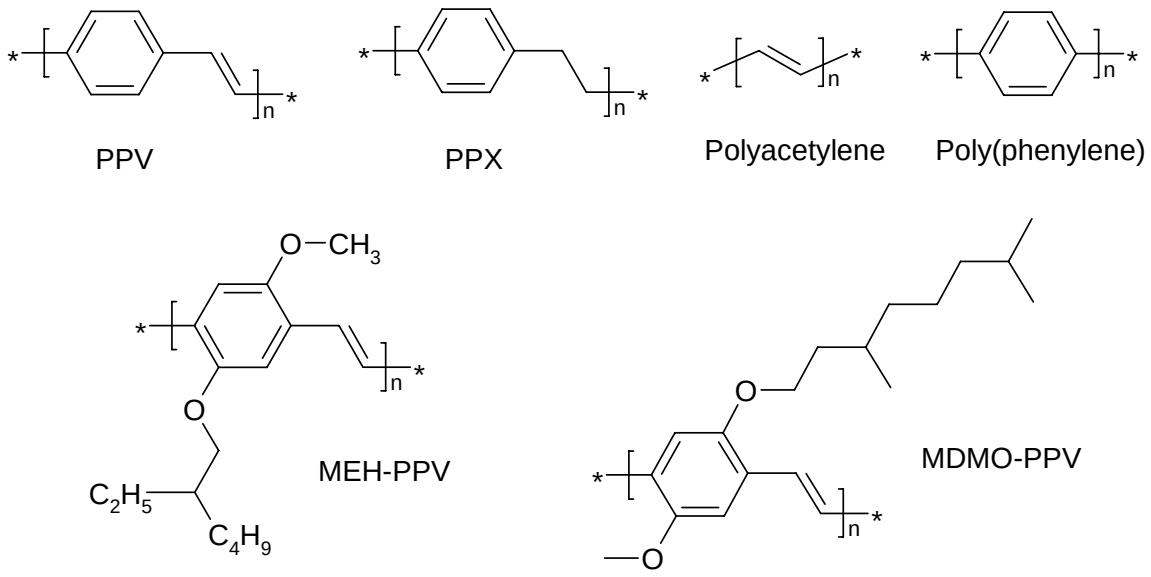

Figure 1.4: PPV and related polymers, including Parylene (PPX, poly(*p*-xylylene), polyacetylene, polyphenylene, poly[2-methoxy-5-[(2'-ethyl-hexyl)oxy]-*p*-phenylene vinylene] (MEH-PPV), and poly[2-methoxy-5-(3',7'-dimethyloctyloxy)-*p*-phenylene vinylene] (MDMO-PPV).

Burroughes *et al*. discovered that it was, in fact, electroluminescent, and successfully integrated undoped PPV into a light emitting device as the emitting layer [9]. This seminal breakthrough was the first for any of the conjugated polymers and opened the door to new areas of research for these materials. Although other conjugated organics are electroluminescent as well, PPV and its derivatives are still widely used as the emitting layer in optical electronic devices such as LEDs and solar cells.

PPV has many useful properties in addition to its photoluminescence and electroluminescence. It has a degradation temperature higher than those of related polymers: PPV at 500 °C [12] compared to poly(*p*-xylylene) (Parylene) at 420 °C [13], polyacetylene at 200 °C [14], and polyphenylene at 450 °C [15].

The crystal structure of PPV films is a monoclinic unit cell with dimensions a = 7.9 Å, b = 6.05 Å, c = 6.6 Å, and an angle α = 123°, as determined by X-ray diffraction studies [16, 17]. The polymer chains have a tendancy to line up in the plane of the substrate

without stretching when deposited from liquid sulfonium precursor [16, 18]; similarly, films deposited from chemical vapor deposition can also be self-orienting depending on the structure of the substrate and at an angle to the substrate [19].

PPV itself is not an ideal polymer. One of the most difficult aspects to overcome is its susceptiblity to the incorporation of oxygen, especially when exposed to UV light. Carbonyl groups formed by the oxygen on the carbon chains linking the polymer break the double bond on those chains and therefore break the conjugated structure. An interruption of this type limits the conductivity of the chains and increases the energy band gap. Thus, polymer synthesis and processing are important steps that must be carefully controlled to prevent the incorporation of defects into the polymer chain.

In addition to organic LEDs, PPV has been used in a variety of other applications. Following the discovery of electroluminescence in PPV, Tessler *et al.* demonstrated optically driven laser activity in a microcavity structure with PPV-based emission [20]. Others have used PPV and its derivatives as electrochemical batteries [21]. Electrical and optical applications for PPV are limited by the material qualities of the films.

1.3 Luminescence of PPV

Luminescence of materials can be stimulated from energy input in a variety of ways, from biological and chemical processes to stimulation by sound or light waves—any process except for thermal excitation, which is known as incandescence. For conjugated polymers, electroluminescence (EL, energy supply from electrical current) and photoluminescence (PL, energy supply from incident light absorption) hold the most attention because of their potential applications in advanced devices such as organic light emitting diodes (OLEDs) and solar cells. Such an interest in developing potentially large area light emitting diodes (LEDs) first spurred Burroughes *et al*. into discovering and studying the electroluminescent properties of PPV [9]. The simple device design of two electrodes (at least one of which was transparent) sandwiching a 70 nm thick layer

of PPV provided yellow-green luminescence visible to the naked eye after applying a voltage of over 14 V. The output spectrum of the device was similar to that of the photoluminescence spectrum, which was centered around 563 nm (2.2 eV) and showed clearly resolved vibronic peaks. Both the electroluminescence and photoluminescence spectra have a similar shape at the same wavelenght, and indeed it has been shown that the same excitation is responsible for both types [22]; namely a singlet exciton. The main difference is the source of the excitations. In electroluminescence, electrons and holes are injected into the material at each electrode and recombine in the material, while photoexcitation causes an electron to move to the conduction band while its associated hole remains in the valence band [23]. As this work is mostly concerned with the study of the photoluminescence properties of PPV, the following discussion will be couched in PL terms but can be extrapolated to include electroluminescence as well.

1.3.1 Stimulation and Emission

The absorption and emission spectra of PPV are shown in Figure 1.5, where the range of absorption stretches through the UV up to approximately 500 nm. Absorbed light stimulates the molecule into an excited state, the level of which is determined by the energy quantum of the light. Higher excited states undergo nonradiative internal conversion to the lowest vibrational level of the first excited state (S_1) (a phenomenon described by "Kasha's rule" [24]), where several pathways for deexcitation exist (Figure 1.6). Radiative decay from this level results in the emission of a photon, or photoluminescence; nonradiative decay produces no photon and will be discussed further in Section 1.3.2. For most practical applications, a high luminescence intensity is desirable and therefore many studies aim to increase the number of radiative emissions or quantum efficiency (ΦE = [number of photons emitted]/[number of photons absorbed]) and/or decrease the nonradiative decay pathways.

The excitation responsible for the luminescence of PPV is a singlet exciton, a neutral bound electron-hole pair. The first excited state is most likely a polaron exciton, a weak-

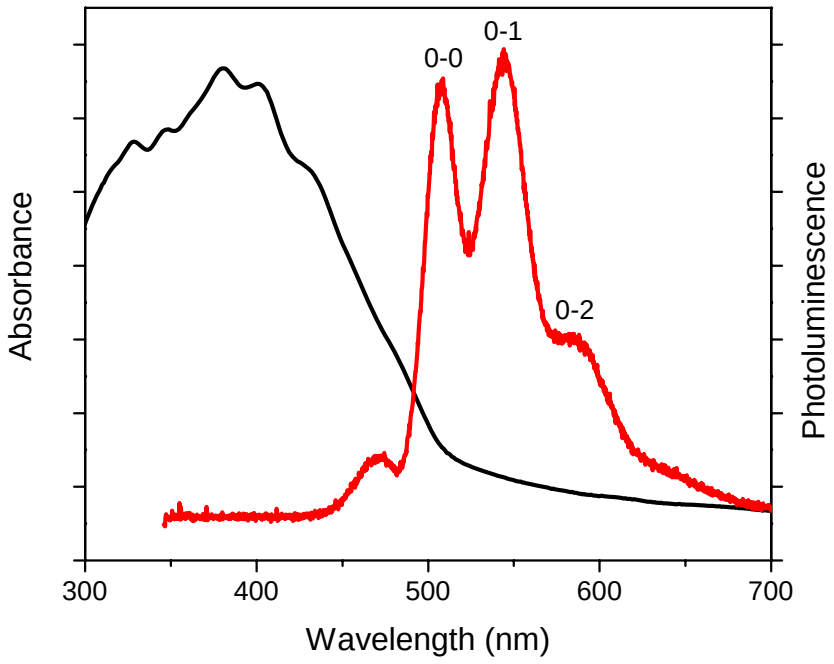

Figure 1.5: Absorption (left, black) and emission (right, red) spectra of PPV. The vibronic peaks of the photoluminescence spectra are marked 0-0, 0-1, and 0-2 at approximately 510 nm, 550 nm, and 590 nm, respectively.

to intermediately bound exciton associated with a lattice distortion [1, 25]. The lattice distortion in the excited state of PPV arises from the change in the π-bond density from the excitation; it typically results in a "flattening" in the polymer backbone as the excitation shifts it into a semiquinoid form [26], where the bonds in the vinylene unit increase (double) and decrease (single) slightly. This effect can spread over 3-4 units of the polymer, but is not otherwise dependent on the chain length [27].

One result of this electron-lattice interaction (electron-phonon coupling) is a strong vibronic progression visible in luminescence spectra as a series of peaks with decreasing energies [25]. As marked in the photoluminescence spectrum of Figure 1.5, the vibronic peaks can be directly associated with vibronic transitions within the excited states. In order of increasing wavelength (decreasing energy) the strongest transitions are 0→0 at about 510 nm, 0→1 at 545 nm, and 0→2 at 585 nm. The first transition, 0→0, also

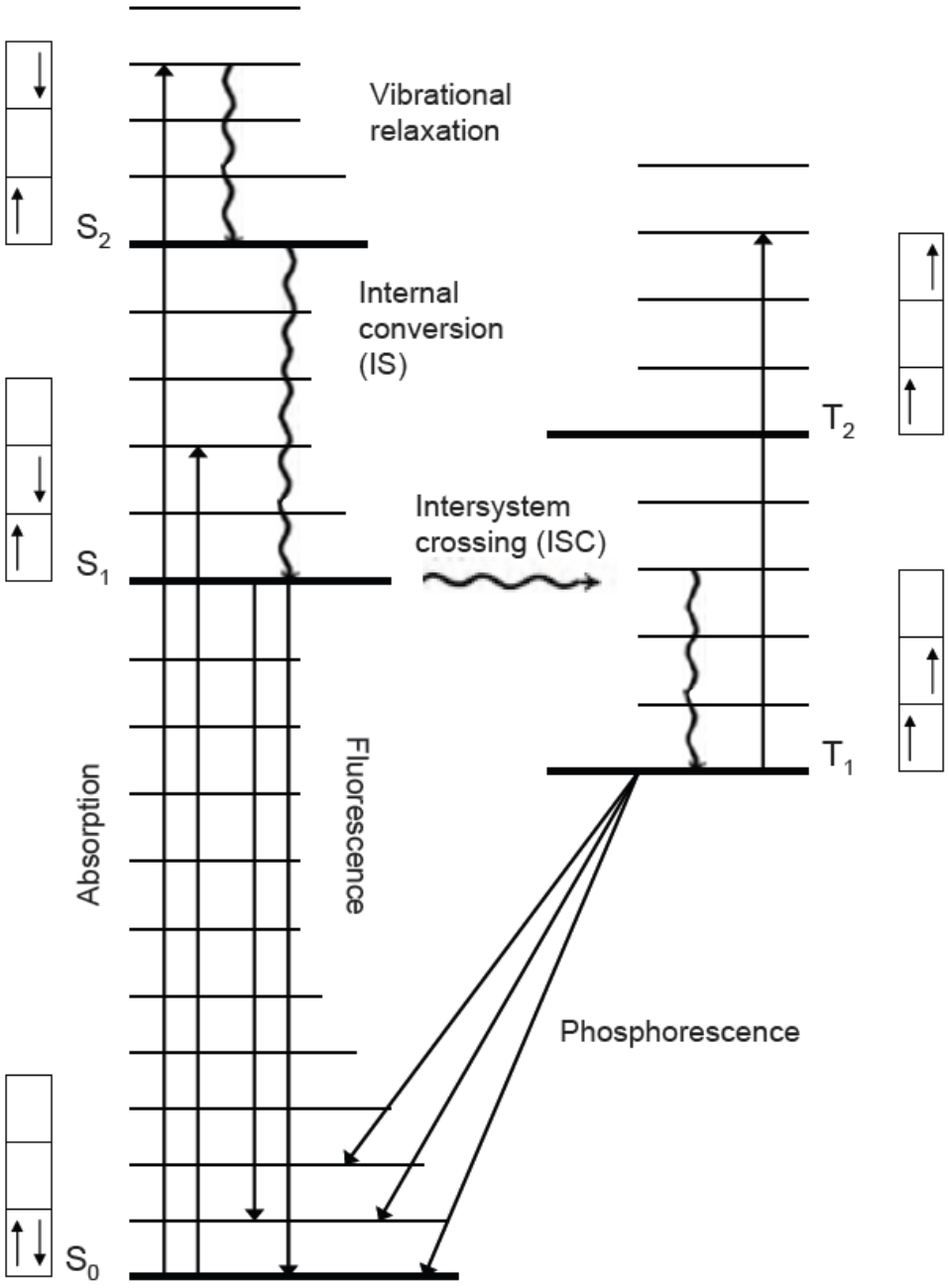

Figure 1.6: Jablonski diagram of energy levels in a molecule and the corresponding spin states [28]. The vertical direction corresponds to increasing energy. Singlet (S_1, S_2, S_3) and triplet (T_1, T_2) states are marked with bold horizontal lines while vibrational levels within those energy states are marked with unbolded lines. Straight arrows pointing up correspond to absorption of light energy; straight arrows pointing down are luminescenct decay (fluorescence or phosporescence); and wavy arrows are nonradiative transitions (internal conversion, intersystem crossing, or vibrational relaxation). (Image based on Ref. [28].)

corresponds approximately to the energy gap between the highest occupied molecular orbital (HOMO) and lowest unoccupied molecular orbital (LUMO) levels, or the π (bonding) and π^* (antibonding) orbitals. Because of the yellow green color of this emission, PPV is already ideally suited to use in organic LEDs [9].

A further influence on the emission spectrum of the polymer is its conjugation length (as opposed to the chain length). Not only the ends of chains break conjugation, but also bends in the chain as well as rotations from the "plane" of the chain can separate sections of the chain into sections known as "conformational subunits," the lengths of which are the conjugation length of that section (Figure 1.7). Conjugation length can be an indicator of the quality of the film, as there are fewer chemical defects and less conformational disorder in longer chains, and can be increased or decreased depending on deposition and processing conditions such as annealing temperature [29] and stretching ratio. In general, longer conjugation lengths result in slightly redshifted luminescence spectra, and for this reason broadened peaks are a result of the distribution of conjugation lengths amongst several polymer chains. The origin of the redshift is explained by Heun *et al*. using low-temperature site-selective fluorescence spectroscopy [30]. They explain that the excitations in PPV execute a random walk along ordered segments of the chains. As an excitation migrates, it relaxes energetically; the longer the conjugated segment in the chain, the more acceptor sites and the less the chance of emission. Thus, longer chains result in redshifted (lower energy) emission spectra. However, even on perfectly straight, conjugated chains, excitations do not migrate to infinity as this would reduce the energy to zero without decay. In fact, excitons have a tendancy to self-localize to a set of about 7-10 monomer units (the effective conjugation length), as calculated by models incorporating both electron-electron interactions and electron-lattice interactions [26, 31] and supported by measurements on PPV oligomers.

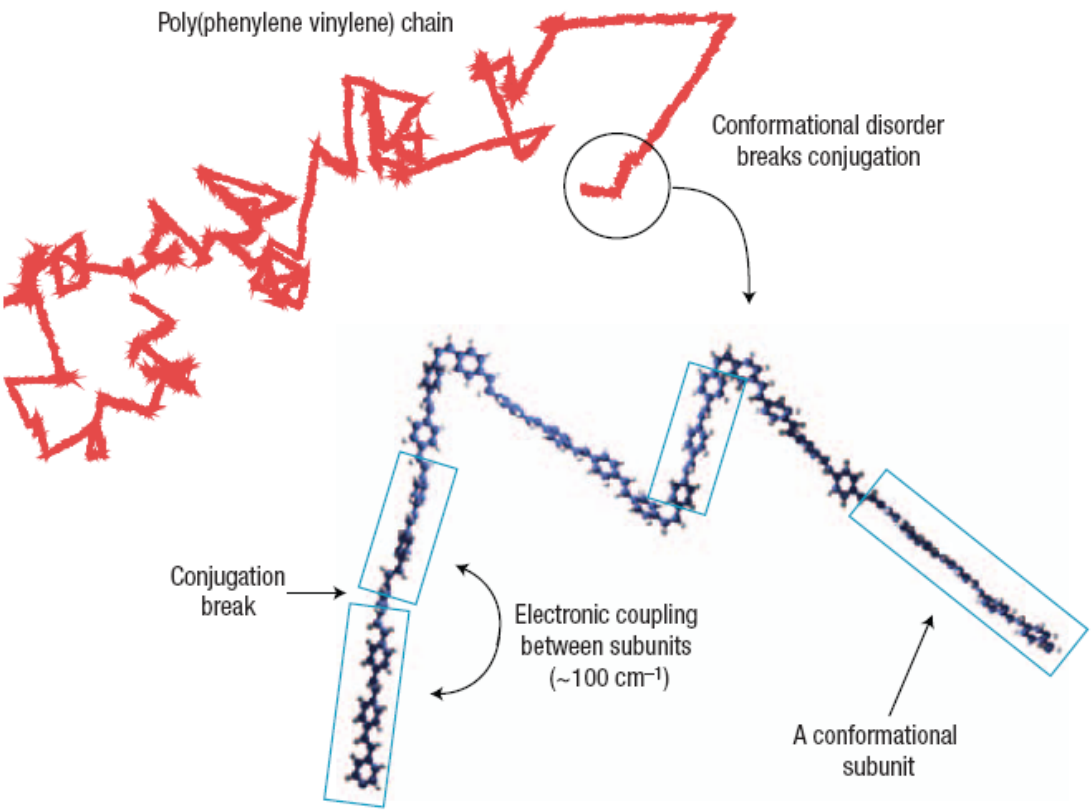

Figure 1.7: Conformational subunits in a disordered chain of PPV. Conjugation is broken when the chain rotates at sufficient angles; the resulting sections are known as conformational subunits and their length is the conjugation length. Excitons migrate to sections with longer conjugation lengths. [Image from Ref. [23]]

1.3.2 Degradation and Quenching

Nonradiative decays are the dominant mechanism for deexcitation of the excited state in PPV because there are many pathways for the decay to follow. Many studies have focused on decreasing the likelihood of a nonradiative transition with varied success in the different methods. The two main photophysical processes responsible for nonradiative decay are internal conversion and intersystem crossing, both of which are shown schematically in Figure 1.6. The first, internal conversion, is a nonradiative transition from higher excited states to the first excited state ($S_n \sim> S_1$ or $T_n \sim> T_1$) or from the first excited singlet state to the ground state ($S_1 \sim> S_0$). In most cases, while the internal conversion rate between higher and lower excited states is very rapid and

therefore dominates over other types of deexcitation, the internal conversion $S_1 \sim> S_0$ is much slower and contributes only partially to the radiationless deactivation of the first excited state [32].

Another pathway for nonradiative deexcitation is known as intersystem crossing (ISC) and involves a transition from a singlet state to a triplet state or vice versa, such as $S_1 \sim> T_1$ and $T_1 \sim> S_0$ (transitions from S_1 to higher triplet states are also possible and typically result in internal conversion to the lower T_1 state). These transitions require a spin inversion of the electron and take place through spin-orbit coupling [32]. Although radiative transitions are possible from triplet states (the origin of phosphorescence), they are typically much weaker than radiation from the singlet state and the nonradiative ISC dominates. The presence of impurities such as oxygens and halogens in the polymer chain can increase the rate of ISC by adding new triplet or low-energy excited singlet states [33]. The triplet states of the impurities are lower than the first excited singlet state of the molecule and so they increase the likelihood of ISC instead of luminescence [24].

In order to increase the luminescence intensity, it is thus desirable to decrease the concentration of impurities in the polymer chain and reduce the number of nonradiative transitions. However, as attested to by the amount of work on this topic, there are many sources of impurities in the polymer: deposition conditions, precursor chemistry, annealing conditions, even substrate material. The most common depostion method, spin coating of a precursor polymer, requires the use of solvents and additives to facilitate the deposition (see section 1.4 for more information on the synthesis of PPV). Many of these compounds contain sulfur groups and/or halogens, both of which can act as dopants and centers for nonradiative recombination as well as break the conjugation of the backbone. Groups have converted precursor polymers at temperatures above 300 °C and still found evidence of the presence of sulfonium and halogen groups in the polymer chains [34]. Others have found that replacing vinylic hydrogens with various substitutents reduce the incorporation of impurities onto the vulnerable carbon-carbon double bond [35].

A different deposition method, chemical vapor deposition, eliminates the need for solvents by sublimating a precursor molecule instead of dissolving it. Although the sulfonium groups and other additives are eliminated, the precursor polymer is a halogenated one, and many studies have found evidence of halogens remaining in the film after conversion to PPV [36].

One of the most damaging elements in terms of reducing luminescence quantum yield is oxygen. Organic groups as a whole are susceptible to reaction with oxygen, especially when facilitated by exposure to an energy source. In addition to increasing the likelihood of nonradiative intersystem crossings, the strong electron affinity of oxygen in carbonyl groups can lead to charge transfer and disassociation of the exciton entirely [37]. As mentioned above, oxygen groups can be incorporated during deposition, during conversion, and during exposure to atmosphere; they typically present themselves as carbonyls on the vinylene carbons [22]. Tran *et al*. found that ketone groups were present in the spin-deposited precursor polymer before conversion to PPV, and actually increased in number when conversion was carried out in the presence of oxygen [38]. Papadimitrakopoulos *et al*. found that the number of carbonyl groups present in a film increased with temperature and the photoluminescence decrease quickly as the carbonyl groups increased [22]. Conversion to PPV in a reducing atmosphere reduced the amount of oxygen in the film, but did not eliminate it entirely.

Even if the deposition and conversion process is designed to minimize the presence of oxygen in the films, exposure to UV light in the presence of oxygen from atmosphere degrades the film by creating carbonyl groups and eventually causing a chain scission reaction to form terminal carboxylic acid groups [39]. It has been shown that the pattern of photo-oxidation in PPV follows the profile of the absorption depth [40] and occurs within minutes of exposure to UV light in atmosphere [41]. Others have found that electrical stress in the presence of oxygen is sufficient to spur degradation of the film [42].

Vaeth and Jensen explored the origin of defects during chemical vapor deposition of halogenated precursor polymers. They found that nearly carbonyl-free films could be

deposited if the entire deposition system was thoroughly baked out and kept from excessive exposure to oxygen [43]. However, they still found evidence of defects in the polymer chain and later determined that nonconjugated sections in the polymer were due to the incorporation of fragmentation or dimerization products during pyrolysis of the monomer, thus requiring careful control of the deposition conditions [36] (Figure 1.8).

The presence of halogens in PPV films is an undesirable side effect of the deposition methods necessary when depositing PPV, during both spin-coating and chemical vapor deposition (CVD). Halogens can act as dopants or electron traps in the films, can break conjugation, and react with some substrates. Thus, they are a contributor to degradation in structures such as organic light emitting diodes [44]. Indium tin oxide (ITO), a clear conductive material commonly used as the hole-injecting material in organic LEDs, has been shown to form indium chloride immediately upon contact with HCl-containing polymer precursor, degrading not only the polymer but the substrate as well [45]. Most halogens from the precursor polymer are removed during the annealing process, with varying degrees of success.

As mentioned in the preceeding section, excitations migrate randomly along ordered, conjugated segments of the polymer chain. In addition to this motion, excitations are also capable of transferring to an adjacent chain and proceeding with deexcitation there. These decays are nonradiative.

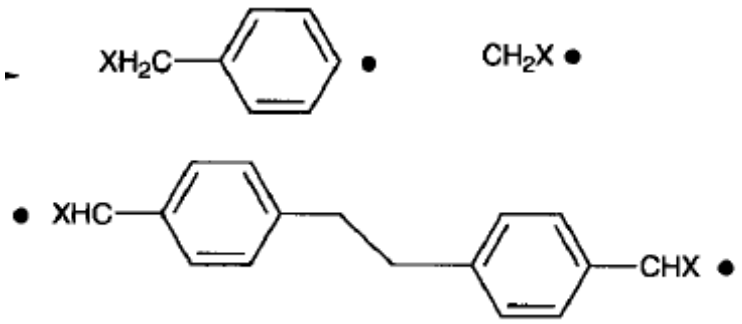

Figure 1.8: Undesirable fragmentation and dimerization products of monomer pyrolysis that can become incorporated into PPV films and break the conjugation of the polymer chains. [Image from Ref. [36]]

1.4 Synthesis of PPV

Poly(*p*-phenylene vinylene) can be deposited using a variety of synthetic processes. One of the first methods was Wittig condensation, which is a common organic synthesis route that utilizes a triphenyl phosphonium ylide (a "Wittig reagent") to form predictable carbon-carbon double bonds. In the case of PPV, McDonald and Campbell first showed that *p*-xylylene-bis-(triphenylphosphonium chloride) reacted with terephthalaldehyde to produce poly-*p*-xylylidene, or PPV, in good amount [46] (Figure 1.9). However, the resulting product is in the form of an insoluble, non-fusible powder and thus has only a limited usefulness due to the difficulty in processing it. Other methods are needed to create more processable and useful thin films.

A common deposition method for materials such as photoresist and soluble polymers is spin-coating. In this procedure, the material is dissolved into solution then applied onto a rotating substrate and dried. The film thickness can be controlled by varying the viscosity and volatility of the solution, the amount of the solution, and the speed of the platform. However, PPV is not soluble, so deposition by spin-coating is not without difficulties, namely finding a suitable soluble precursor polymer that can easily be converted to PPV. One of the earliest and most common "precursor-route" deposition methods is called the Wessling route or the sulfonium route. In this procedure, water-soluble polyelectrolytes with bis-sulfonium substitutents are prepared by polymerizing monomeric sulfonium salts in solution, as in Figure 1.10 [47]. By spin-depositing the polymer solution, drying it, and then annealing it at elevated temperatures (usually 100-300 °C), the sulfonium groups leave and are replaced with the carbon-carbon double bonds characteristic of PPV. Typical precursor polymers include poly(*p*-xylylene-α-dimethylsulphonium chloride) [48] and poly(xylylidene tetrahydrothiophenium chloride) [49] (Figure 1.11); other precursor-route depositions are variations on this method, utilizing different leaving groups, ions, or solvents to further refine the resulting films.

Other deposition methods can take advantage of the Wessling route precursors to produce ultrathin Langmuir-Blodgett (LB) or self assembled monolayer (SAM) PPV

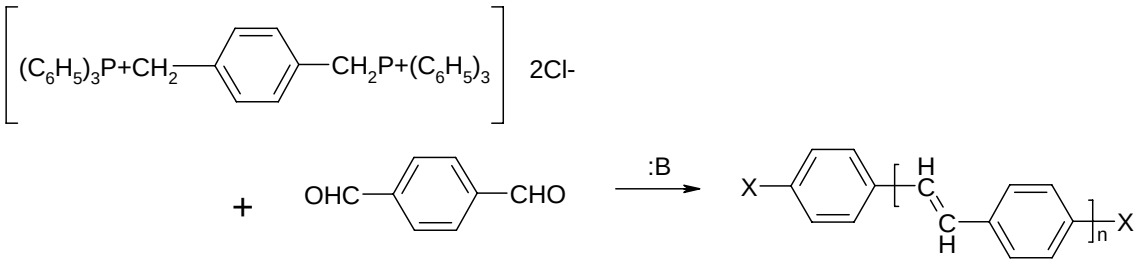

Figure 1.9: Wittig reaction for formation of PPV. The polymer product is an insoluble, infusible polymer.

Sulfonium salt:

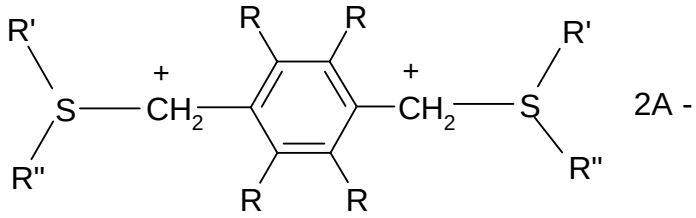

Water soluble polyelectrolyte precursor:

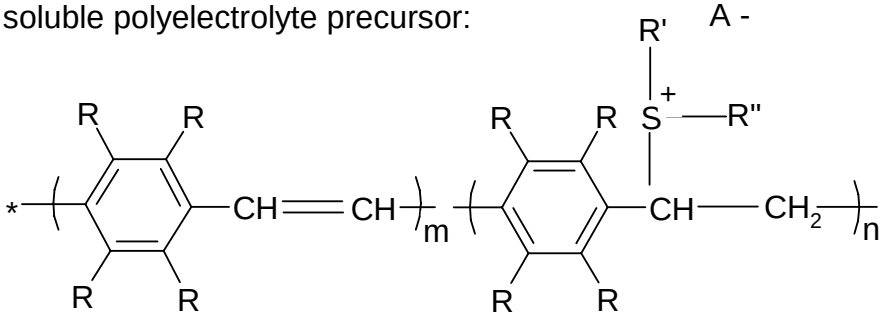

Figure 1.10: Wessling (sulfonium) route precursor and soluble polymer precursor. Polymerization of the sulfonium salt monomer occurs in strongly basic solution. In both cases, R represents hydrogen or a methyl group, R' and R" each represent an alkyl group containing 1-4 carbon atoms, and A represents a counterion from a low molecular weight acid that does not precipitate or react in the aqueous polymer solution [47].

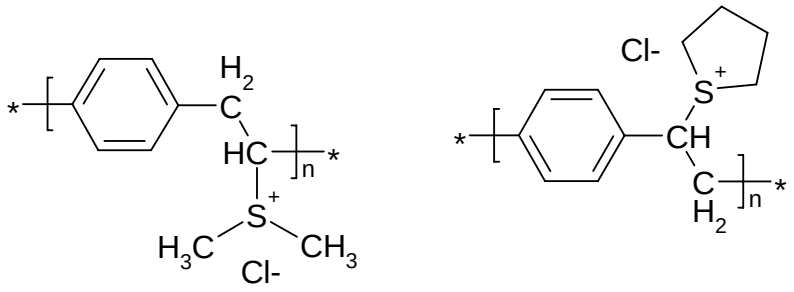

Figure 1.11: Common sulfonium route precursor polymers poly(*p*-xylylene-α-dimethylsulphonium chloride) and poly(xylylidene tetrahydrothiophenium chloride). Another polymer, poly(*p*-xylylene-α-diethylsulphonium chloride), has the same structure as the former but with -CH_2CH_3 groups replacing the -CH_3 groups.

films. For LB films, substrates are dipped into solutions containing the precursor polymers. The molecules are transferred to the substrate in one monolayer increments, allowing for precise thickness control as well as alignment of long chains. In order to achieve the conditions necessary for LB film deposition, Wessling precursors such as poly(*p*-xylylene-α-diethylsulfonium chloride) are modified by replacing the chloride counterion with long-chain replacements such as $C_{18}H_{37}SO_3$ [50] or long chain dodecylbenzenesulfonate [51]. A similar modification allows the creation of self-assembled monolayers (SAM) of PPV, which can be formed by dipping the substrate alternately into the precursor polymer solution and the counterion solution for each layer [52]. Both methods allow the depositions of films a few angstroms in thickness.

However, even with the success of these methods, many problems still exist, often due to the use of solution in the deposition process. Impurities from the variety of chemicals and from the deposition process abound. The leaving groups can damage the film or the substrate as they leave, and even then the conversion process isn't always efficient, requiring long annealing times while still failing to remove all of the precursor (see Section 1.3.2 for further details). Additionally, the spin deposition method has fundamental limitations that prevent thin, conformal coatings on nanostructured substrates without post-processing.

Partially in response to these difficulties, researchers have developed methods for the chemical vapor deposition of PPV. In this method, a solid precursor is sublimated, pyrolized to a reactive form, and deposited onto a variety of substrates. The first successful chemical vapor deposition of PPV was developed by Iwatsuki *et al*. in 1991 [53], who was inspired by the successful CVD of xylenes by Gorham to form poly(*p*-xylylene) (Parylene or PPX) and its derivatives [54]. In his deposition process, Gorham used the precursor [2.2]paracyclophane (or di-*p*-xylene), which cleaves at the carbon-carbon bonds during pyrolysis to form two molecules of the reactive intermediate *p*-xylylene that then spontaneously polymerize to form PPX on room temperature substrates (Figure 1.12). Significantly, the films thus deposited were conformal and pinhole free [54]. Since PPX has the same chemical structure as PPV without the adjoining double bond, adding a halogen leaving group to the paracyclophane precursor allowed a halogenated precursor polymer to deposit that could then be heat treated to convert to PPV. Iwatsuki et al. used the precursor 1,9-dichloro[2.2]paracyclphane to deposit chlorinated precursor polymers, then converted the films to PPV at 300 °C [53]. Efforts to improve yield and molecular weight of CVD PPV were carried out by groups such as Staring *et al*. [55] and further developed by Schäfer *et al.* [56], who investigated the use of *p*-xylenes substituted with two halogen groups as the precursor molecule. In this case, one of the halogens leaves during the pyrolysis of the precursor molecule, creating a resonant quinone intermediate that polymerizes upon deposition on a room-temperature substrate. The resulting halogenated precursor polymer then must be annealed in order to remove the remaining halogen and create the final PPV film (Figure 1.13). Although the method still requires a precursor polymer, the CVD method has advantages over the traditional spin coating method in that there is no need for a solvent and films can be deposited conformally on a variety of nanostructured substrates, eliminating the need for some types of post-processing. Additionally, CVD growth can be selective on certain substrates, allowing the possibility of patterned depositions without post-processing of the polymer [57-59].

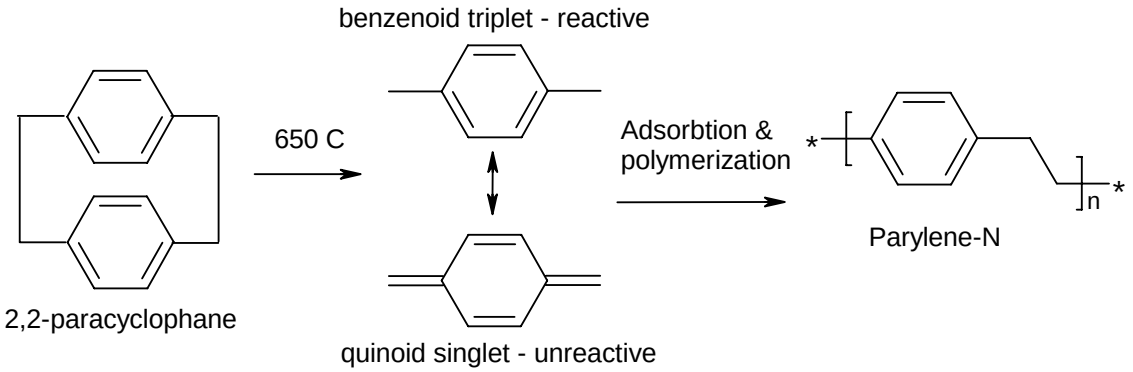

Figure 1.12: Parylene chemistry. Gorham method for deposition of Parylene-N [60].

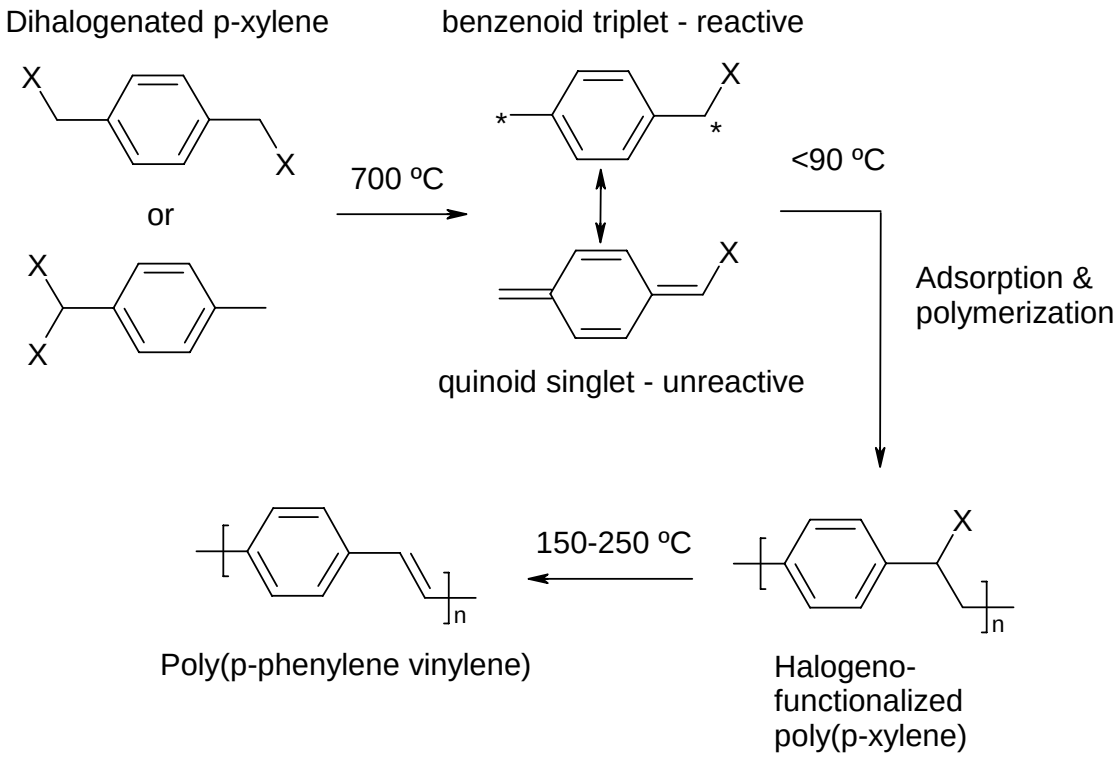

Figure 1.13: Reaction steps involved in depositing a film of PPV. X = Br, Cl, I

1.5 Outline of Thesis

This thesis is organized into seven chapters. Chapter 2 discusses the design and setup of the reactor for PPV. Experimental details for the deposition of PPV are provided, as

well as properties of the substrates used. Additionally, the techniques of film analysis and characterization are described.

Chapter 3 contains work on the annealing of the precursor polymer to form PPV. Methods to minimize the amount of bromine present in the converted films are explored.

Chapters 4 and 5 focus on the thermal degradation and the photodegradation of PPV, respectively. Thermal degradation analysis takes place under isothermal and dynamic heating conditions. Photodegradation is measured on a variety of substrates and methods to prevent degradation are presented.

Chapter 6 analyzes the photoluminescence of PPV under varying conditions, including thickness, temperature, and substrate structure. Finite size and interface effects are examined in these films.

Chapter 7 contains the summary and conclusions of the work in this thesis. In addition, a selection of future work is provided.

Finally, Chapter 8 provides the references for this complete work.

2. Experimental Design

This chapter presents the setup for preparation and study of poly(p-phenylene vinylene) films used in this work. First, the design for construction and use of the chemical vapor deposition (CVD) reactor is discussed. Next, the conditions for deposition are presented, as well as the conditions and considerations for annealing of the precursor polymer and conversion to PPV. A discussion of the types of substrates used ensues. Finally, an overview of the characterization methods used is given, including several optical spectroscopy techniques.

2.1 Reactor Design

A custom built vacuum chamber was constructed for the chemical vapor deposition of poly(p-phenylene vinylene) in this thesis. The CVD system design is based on that of Schäfer et al [56], and was built piece-by-piece using a variety of aluminum and stainless steel parts. There are four main sections of the system: sublimation furnace, pyrolysis furnace, deposition chamber, and mechanical pump with traps (Figure 2.1). Valves are used in between all the different sections of the system, and heating tape above 90 °C covers all the lines in order to prevent premature condensation of the precursor gas. Metal-to-metal seals consist entirely of Viton o-ring Quik Flanges except for the metal Conflat Flanges on either end of the furnace due to the high heat involved there. Two pressure gauges are used: a gas-independent heated MKS Baratron capacitance manometer attached to the side of the deposition chamber, and a thermocouple gauge attached between the chamber and the mechanical pump to monitor foreline pressure.

The deposition process begins with the sublimation furnace, which consists of a glass-to-metal ampoule wrapped in heating tape. A carrier gas (nitrogen gas from lab lines) is flowed through the ampoule, on top of the solid precursor, and out into the system. The combined carrier and precursor gas flows from there through a custom-made stainless steel tube inside the pyrolysis furnace. This furnace is a Thermolyne 21100 tube furnace

that is cylindrical in shape, 15 inches long, and heated to a controlled temperature of 700 °C during deposition. The substrate is held at room temperature inside the deposition chamber. Gas removed from the chamber by the vacuum pump is first sent through a series of filters, including water cooled, liquid nitrogen cooled, and stainless steel or copper element, before being removed to the exhaust system. The mechanical pump is capable of base pressures on the order of 10^{-3} Torr.

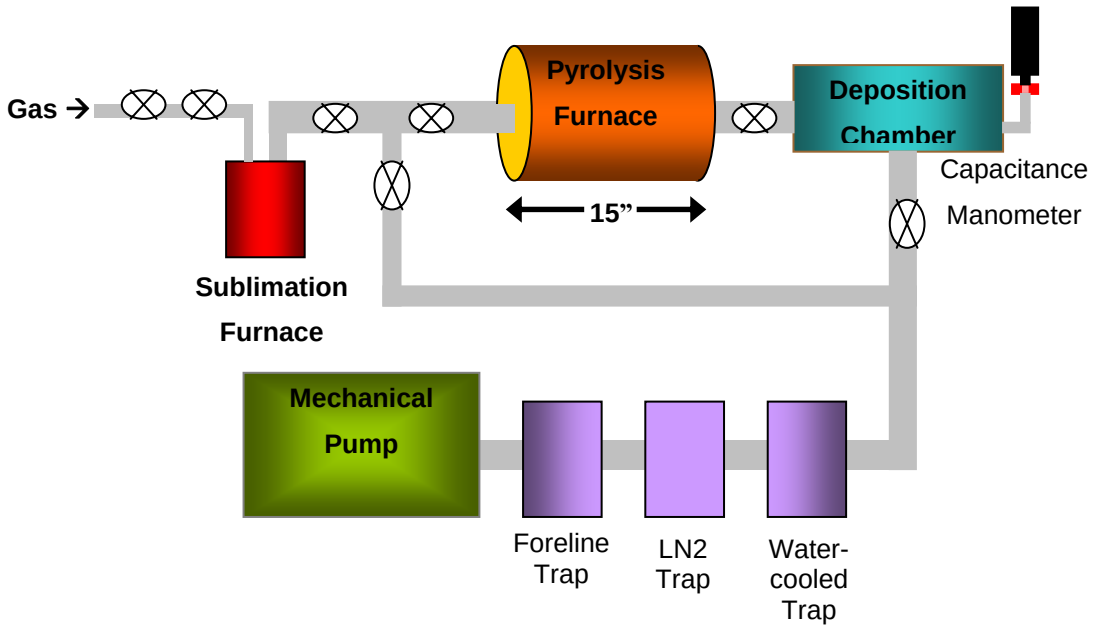

Figure 2.1: Schematic for the Chemical Vapor Deposition (CVD) system.

2.2 Deposition Conditions

The sublimation furnace typically contains 0.5 – 3.0 g of the precursor α,α′-dibromo-p-xylene and is heated to temperatures between 100 and 130 °C, above the sublimation temperature (90 °C) of the precursor but below its melting point of 143 °C (97 %, Sigma-Aldrich, St. Louis, MO USA). Nitrogen gas is flowed during the deposition to increase the deposition rate and provide a more even precursor flow. Typical gas pressures in the deposition chamber range from 10 – 50 mTorr. Deposition rates depend

on the pressures of both the carrier gas and the precursor gas; a selection of typical rates is given in Figure 2.2.

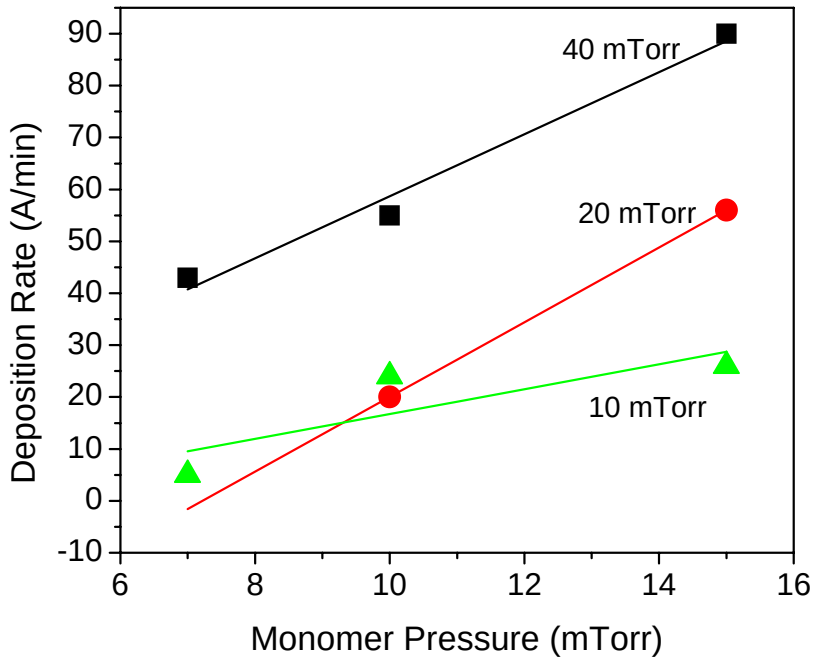

Figure 2.2 Sample deposition rates in CVD system, including carrier gas pressures of 40 mTorr (■), 20 mTorr (●), and 10 mTorr (▲). Lines are guides to the eye.

2.3 Annealing

The most common method of converting the precursor polymer to insoluble PPV is annealing, although alternatives such as UV exposure exist [61]. For this work, annealing was done in one of two furnaces. Most films were annealed in a home built system using a heated substrate. The heating unit is enclosed in a vacuum-ready chamber connected to a mechanical pump, a diffusion pump, and nitrogen gas lines. Typical annealing conditions were in vacuum with a pressure of about 5 mTorr and a temperature of 250 °C, although some annealing was done under gas flow or at different pressures or temperatures, as noted in the results sections.

The second furnace was designed for more complicated temperature control patterns and access to a mass spectrometer. The furnace itself is a Mini-Lamp Annealing system (MILA-3000, ULVAC Technologies Inc., Methuen, MA USA) and uses an infrared lamp as the heat source. The sample holder is made of quartz and the temperature is programmable and controlled with a thermocouple. The furnace is connected to a mechanical pump and a high vacuum pump, either a diffusion pump or a turbo pump. Pressure during heating was in the 10^{-6} Torr range, as the mass spectrometer requires a pressure of less than 10^{-4} Torr to avoid damage (see Section 2.5.3 for further discussion of the mass spectrometer as well as a figure of the setup of the furnace/mass spectrometer/pumping system).

2.4 Other Materials

2.4.1 Substrates

Unless otherwise noted, films were deposited on silicon <1 0 0> wafers (Silicon International, Hong Kong). Films for characterization requiring a transparent substrate (FTIR, transmission spectroscopy, etc.) were deposited on either potassium bromide (KBr) pellets from Pike Technologies (Madison, WI USA) or quartz glass disks from McMaster-Carr (Chicago, IL USA).

Porous methyl silsesquioxane (MSQ) with pore size ~4 nm was obtained from TI and Freescale. Deposited by the sol-gel method, the MSQ was 300 nm thick on top of 6.8 nm SiO_2 on n-doped Si with a resistivity of 10 Ω-cm. Bulk MSQ has a stoichiometry of $SiO_{1.5}CH_3$; the structure is shown in Figure 2.3.

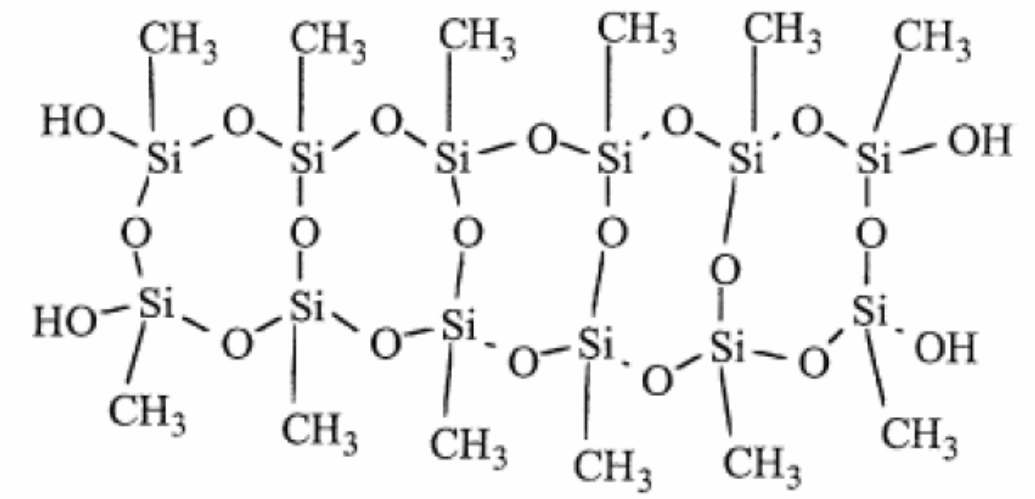

Figure 2.3: Methyl silsesquioxane (MSQ) structure. [Image from Ref. [62]]

2.4.2 Other Films

Parylene (PPX) films were deposited from [2.2]-paracyclophane precursor using the Gorham method [54] in a system very similar to that for PPV deposition, including a sublimation furnace, pyrolysis furnace, and deposition chamber. In this system, the base pressure reached approximately 10^{-6} Torr through use of a diffusion pump in addition to the mechanical pump. Deposition rates could be varied from 0.7-500 Å/min by increasing the chamber pressure from 1-15 mTorr for depositions. Further system details are given by Fortin and Lu [60].

Thin aluminum films were deposited using a Temescal e-beam evaporator Model CV-8 in high vacuum (base pressure of 5×10^{-7} Torr). The aluminum charge used was 99.999 % pure. In order to prevent destruction of the polymer during aluminum deposition, a low deposition rate was maintained. The thickness was monitored by a quartz crystal microbalance and gave a final thickness of 5.6 nm. The aluminum oxidized after exposure to atmosphere.

2.5 Characterization

Characterization of the various films and structures created and utilized in this work were performed on a variety of equipment, predominantly spectroscopic in nature.

2.5.1 Photoluminescence

Photoluminescence is the generation of light stimulated by an outside light source, as opposed to luminescence stimulated by other sources such as a chemical reaction (chemiluminescence) or an applied electric field (cathodoluminescence), and excluding incandescence, the light given off by heated elements. There are two types of photoluminescence: fluorescence and phosphorescence, which can be distinguished by the state from which they decay (singlet and triplet, respectively) and the lifetimes of the respective excitations responsible for the radiation.

Photoluminescence measurements were made on USB2000 and USB4000 mini spectrometers from Ocean Optics. The USB2000 detector has a Sony ILX511 linear silicon CCD with a range of 200-1100 nm, 2048 pixels, and a sensitivity of 75 photons/count at 400 nm. This detector was eventually replaced by the improved USB4000 model, which contains a Toshiba TCD1304AP linear CCD array with a range of 200-1100 nm, 3648 pixels, a signal-to-noise ratio of 300:1, and a sensitivity of 130 photons/count at 400 nm. Spectra in this work were taken on the USB4000 unless otherwise noted.

The excitation source for the photoluminescence spectra depended on the detector. The USB2000 measurements used either a UV LED with peak wavelength ~400 nm or a blue LED with peak wavelength of either 430 nm or 450 nm as noted. The USB4000 source is an LS-450 Blue LED light source from Ocean Optics that is powered through the detector and has a peak wavelength of 470 nm.

2.5.2 Spectroscopic Ellipsometry

Spectroscopic Ellipsometry (SE) is a standard method for measuring the thickness and optical parameters of thin films. This characterization technique measures the change in the polarization state of light reflected from a material structure through the use of two independent parameters: the change in relative phase, Δ, and the change in relative amplitude, Ψ, of the orthogonal electric field components of the light after reflection. Variable Angle Spectroscopic Ellipsometry (VASE) measures the ratio of reflection coefficients (ρ) as a function of wavelength and the angle of incidence as follows:

$$\rho(n,k,d) = \tan(\Psi)\cdot e^{i\Delta}, \qquad (2.1)$$

where n and k are the real and complex parts of the refractive index and d is the thickness of the substrate.

All measurements in this work were made on a VASE M-44 Spectroscopic Ellipsometer from J. A. Woollam Co., Inc. (Lincoln, NE). Data was gathered at three incident angles (65°, 70°, and 75°) and either at 44 wavelengths from 410 nm to 742 nm for nonluminescent (precursor) material or at 19 wavelengths from 603 nm to 742 nm for samples photoluminescent in the yellow-green range. Spectra were fitted with uniaxial Cauchy and biaxial (x-y and z) Cauchy models.

2.5.3 Mass Spectroscopy

Mass spectroscopy (MS) is an extremely sensitive technique that is capable of identifying, quantifying, and evaluating the properties of a wide variety of chemicals. In mass spectroscopy, samples are ionized and sent through a magnetic field, where they are separated and detected based on their mass-to-charge (m/z) ratio. There are many different types of mass spectrometers, but each includes three basic components: the ionizer, the analyzer, and the detector. In this work, we utilize an electron impact ionizer, a quadrupole mass analyzer, and a Faraday cup detector.

The ionizer is responsible for giving analyte molecules a charge and often fragments those molecules in the process. An electron impact ionizer (EI) produces electrons using thermionic emission, where a wire (dual thoriated-iridium) filament with current running through it is heated. Resulting electrons are accelerated through space to an anode. As molecules pass through this space, impact with electrons results in charged, fragmented molecules. The fragmentation pattern depends on the type of molecule as well as the energy of the electrons.

This particular mass spectroscopy system is from Stanford Research System RGA300 (Sunnyvale, CA). Parameters included a focus voltage of 90 V, filament current of 1 mA, and electron energy of 70 eV. The system was differentially pumped with a base pressure of ~1 x 10^{-6} Torr, provided by a diffusion or turbo pump. The mass spectrometer was also connected to the MILA furnace discussed in Section 2.3 for in-situ measurements during heating. A schematic for the set up is shown in Figure 2.4.

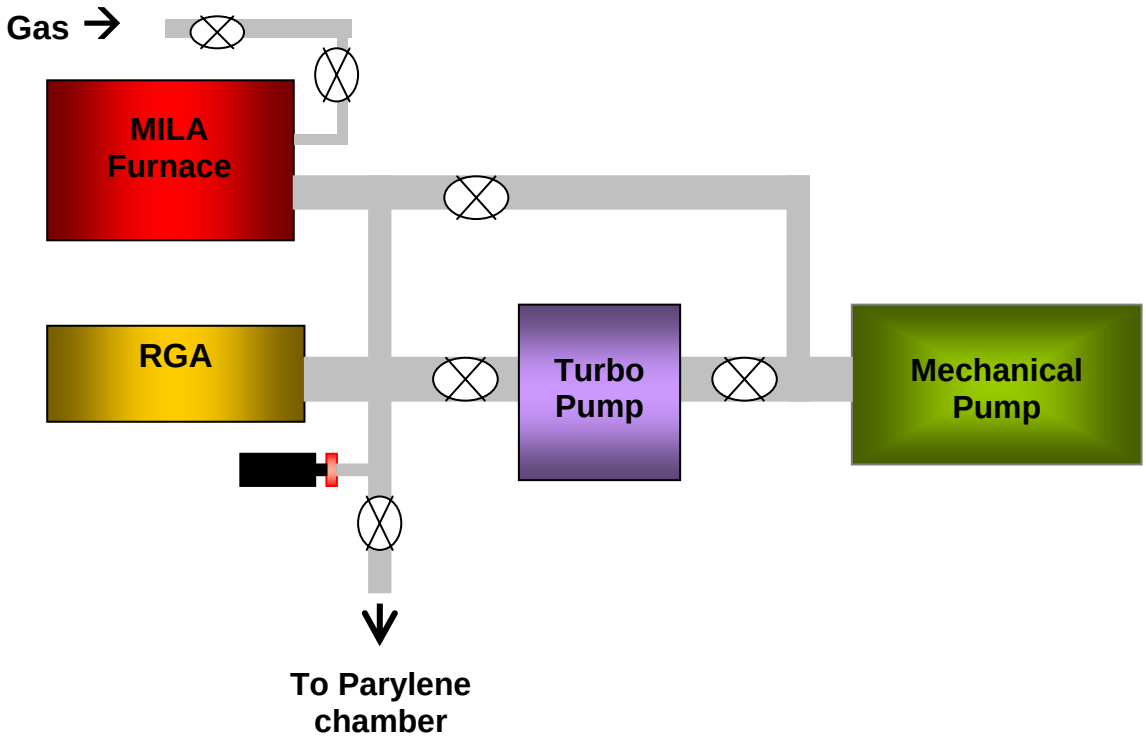

Figure 2.4: Furnace and mass spectroscopy system layout.

2.5.4 Rutherford Backscattering Spectroscopy

The underlying principle of Rutherford Backscattering Spectroscopy (RBS) is that particles traveling through a material will lose energy due to collisions, and the amount of energy lost is dependent on the type and amount of different atoms present in the material. This technique uses a collimated, monoenergetic stream of particles at energy E_0 directed at the sample. Particles that have been backscattered at very small angles from the sample are collected and the energy E_1 is measured. Analysis of the energetic information, including the kinematic factor $K = E_1/E_0$, provides information about the elemental composition as well as the depth profile [63].

In this work, measurements were made using 2 MeV $^4He^+$ incident ions from a Dynamitron accelerator in the Ion Beam Laboratory located at SUNY Albany. The beam current was kept at 5 nA or lower to prevent damage to the samples. The spot size was 20 mm^2 and the beam contained 2-4 mC of charge. The backscattered ions were detected with a surface barrier detector and the resulting spectra were analyzed using the RUMP program.

2.5.5 Nuclear Resonance Analysis

A similar procedure to RBS is Nuclear Resonance Analysis (NRA). In this case, the energy of the incoming particles is carefully calibrated to resonate strongly with a particular element. This technique is useful for elements with smaller atomic weights, such as carbon and oxygen, that may be masked from accurate detection by large amounts of a more abundant element such as silicon. In this study, the nuclear reaction of ^{12}C was utilized to detect small changes in carbon depth profiling. Strong (α,α) elastic scattering is exhibited in the energy region 5.5-5.8 MeV and at 4.28 MeV [64]. Thus, incoming He^+ particles were given an energy of 4.28 MeV and directed onto the carbon-containing films. Comparison with "blank" substrates allowed the increased carbon content of the film samples to be calculated using the stoichiometric carbon content of

PPV, C_8H_6. NRA measurements were performed at the SUNY Dynamitron facility and the data was analyzed using RUMP software.

2.5.6 Scanning Electron Microscopy

Scanning Electron Microscopy (SEM) creates images of film surfaces by focusing high-energy electrons onto a sample surface and detecting the returning signals. One such signal, secondary electrons (SE), originates from near the surface of the sample and the variation of intensity of these particles results in high-relief images of the sample surface.

SEM images were taken with a Carl Zeiss Supra using an SE Inlens detector. Electron energies were capable of ranging from 100 V to 30 kV with up to 1.5 nm resolution at 15 kV. Image parameters were varied for each sample as necessary.

2.5.7 Fourier Transform Infrared Spectroscopy

Molecular bonds vibrate at quantized energies, the levels of which depend on composition and environment. Polar bonds can absorb infrared light in the range 4000 – 400 cm^{-1} to transition to higher vibration energy levels. Measuring the absorption pattern in this range of light and comparing to known patterns associated with the various bond types gives information about the composition of the sample. A Fourier transform is a mathematical operation performed on the spectrum to clarify the peaks.

Fourier Transform Infrared Spectroscopy (FTIR) was done on a Bruker IFS66v/s (Billerica, Massachusetts) in the mid-IR range (4000 – 400 cm^{-1}). Spectra were recorded in a nitrogen environment in order to reduce interference effects of oxygen and moisture from the atmosphere.

2.5.8 Transmission Electron Spectroscopy

As light has a wave-particle duality in its structure, so do electrons. Transmission electron spectroscopy (TEM) takes advantage of this phenomenon to diffract beams of electrons through crystal structures to form diffraction patterns depending on the sample. Samples are prepared by cutting slices and adhering them top-to-top with epoxy, then milling the sample down to a thickness of about 500 Å. This process allows direct observation of the cross section of the samples. TEM for this work was performed on a JEOL JEM-2010 at 200kV. The energy filtered imaging technique was adopted for compositional maps using post column filter attachment (Gatan, Inc.) in TEM.

3. Conversion of the Precursor Polymer to PPV

The insoluble nature of PPV creates challenges in producing clean, impurity-free, pinhole free films without contamination from solvents or precursors. The necessity of depositing precursor films to convert to the final polymer film brings complications as well. Solution-based precursor polymers have a wide range of leaving groups, resulting in a wide variety of attempts to convert the precursor film into PPV and find the most successful conditions. The most common leaving groups are sulphur based and can require acid-based counterions necessary for deposition, all of which can inadvertently dope the film or damage the substrate or other components in a device during the conversion process (see Section 1.3.2 for more information). Efforts to minimize damaging effects from precursor components during conversion have varied the annealing temperature, atmosphere, and time with mixed results. Temperatures have ranged from 150-350 °C; atmosphere has varied from high vacuum to gas mixtures such as hydrogen chloride and argon; and conversion times have ranged from minutes to days [49, 65-68]. Each process depends on the solvents and exact precursors used in the solution. Adding to the complexity, some groups have focused instead on producing partially converted films in order to increase luminescence intensity or change the peak color emitted [69, 70].

As an alternative to liquid precursors, chemical vapor deposition eliminates the need for a solvent, although it still requires the use of a precursor polymer. The halogen leaving group that is typically a part of this precursor is itself capable of damaging the substrate or incorporating into integrated circuits or other delicate systems. Trace amounts of the halogen are often left behind in the film [36]. The annealing process can sometimes even destroy substrate layers such as ITO [45, 71, 72], making devices such as OLEDs less efficient and requiring the use of protective coatings between the polymer and the substrate.

Although there has been much work done to determine the best annealing conditions for conversion of precursor polymers from solution, much less study has been done for precursor polymers deposited by CVD.

3.1 Characterization Process

For this work, the precursor consists of α,α′-dibromo-p-xylene, so the halogen leaving group in this case is bromine. In an ideal system, one of the bromines on the precursor molecule breaks off during pyrolysis and leaves the resulting monomer ion reactive in a resonant brominated quinone form. The film then deposits on the substrate surface and polymerizes into a brominated xylylene polymer. Upon annealing, the polymer undergoes dehydrobromination (Figure 3.1) on each of the polymer units, leaving behind the characteristic double bond of the PPV polymer unit (see also Figure 1.13).

Bromine is a heavier element that is easily distinguishable from the typical constituents of carbon, hydrogen, and oxygen in most polymer films. In order to measure the effectiveness of our methods for removing bromine from PPV, two main characterization techniques were employed. First, during conversion, mass spectroscopy was used to monitor the intensity of bromine ions leaving the film. The characteristic mass-charge fragments of HBr are 79, 80, 81, and 82 a.m.u., which are assigned to the mass fragments $[^{79}Br]^+$, $[^{1}H\text{-}^{79}Br]^+$, $[^{81}Br]^+$, and $[^{1}H\text{-}^{81}Br]^+$, respectively (in its natural state, bromine has an almost equal distribution between the 79 and 81 a.m.u. isotopes). These ion mass fragments were monitored in real time during in-situ heating of the films under controlled temperature and atmosphere conditions. Overall fragment intensities depended on the thickness of the film and the relative abundances of the characteristic abundances. An example of the typical spectrum of the bromine mass fragments during annealing from the precursor polymer is shown in Figure 3.2. It should also be noted that in this figure the intensity of the bromine ion mass fragments peaks at around 8 minutes, has nearly returned to its original intensity at 20 minutes, and completely drops off before 30 minutes.

Second, Rutherford Backscattering Spectroscopy (RBS) was used before and after annealing to measure the percent of bromine left in the film. Supplementary analysis techniques include photoluminescence (monitoring the evolution of the spectrum) and ellipsometry (measuring the change in thickness before and after heating).

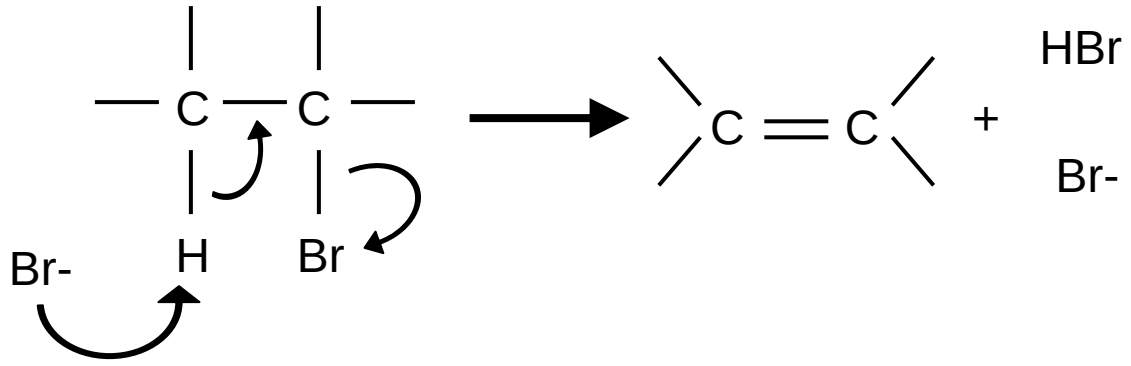

Figure 3.1: Dehydrobromination in an organic molecule. The carbon containing the halogen is known as the β carbon, so this is one type of a reaction also known as β elimination.

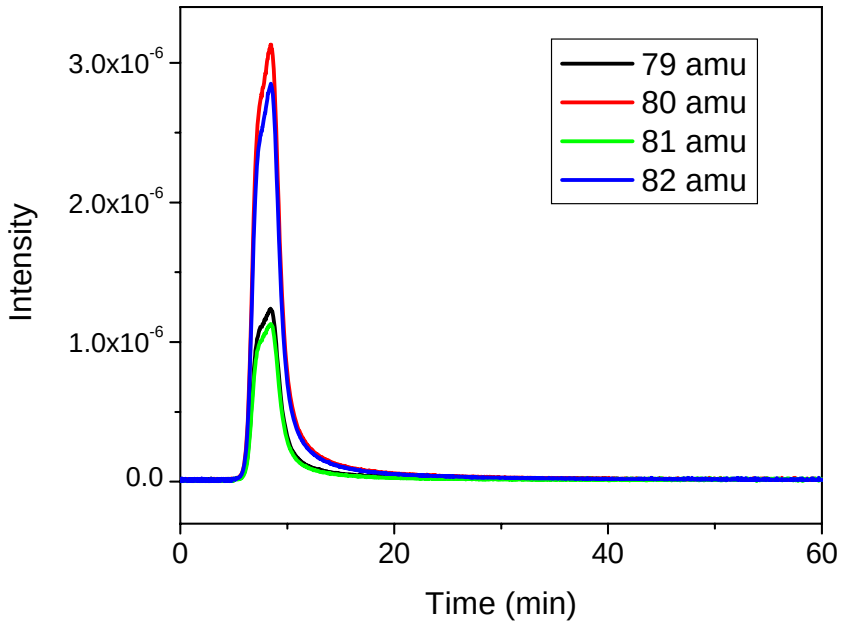

Figure 3.2: Bromine ion mass fragments during annealing at 250 °C.

3.2 Temperature of Conversion

In order to characterize the effect of long annealing times on bromine removal, we annealed films at different temperatures for several hours. The results as determined by modeling the bromine peak from Rutherford Backscattering Spectroscopy (Figure 3.3) are shown in Table 3.1. For these tests, the samples annealed at 300 °C had less bromine remaining than the samples annealed at 150 °C, 0.57 % and 0.99%, respectively. For both temperatures, the time of the anneal had no significant effect on the amount of bromine: samples annealed for 6 hours had the same amount of bromine remaining in them as samples annealed for 2 hours at the same temperature. The temperature of the anneal evidently has a larger effect on the amount of bromine left in the film than the time of the anneal. This is consistent with the results in Figure 3.2, where peaks from the bromine ion mass fragments have returned to the original intensity before 30 minutes. However, the amount of bromine in the sample can be further reduced by flowing gas into the furnace during annealing.

Although the bromine may be removed as completely as possible in less than two hours, the film itself is not necessarily completely converted to PPV in the same amount of time. Figure 3.4 shows the photoluminescence spectra of the samples annealed in vacuum at 150 °C and 300 °C for 2 and 6 hours. It can be seen that the 6 hour spectrum of the 150 °C sample is redshifted from the 2 hour spectrum, and both 300 °C spectra are redshifted from those. Redshifted peaks in photoluminescence spectra indicate longer conjugated chains because excitons that migrate to longer chain sections lose more energy before deexcitation and so they appear at higher wavelengths [30] (see Section 1.3 for more on the luminescence of PPV).

Additionally in Figure 3.4 the two 300 °C spectra are nearly identical, indicating that those samples have converted to PPV to approximately the same degree. However, they also have lower intensities than the 150 °C samples, which may be due in part to the slightly larger thicknesses in the 150 °C samples but is more likely due to a higher degree of defects in the films. It is well known that increased temperatures are more

Table 3.1: Atomic percentage of bromine in films after annealing. Before anneal: Br = 1.75 %

	150 °C	300 °C
2 hours with gas	0.57 %	0.36 %
2 hours in vacuum	0.99 %	0.57 %
6 hours in vacuum	0.99 %	0.57 %

damaging to the films during conversion; Papadimitrakopolous *et al*. point out that higher temperature conversion can lead to a higher quencher concentration, lowering the overall quantum efficiency even though there is a longer conjugation length [22]. In these films, the bromine has been removed to a greater extent than in the 150 °C films, but they are more likely to contain oxygen from the annealing process.

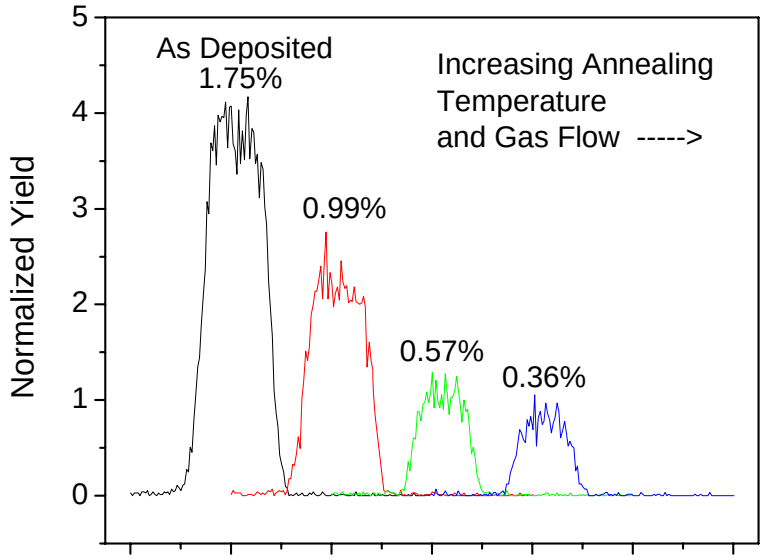

Figure 3.3: RBS peaks of bromine in decreasing amounts in PPV films. See Table 3.1 for corresponding annealing conditions.

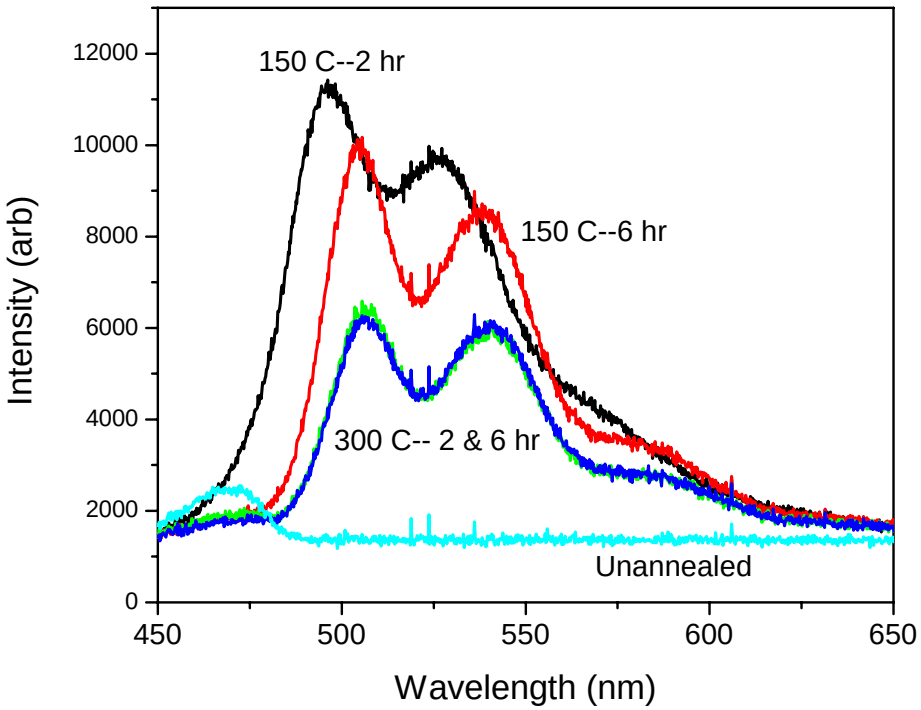

Figure 3.4: Photoluminescence spectra of PPV annealed at 150 °C for 2 hours (----) and 6 hours (----) and at 300 °C for 2 hours (----) and 6 hours (----). Also shown is the spectrum measured for the unannealed (nonluminescent) sample (----) with a reflection peak for the excitation source at about 470 nm. Sample thicknesses were 220 nm, 190 nm, 180 nm, 180 nm, and 210 nm, respectively.

3.3 Short Time Anneal

From the results in the previous section, it is clear that most of the bromine is released from the polymer film during the first 30 minutes of the anneal. The progress of the conversion can be monitored with mass spectroscopy of the characteristic bromine ion mass fragments during short anneal times. Figure 3.5 shows the intensity of the bromine ion mass fragment at 80 a.m.u. during anneal at 250 °C for 5, 10, 15, and 30 minutes and during subsequent cooling. The sample took 11 minutes, 45 seconds to reach the annealing temperature (first dashed line). Dashed lines mark the time in 5

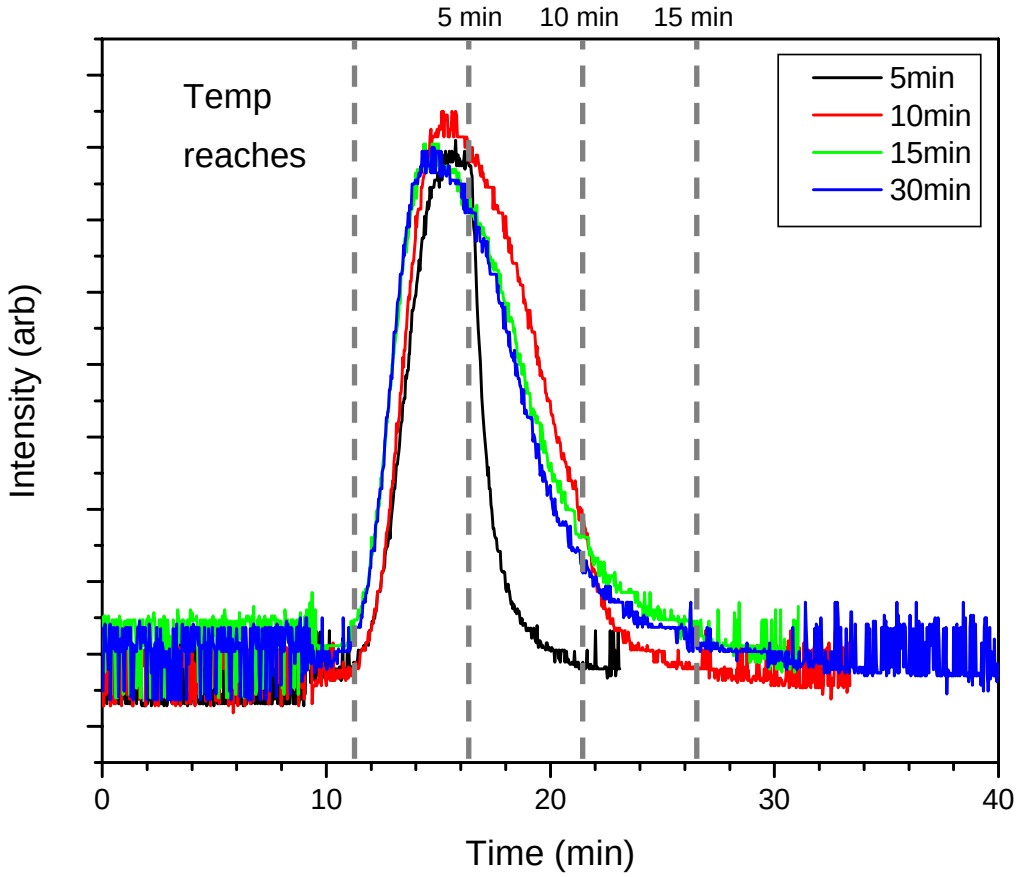

Figure 3.5: Intensity of ion-mass fragment 80 a.m.u. during short time anneal. Sample took 11.75 min to reach 250 °C; heating times are counted after this point was reached as marked, including 5 min (black line), 10 min (red), 15 min (green), and 30 min (blue).

minute increments after the temperature is reached. Each line peaks at about 15 minutes, or about three minutes after the annealing temperature is reached. The spectrum corresponding to the 5 minute anneal clearly discontinues the concave shape of the peak to turn convex as the temperature drops (although the temperature does not immediately return to room temperature, there is a significant drop (~75 °C) immediately and the temperature continues to cool at a rapid pace afterwards). The other lines maintain their shape because the majority of the fragments have already passed through.

Comparison of the photoluminescence spectra after the short time anneal (Figure 3.6) shows that even though the intensity of the bromine ion mass fragment is mostly back to the original intensity after 10 minutes at the annealing temperature, the conversion is still not complete, similar to the results from the previous section. Again, the spectrum intensity decreases slightly and the peaks redshift with increasing annealing time. Additionally, the thickness of the film decreases as the annealing time increases (Figure 3.7). Shorter times have a larger change in properties that converge to a final state.

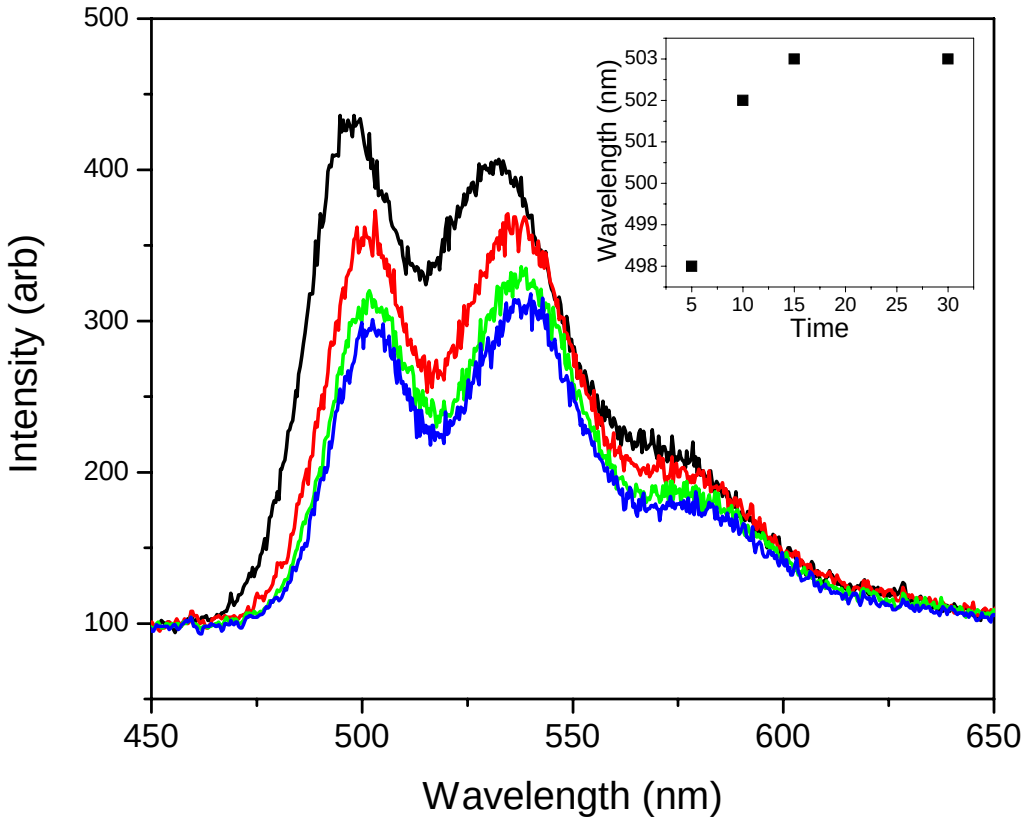

Figure 3.6: Photoluminescence spectra of PPV annealed for 5 (black), 10 (red), 15 (green), and 30 (blue) minutes. Insert: Wavelength of the maximum of the 0-0 peak for each of the annealing times.

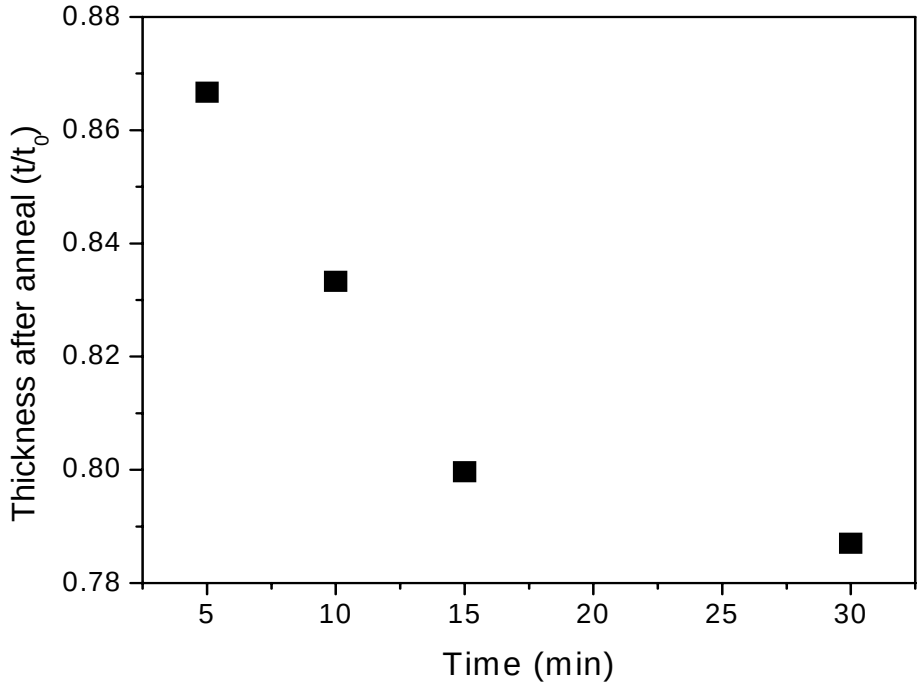

Figure 3.7: Thickness change after annealing at 250 °C at short times in vacuum.

3.4 Conclusions

The properties of the conversion of the brominated precursor polymer to poly(*p*-phenylene vinylene) have been discussed in terms of removal of the bromine from the film. Mass spectroscopy of the characteristic HBr ion fragment masses shows that most of the bromine is removed during the first thirty minutes of the anneal. Long time anneal at two different temperatures, 150 °C and 300 °C in vacuum, shows that the temperature of the anneal had a larger effect on the amount of bromine removed from the film than the time of the anneal did, as calculated from the bromine peak in Rutherford Backscattering Spectroscopy. Since a greater amount of bromine could not be removed by annealing at longer times, nitrogen gas was flowed into the chamber during the anneal and successfully reduced the amount of bromine further than in vacuum.

Additionally, although the 300 °C anneal removed more bromine than the 150 °C anneal did, photoluminescence spectroscopy revealed that the 300 °C films were more completely converted but less intense than the 150 °C films. Since longer annealing times and higher temperatures both reduce the quality of the film, a median time and temperature was chosen as the standard for annealing subsequent PPV films: 2 hours at 250 °C.

The 250 °C anneal was studied further at short times. 5, 10, 15, and 30 minute anneals were monitored with mass spectroscopy for the bromine ion mass fragment peaks. The bromine lines peaked about 3 minutes after the furnace reached the annealing temperature of 250 °C, or 15 minutes total during heating. All of the films were not completely converted, as the photoluminescence spectra and thickness changes show, but as the time increased the properties reached toward a stable state for the film.

4. Onset of Thermal Degradation

It is known that at high temperatures (>800 °C) PPV can be converted to graphite, and both doped and undoped films have been studied extensively before and after this conversion [73-76]. Several theories have been put forth as to how the graphitization of PPV begins, including: crosslinking and forming polyaromatic structures [73]; reduction of hydrogen during graphitization [75]; and aromatization and removal of hydrogen which causes the structures to become more compact [76]. The transition of the conjugated PPV structures to the planar graphite structures is an area of interest for high temperature applications. This chapter examines this transition; the work included here has been published by the author [12].

4.1 High Temperature Studies of PPV

The most common application of PPV has been in organic LED's, where much work has been done on both the polymer and several of its derivatives [1]. Further inclusion of PPV into more complex electronic circuits may require exposure to high temperatures during manufacturing and processing. PPV itself has a higher degradation temperature (~500 °C) than other related polymers such as poly(p-xylene) (Parylene) at 420 °C [13] and the conjugated polymers polyacetylene and polyphenylene at 200 °C [14] and 450 °C [15], respectively. It is known that at high temperatures (>800 °C) PPV can be converted to graphite [73] (Figure 4.1). The carbonization of this conjugated polymer by pyrolysis of both doped and undoped films has been studied extensively. In one case, Ohnishi *et al.* found that PPV obtained from solution-based precursor is converted to pure graphite above 2750 °C, but TGA analysis showed degradation beginning around 500 °C [73]. Since the film pyrolysed without melting, they suggested that the film crosslinks and forms polyaromatic structures before complete graphitization. A separate TGA analysis of the solution-based precursor polymer during conversion to PPV done by Mates *et al.* showed a multistep weight loss, including a stage starting at approximately 500 °C [74]. The most significant drops, however, occurred below 250 °C and correspond to

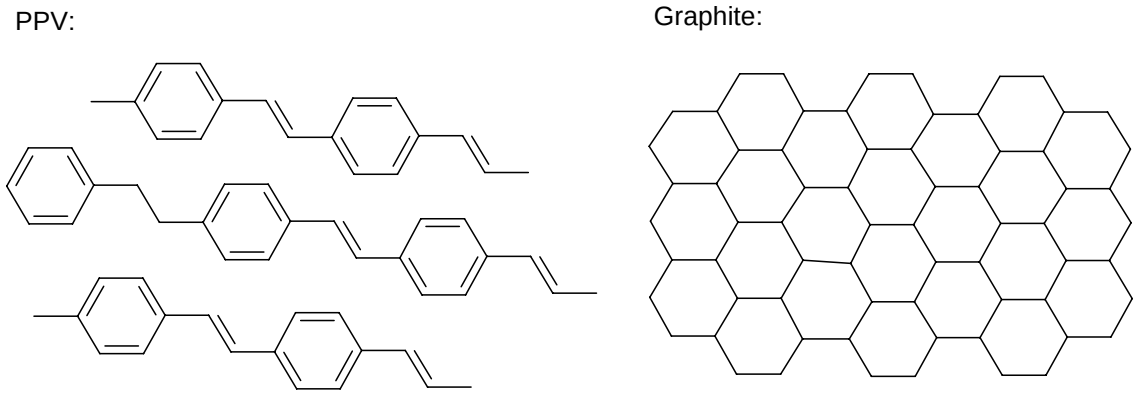

Figure 4.1: Comparison of PPV chains and a graphene sheet in the graphite form of carbon. No hydrogens are present in the graphite.

elimination of the chlorine-containing leaving group, HCl. In PPV formed from solution, neither the HCl nor the sulphonium side groups from the precursor molecule are completely removed by annealing, so removal continues throughout heat treatment. In contrast, PPV films deposited by chemical vapor deposition (CVD) have only a halogen as the side group, so only residual HX will be present from deposition and annealing.

The dependence of graphite conductivity on PPV conversion temperature was studied by Ueno and Yoshida [75]. They found a large jump in conductivity from pristine PPV films when the films were heat treated at a temperature of 600 °C for one hour. This effect was attributed to increased carrier density caused by the reduction of hydrogen during graphitization. Again, PPV films were obtained from solution-based precursor polymers and little else was done to characterize the transition from PPV to graphite.

More recently, carbon nanotubes and carbon nanorods were created by graphitizing amorphous nanostructured PPV deposited using CVD [76]. Because of the conformal coating allowed by CVD, polymer films were deposited inside porous material, annealed, and the porous material removed to leave behind PPV nanorods and nanotubes, depending on the size and configuration of the pores. After heat treatment of the PPV nanostructures, a noticeable decrease in rod thickness and tube wall thickness

occurred. This was attributed to aromatization and removal of hydrogen, causing the structures to become more compact, where rod diameter decreased by ~30% and tube wall thickness decreased by ~50%. Conversion to carbon was done at 850 °C for one hour; a more complete conversion (and further contraction) was expected at higher temperatures.

Although the chemical structure and changes of PPV have been studied, little work has been done to document the beginning of the transition between PPV and graphite. Knowing the properties of the film at this transition point is important if PPV is exposed to temperatures at or near its degradation point. This study aims to examine the transition between pristine PPV and graphitized PPV in order to give a more accurate picture of thermal degradation mechanisms.

4.2 Characterization of Degradation

Figure 4.2 shows a mass spectrum of PPV taken during dynamic heating at a rate of 20 °C/min when the film reached 600 °C. Various ion fragment masses between 1 and 150 a.m.u. are visible. The lower mass peaks (2-45 a.m.u.) are generally from small molecules such as those found in the atmosphere, including water at 18 a.m.u., nitrogen at 28 a.m.u., oxygen at 32 a.m.u., and carbon dioxide at 44 a.m.u. The higher mass peaks above 50 a.m.u. are mostly due to organic groups consisting of carbon and hydrogen atoms. These ion fragments cluster around masses separated roughly by the mass of another carbon atom, starting at 65 a.m.u. and continuing through 78, 91, and 105 a.m.u. Of these, the ion fragments at 91 and 105 a.m.u. are of special interest because they correspond to large toluene ($C_7H_7^+$) and xylene fragments ($C_8H_9^+$), respectively. Since they do not appear at room temperature, they are considered to be a thermal decomposition product of the film, similar to the related polymers Parylene and polyphenylene [15, 77].

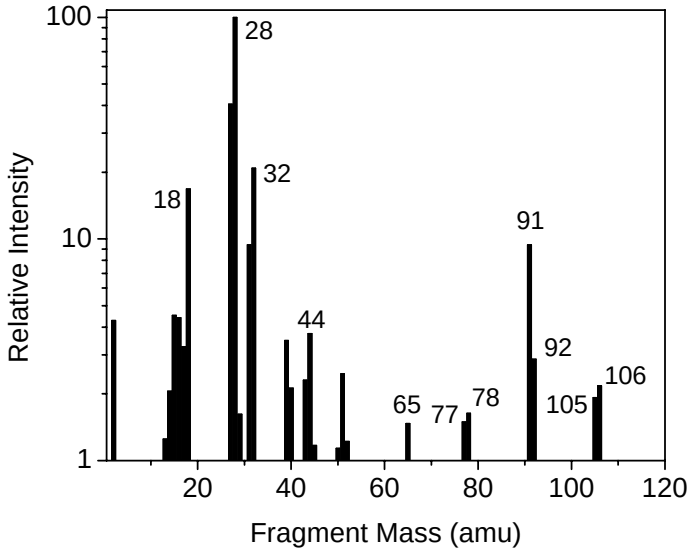

Figure 4.2: Mass spectrum of PPV taken at 600 °C. The film in this case was in the process of being heated at a constant ramp rate of 20°C/minute.

4.3 Dynamic Temperature Ramp

None of the major masses shown in Figure 4.2 have a significant increase in intensity during dynamic heat treatment below the temperature 500 °C, especially the higher mass peaks. Because of the interest in the ion fragments at 91 and 105 a.m.u., the time/temperature dependent intensity of these masses are shown in Figure 4.3 from a PPV film heat treated with a constant temperature increase of 20 °C/min. The peaks emerge at about 500 °C and peak near 600 °C before decreasing. This is an indication of film degradation as these large mass fragments leave the polymer films. With only a few exceptions, the ion fragment masses visible in Figure 4.2 display similar behavior during dynamic ramping. The exceptions include water (18 a.m.u.) and carbon dioxide (44 a.m.u.), whose intensities increase without peaking during the entire period of temperature increase, and which may have been incorporated into the film during exposure to atmosphere and released as the film begins to degrade and become more reactive.

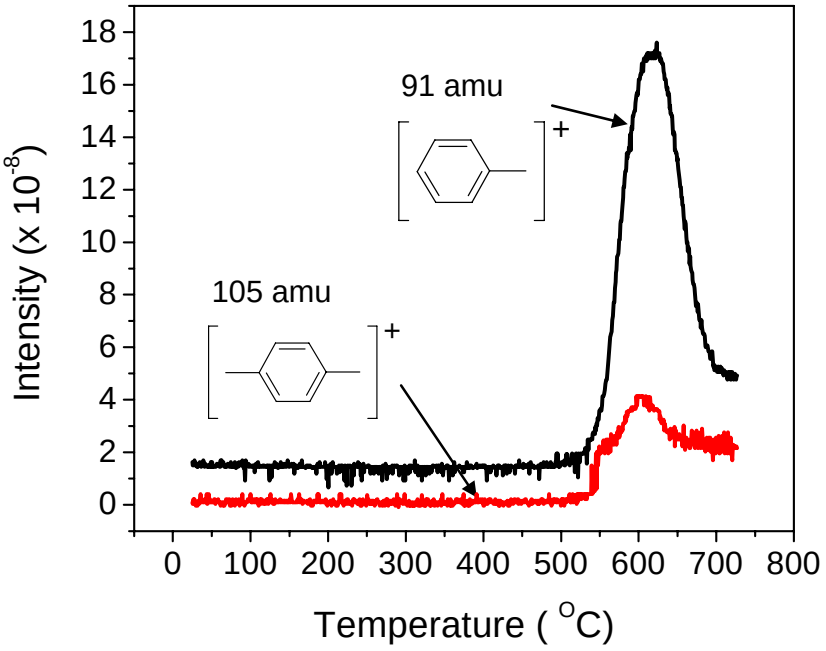

Figure 4.3: Continuous mass spectra of two ion fragment masses, 91 a.m.u. and 105 a.m.u., taken during temperature ramping at a constant ramp rate of 20°C/minute. No significant intensity increases are observed at 450 °C or below, but at around 500 °C clear 91 and 105 a.m.u. signals are visible, suggesting the removal of toluene and xylene fragments, as shown in the insets.

Notably missing from the mass spectra in Figure 4.2 are the ion fragments at 79, 80, 81, and 82 a.m.u., which are the characteristic peaks of HBr. Since bromine is incorporated into the film as part of the precursor polymer, this lack indicates that, although all the bromine may not have been removed during annealing [36], further heat treatment of the film does not cause a significant amount to be removed compared to the amount of fragments leaving due to degradation.

4.4 Isothermal Heat Treatment

In order to investigate the effects of temperature on the bulk characteristics, converted PPV films were heat treated by first ramping the temperature at 20 °C/min for 21.25 or 23.75 minutes to 450 °C or 500 °C, respectively, and then held at that temperature for periods of either 30 or 60 minutes. During this time, the characteristic degradation masses 91 and 105 a.m.u. were monitored as well as one of the characteristic ion fragment masses of HBr at 79 a.m.u. Figure 4.4a shows the mass spectrum of a PPV film during heat treatment at 450 °C for 60 minutes. Although the intensity of the HBr

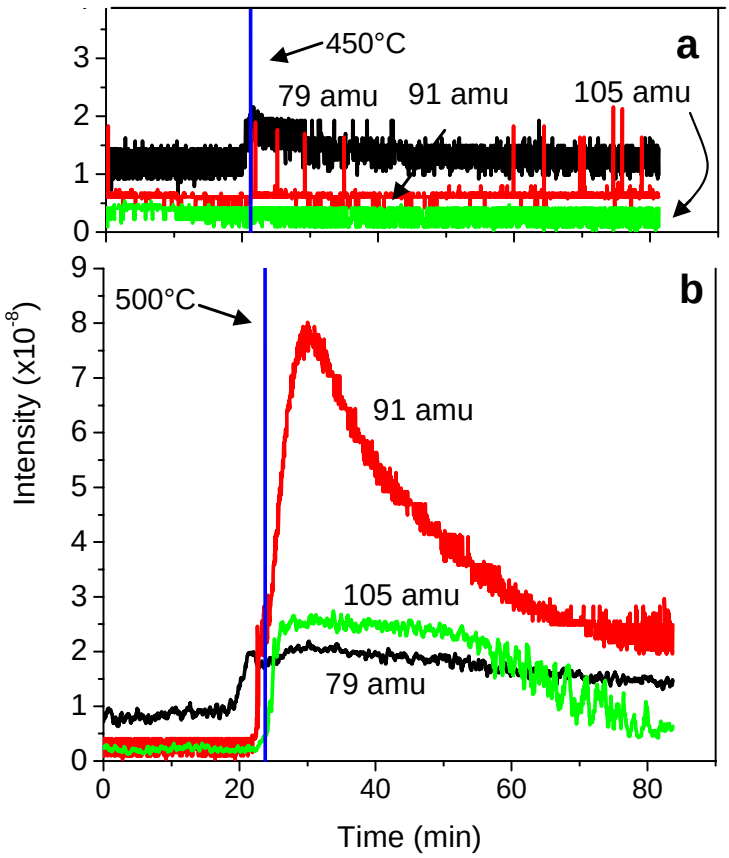

Figure 4.4: Continuous mass spectra of the ion fragment masses 79, 91, and 105 a.m.u. taken while the temperature was ramped at 20°C/minute up to a) 450°C and b) 500°C, then held at that constant temperature for 60 minutes. The vertical lines in a) and b) are at 21.25 minutes and 23.75 minutes, respectively, indicating the times at which the temperatures reached their steady state.

mass peak increases slightly as the temperature reaches 450 °C, there are no significant peaks visible for the higher masses. Comparison to Figure 4.4b, which shows the intensities of the same ion fragment masses during heat treatment at 500 °C, shows a dramatic increase in the intensity of the 91 a.m.u. mass peak but very little change in the behavior of the bromine peak from heat treatment at 450°C. This further confirms that at higher temperatures the degradation of the film plays a larger role in affecting the film than continuation of conversion by bromine removal, which occurs when the film has not been entirely transformed into PPV during the annealing process.

4.4.1 Thickness Effects

Figure 4.5 shows the effect that heat treatment has on the thickness of the samples. The samples annealed at 450 °C for 30 and 60 minutes both show little change from their original thicknesses. However, the samples annealed at 500 °C for 30 and 60 minutes show a decrease to 80% and 70% of their original thicknesses, respectively. These results corroborate the mass spectra in Figure 4.4, where only a small increase in mass fragment intensity was seen when the film was heat treated to 450 °C, but at 500 °C significantly larger peaks of high-mass ion fragments appeared. Additionally, since the temperature at which the intensity of high mass ion fragment peaks appear can change depending on ramp rate [77], these results confirm the stability of the film up to 450 °C. This is also consistent with the weight loss at 500 °C measured by Ohnishi *et al.* using thermal gravimetric analysis [73]. Thus elimination of previously mentioned ion fragments such as the ones at 91 and 105 a.m.u. is responsible for the thickness change, not densification alone.

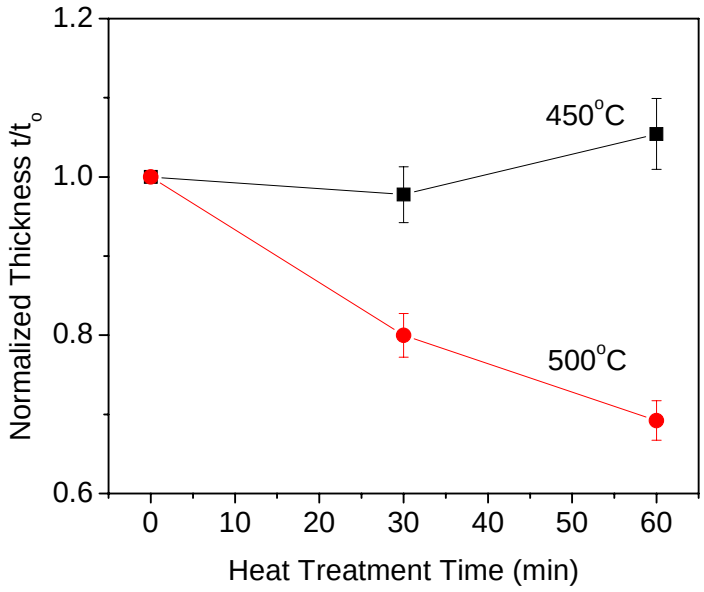

Figure 4.5: Percent change in thickness (t/t_0) after PPV films were heat treated for 30 and 60 minutes at either 450°C (■) or 500°C (●). A different sample was used for each thickness change measurement.

4.4.2 Chemical Bonds

Finally, the films were examined to determine the extent, if any, of changes to the chemical backbone of the polymer after heat treatment at these temperatures. Figure 4.6 shows the FTIR spectra of both PPV and PPV treated at 500 °C for 60 minutes. All the strong peaks of the characteristic PPV spectrum [78] appear in both spectra. This includes several peaks of ring bending and stretching, but also a vinylene C-H bend at 960 cm^{-1} and stretch at 3020 cm^{-1} and a pair of aliphatic C-H stretches at 2845 and 2915 cm^{-1}. The peak intensities are relatively unchanged before and after heat treatment, indicating that there is no major change in the structure of the polymer chains. In particular, the vinylene C-H bend and stretch do not decrease in intensity and the aliphatic C-H stretches do not increase after heat treatment, indicating that neither the double bonds are broken nor additional double bonds formed during heat treatment. Thus, for these CVD

PPV films, neither the cross linking of polymer chains nor the aromatization suggested by Kim and Jin [76] begins when the film degradation commences at ~500 °C.

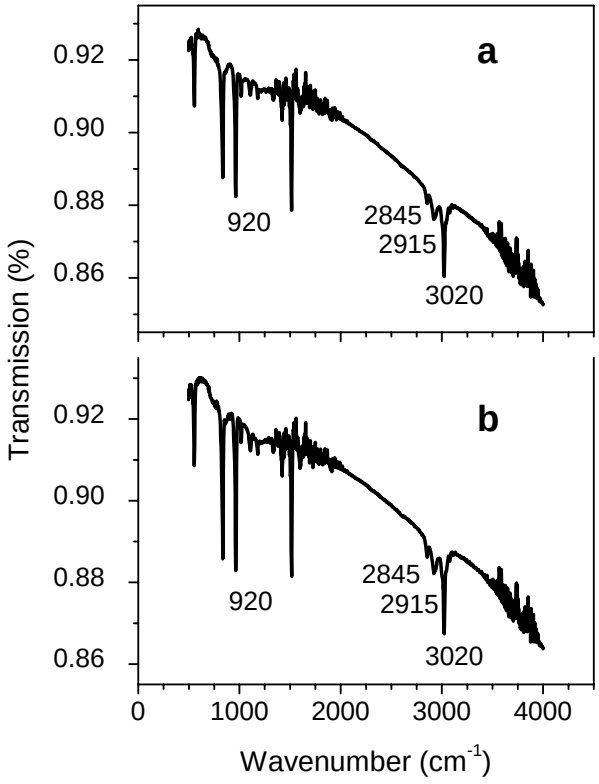

Figure 4.6: FTIR spectra in the mid-IR range of ~100 nm PPV on KBr substrates. Both samples were annealed at 350 °C, but sample a) PPV was additionally heat treated at 500°C for 60 minutes, while sample b) is PPV with no further heat treatment.

4.5 Conclusions

Poly(*p*-phenylene vinylene) can be converted to pure graphite at high temperatures. In order to understand the conversion process more fully, CVD PPV films were treated at temperatures of 450 °C and 500 °C while mass fragments from the film were analyzed

and changes in thickness were measured. Degradation in PPV thin films has been shown to take place at 500 °C through thickness changes and mass spectra that show high molecular weight fragments eliminated from the film. This agrees with previous TGA curves that show weight loss at that temperature [73]. Since there is no thickness change or increased intensities of mass fragments during annealing at 450 °C, this is the minimum temperature for the start of degradation. However, FTIR spectra show no significant change in bond intensity before and after heat treatment at 500 °C, so neither crosslinking nor bond breaking occur to a significant degree at this temperature. Degradation thus proceeds through densification and removal of unreacted or weakly bonded fragments. Additionally it was found that continued bromine elimination from unconverted segments of the polymer does not play a significant role in the weight loss behavior of heat treated PPV.

5. Photodegradation

PPV degrades when exposed to light in the blue-to-ultraviolet range while in the presence of oxygen due to the formation of groups such as carbonyls that break the conjugation of the polymer backbone [22, 79, 80]. One reason for oxygen's powerful quenching effect on luminescence is due to its strong electron affinity that is capable of dissociating excitons, the primary source of luminescence [37]. Additionally, oxygen has a triplet ground state of lower energy than the first excited state (S_1) of PPV. Because of this, the likelihood of nonradiative intersystem crossing between S_1 and various triplet states increases, the higher energy triplet states undergo nonradiative internal conversion to the first excited triplet state (T_1), and, since nonradiative transitions are more likely than phosphorescence from T_1, the overall quantum efficiency of the polymer is reduced [32] (see Figure 1.6). These quenching effects demand the presence of an encapsulation layer to prevent oxygen and other impurities from incorporation into PPV layers, increasing device processing complexity and limiting commercialization potential [81]. Encapsulation materials must prevent transmission of oxygen and water vapor through the layer while still allowing transmission of UV and visible light through the barrier.

5.1 Aluminum

One potential encapsulation material is aluminum, which has been widely used in the development of organic devices. It has frequently been applied as the cathode/anode in OLEDs due to its small work function and stability [1]. Additionally, its oxide form has proven useful in a variety of ways as a layer in organic devices. For example, a thin aluminum oxide layer has been shown to improve the quantum efficiency of OLEDs by improving injection of minority charge carriers into PPV devices [82]. It has also been demonstrated to increase the thermal stability of crystalline organic films when applied in layers thinner than 50 nm, where the oxide acts as a buffer against the film's defects and inherent stresses [83]. Furthermore, films in the tens of nanometers of thickness have been shown to prevent the transmission of water and oxygen gas [84], leading to the use

of 180 nm of the oxide as an encapsulation material for organic devices in high temperature and humidity conditions [85]. Other groups have found that aluminum oxide films as thin as 5 nm are effective barriers to water vapor and oxygen gas diffusion [86], as determined by oxygen and water vapor transmission rates.

Although very thin aluminum and aluminum oxide (AlOx) films have been used as electrodes in electroluminescent devices with PPV [9], the usage of a very thin film of AlOx as a protection layer for PPV degradation has not yet been studied.

Figure 5.1 shows the normalized intensity of the photoluminescence spectra of PPV captured at 5 minute intervals during exposure to blue and UV light. When excited by blue light, the uncoated PPV film shows an initial dramatic decrease in the intensity before leveling off to approximately 20 % of the initial value, which is similar to previously reported degradation [79]. The AlOx coated PPV film, however, has a different time-dependent intensity pattern that depends on the excitation wavelength. The sample exposed to blue light shows only a small decrease in intensity if any at all. The UV light, however, causes a decrease to about 70 % of the original intensity over the 6 hours of exposure and does not level off as the intensity of the uncoated sample does. The AlOx layer thus successfully prevents the PPV from degradation during blue light exposure, but only partially prevents degradation under exposure to the UV light. The reason for this is most likely due to the absorption spectrum of PPV, as shown in Figure 5.2 along with a photoluminescence spectrum for comparison. The highest wavelength for maximum absorption is approximately 400 nm, the wavelength of the UV LED. The absorption intensity quickly drops as the wavelength increases. Since blue light is not absorbed as intensely as UV light is, the blue light is less reactive in the PPV film.

One additional effect of the change in excitation light is the change in intensity of the photoluminescence spectra. Because the blue light is not absorbed as much as the UV light is, the intensity of the PL decreases as well, which is one of the causes of the intensity fluctuations of the blue-excited AlOx-coated time dependent line in Figure 5.1.

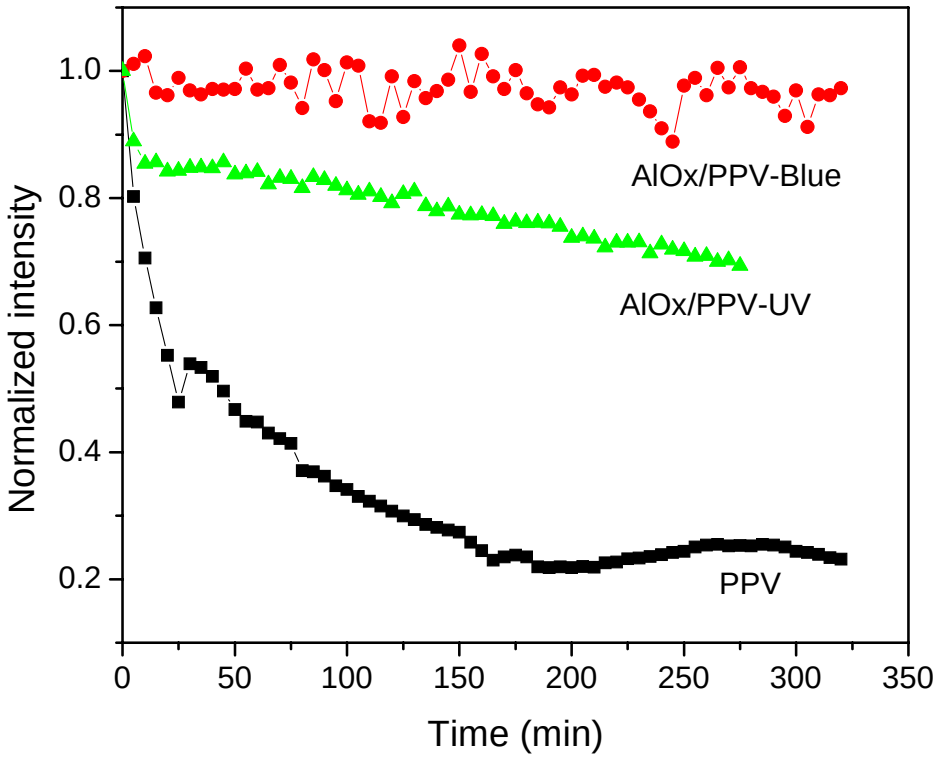

Figure 5.1: Photoluminescence decay over time of PPV exposed to blue light (■), AlOx/PPV exposed to blue light (●), and AlOx/PPV exposed to UV light (▲). The intensity of the first peak in the spectrum (0→0 transition) was measured at each point in time and normalized to the intensity of the initial (time = 0) spectrum.

Further, the overall PL intensity of the AlOx coated samples is much less than that from uncoated ones, approximately 1:7 when excited with blue light. This is due to the slight opacity of the aluminum film blocking some of the intensity from the light source. The transmission spectrum of our AlOx film is shown in the inset of Figure 5.2; as can be seen, the transmission is approximately 55.5 % for wavelengths between 400 and 600 nm. The light reaching the film is decreased by half before reaching the film then decreased half again as the luminescence is transmitted outward. Because the transparency of AlOx depends on the structure and morphology of the deposited films [87], using different deposition conditions could produce a more transparent oxide film.

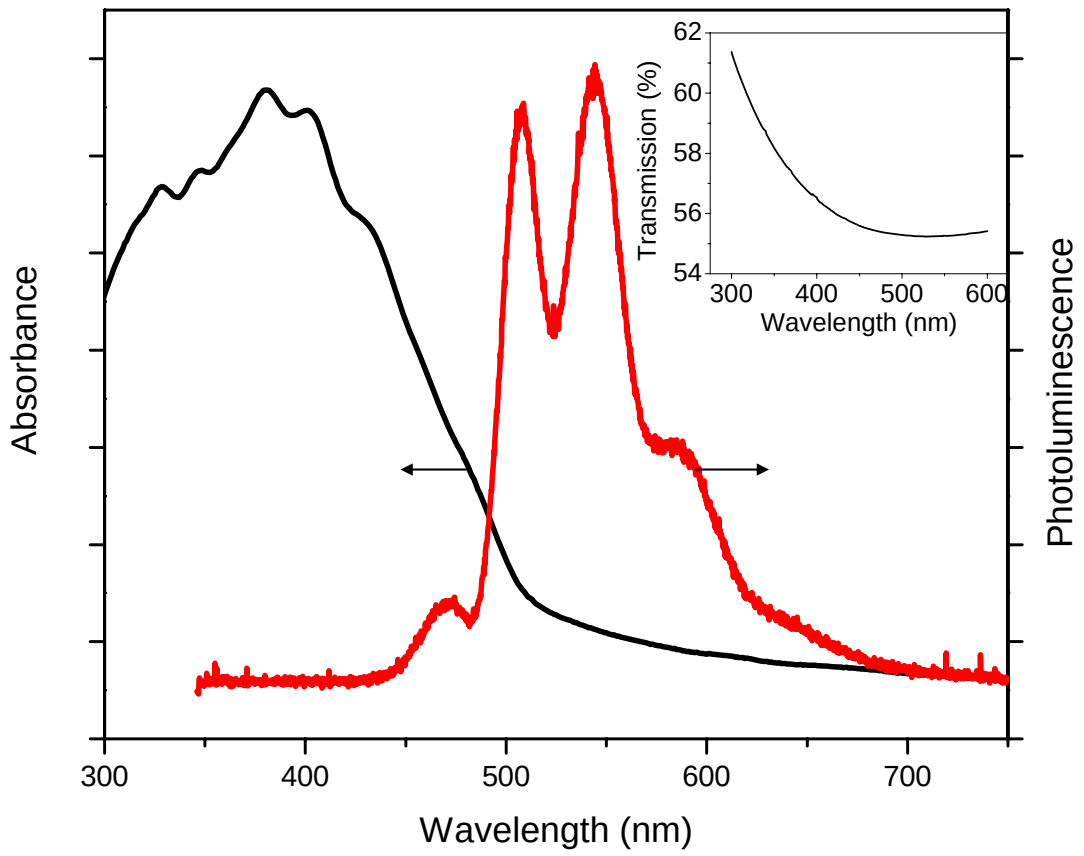

Figure 5.2: Absorbance and photoluminescence spectra of PPV films. The 0→0 transition in the luminescence spectrum is at about 510 nm. Inset: Percent transmission of light through aluminum oxide film on quartz. The transmission from 400-600 nm is approximately 55.5 %.

The transmission of this film is consistent with those typical for AlOx films not completely oxidized [88].

Furthermore, it is possible that the AlOx itself is responsible for quenching some of the overall luminescence intensity. In addition to the possibility of damage to the polymer film during aluminum deposition, it has been reported that luminescence quenching can occur in conjugated polymers due to metal and metal oxide layers, which is conjectured to be due at least in part to charge transfer between the layers, even in small doses and irregardless of the metallicity [89].

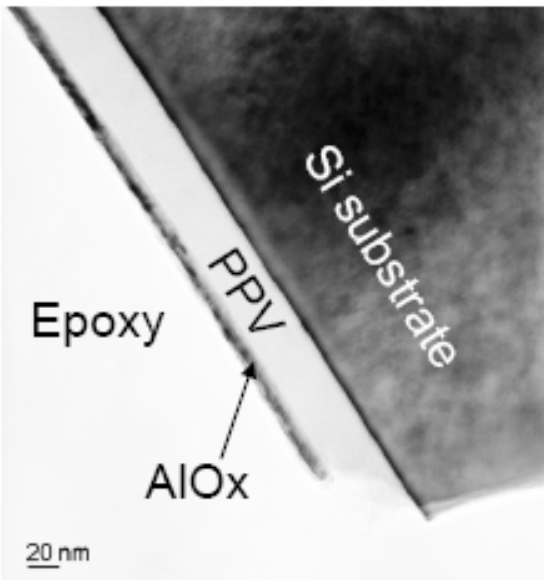

Figure 5.3: TEM images of AlOx/PPV/Si. Left to right (as marked): Epoxy (from sample preparation), AlOx, PPV, and silicon (with thin oxide).

Figure 5.3 shows TEM images of the aluminum oxide/polymer/silicon structure taken after exposure to the light source. The layers are epoxy (applied in TEM cross section sample preparation), AlOx, PPV, and silicon oxide/silicon, as indicated in the figure. The AlOx layer, which appears darker than the PPV and epoxy layers, is about 10 nm thick. The increased thickness after the original QCM reading is due to the expanded volume after oxidation and measurement uncertainty. Notably, this AlOx film is continuous; no visible cracks or pinholes are detected.

The compositional maps of the film structure are shown in Figure 5.4. The zero loss image (energy window 10eV) includes the PPV, AlOx, and epoxy layers, as indicated in the figure. The inhomogeneous contrast in the AlOx layer can be due to its roughness and difference in crystalline orientations. The Al, C, and O elemental maps are collected respectively using Al $L_{2,3}$, C K and O K edges, where increasing brightness indicates higher elemental concentrations. The significant differences of Al and C concentration in the AlOx and PPV layer suggest that the diffusion of Al into PPV is negligible. It is obvious that in the AlOx layer the O concentration is much higher than

in the PPV and epoxy, which confirms that the aluminum film is oxidized. The nearly homogenous brightness of Al and O along the AlOx layer further evidences the continuity of the film.

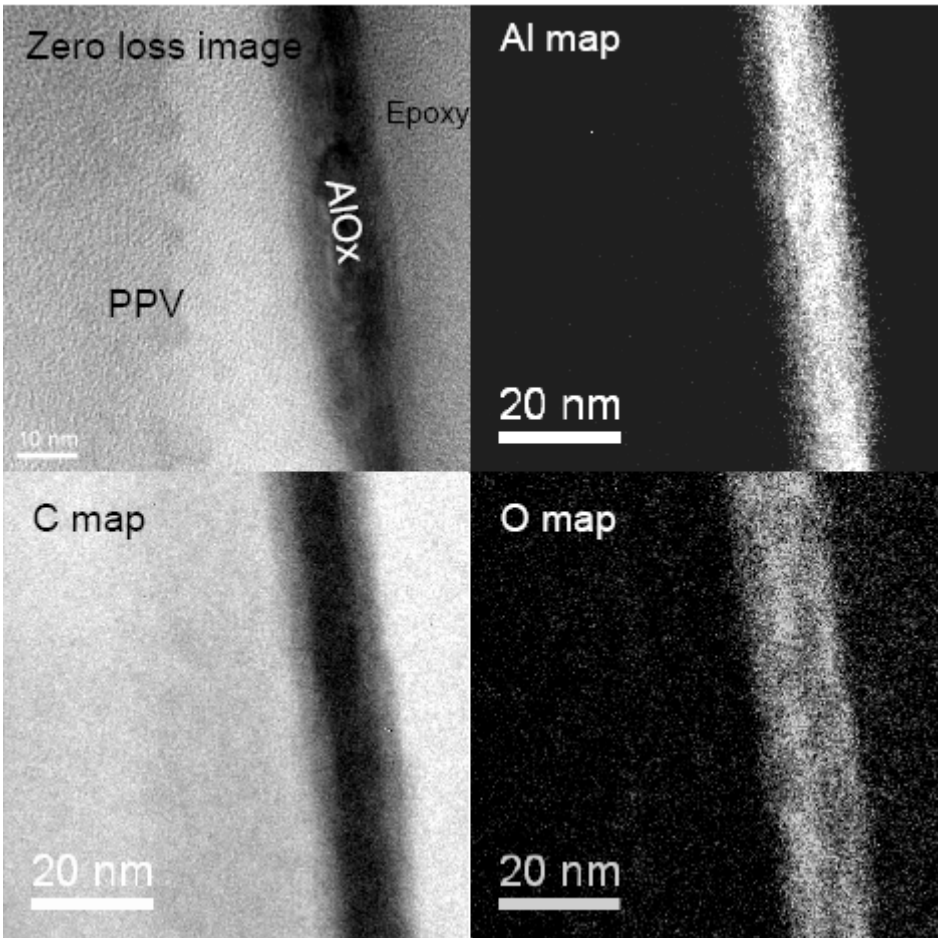

Figure 5.4: Composition mapping of Epoxy/AlOx/PPV, including zero field image, aluminum map, oxygen map, and carbon map, as marked.

5.2 Parylene

Parylene (poly(*p*-xylylene), PPX) has the same polymer backbone as PPV without the conjugation (see Figure 1.4 for structure comparison). As such, it has many useful properties that have led to its widespread study: it is nonreactive, it has a low dielectric

constant (k = 2.65) [54], it is thermally stable up to 400 °C [77], and it can be deposited using chemical vapor deposition for selective [58, 90], conformal, and pinhole-free films [54]. Additionally, Parylene is transparent in the visible range and in the UV above wavelengths of about 250 nm (Figure 5.5). Additionally, Parylene has been successfully used as a barrier layer in OLEDs, improving the performance of the device by increasing the adhesion of organic layers, providing more uniform coverage, promoting the transmission of holes through tunneling, and preventing degradation due to oxygen and water transmission [91]. Most importantly, PPX has excellent barrier properties for gases [54] as well as other molecules deposited with chemical vapor deposition [92, 93]. For these reasons, PPX seemed an interesting candidate to use as a sealant for PPV during photoluminescence. In these experiments, PPV precursor was deposited and converted to PPV through heat treatment before Parylene was deposited.

Figure 5.6 shows the time dependent photoluminescence of PPV (110 nm thick) and PPV capped with 5 nm and 160 nm of Parylene using an excitation wavelength of 450 nm. Although there is a slight decrease in degradation, the Parylene capping layer does not improve the photodegradation characteristics of PPV to a significant extent. After 200 minutes, bare PPV has an intensity of about 20 % of the original, PPV with 5 nm PPX has about 30 %, and PPV with 160 nm of PPX has about 40 %. Since the photodegradation of PPV is typically caused by the presence of oxygen during exposure to UV light, the degradation of the films when capped by Parylene can have two sources: oxygen diffuses through the Parylene layer to reach the PPV layer; or oxygen is already present in the Parylene layer and transfers to the PPV layer during exposure.

In order to prevent diffusion of oxygen through from atmosphere through the Parylene film, a 5.6 nm film of aluminum was deposited on the PPX/PPV structure and allowed to oxidize in atmosphere. From the results in Section 5.2 of this work, it has been shown that aluminum oxide is successful at reducing the photodegradation of PPV in blue light. An example of this time dependent luminescence is shown in Figure 5.7 along with that of 73 nm PPV capped with and without 65 nm Parylene and with and without about 10 nm of aluminum oxide. Although there is a decrease in the photo-

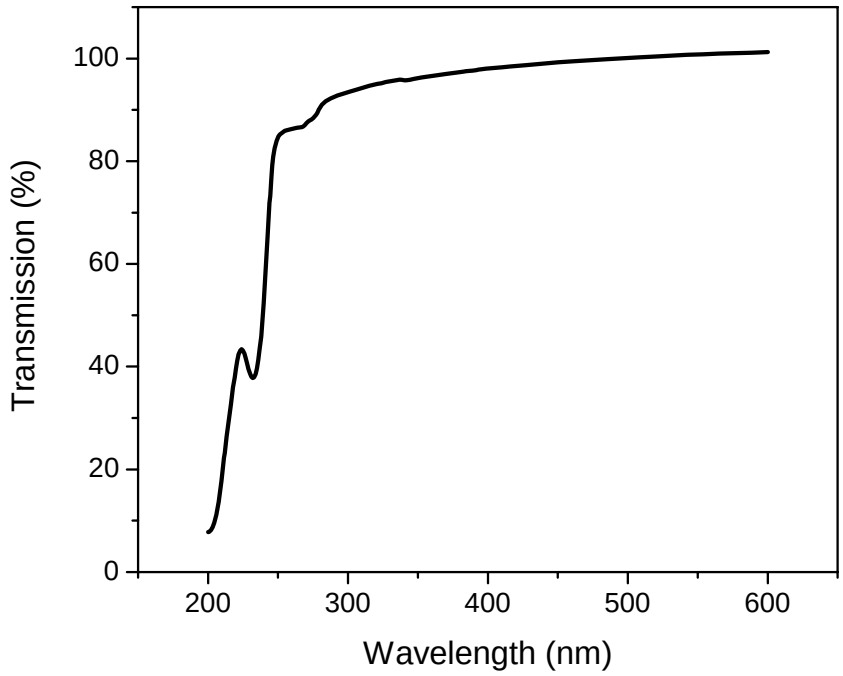

Figure 5.5: Transmission spectrum of Parylene in the UV and Visible ranges.

degradation in the AlOx/PPX/PPV structure compared with uncapped PPV, the intensity still decreases to 60 % of its original value compared to 20 % for bare PPV and 30 % for PPX/PPV. From these results, it can be estimated that oxygen present in the Parylene film accounts for approximately 40 % of the degradation while diffusion through the film accounts for the other 30 % of the luminescence decrease.

Other studies have confirmed the presence of surface oxygen in the Parylene films. It has been shown that ultrathin Parylene films react with oxygen when exposed to atmosphere due to the presence of unterminated chain endings on the surface of the film [94]. Further, the presence of oxygen in the Parylene films make layers such as copper vulnerable to reaction with the oxygen, eliminating the desirable qualities of the films [94]. However, heat treatment at 250 °C reduces the presence of oxygen to the extent that it no longer reacts with succeeding layers. To this end, two samples of 110 nm thick of PPV were capped with 25 nm of Parylene and one was tested as-is while the second was

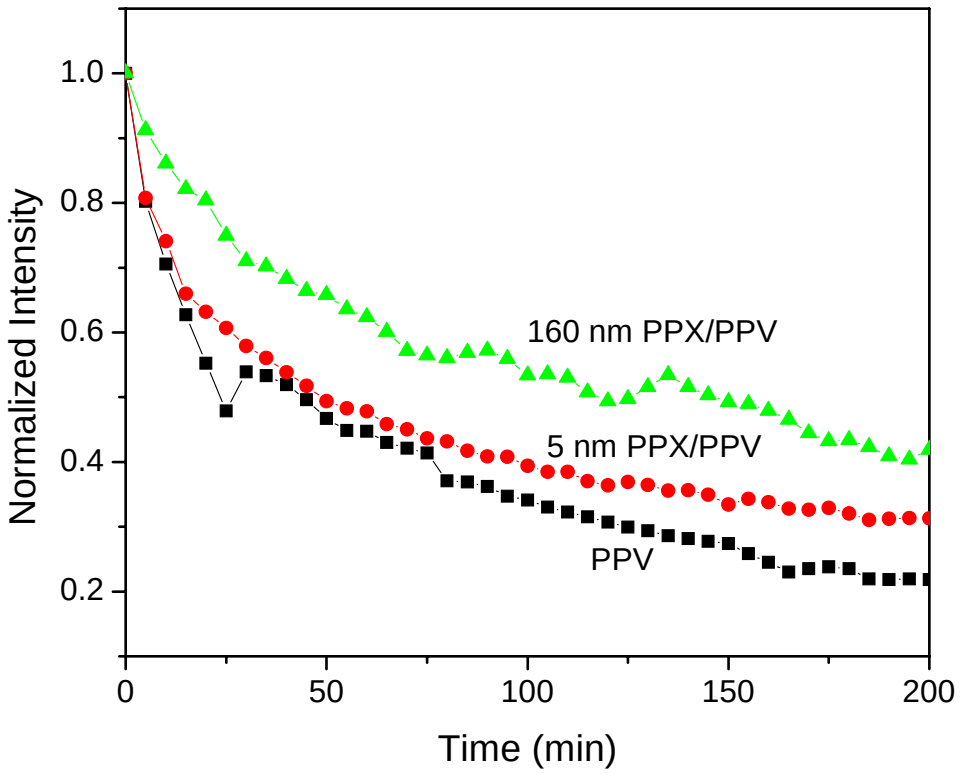

Figure 5.6: Time dependent photoluminescence of bare PPV (■) and PPV capped with 5 nm (●) and 160 nm (▲) of Parylene.

annealed again at 250 °C in vacuum after the Parylene deposition. Figure 5.8 shows that, contrary to expectations, the film that was annealed after Parylene deposition has a larger decrease in intensity than the film left as-is.

In order to clarify the results from photoluminescence degradation with an encapsulation layer of Parylene on top of PPV, FTIR spectra were taken of the samples before and after 5 hours of exposure to blue light. Figure 5.9 shows the spectra for Parylene, PPV, PPV after exposure, PPX on PPV, and PPX on PPV after exposure. The PPX and PPV spectra each show the characteristic peaks associated with their structure; the layered film shows peaks from both the samples. However, neither of the samples show significant changes in the intensity of the peaks after exposure, except for a small

increase in the strongest peaks that may be due to fluctuations in the thickness in the area of analysis. Because the capped and uncapped films behave in the same way there is no apparent benefit to using Parylene as an encapsulation layer for PPV.

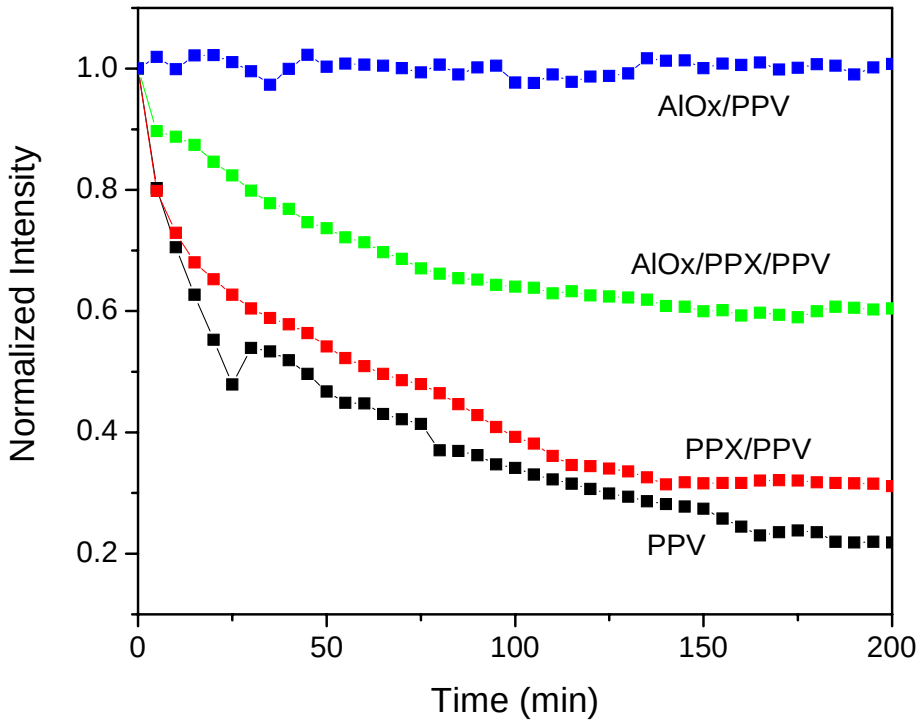

Figure 5.7 Time dependent photoluminescence of PPV capped with 25 nm Parylene and ~ 10 nm aluminum oxide. In order of decreasing final intensities: Blue: AlOx/PPV; Green: AlOx/PPX/PPV; Red: PPX/PPV; Black: PPV. The AlOx/PPV spectrum has been adjusted to account for variations in the intensity of the light source.

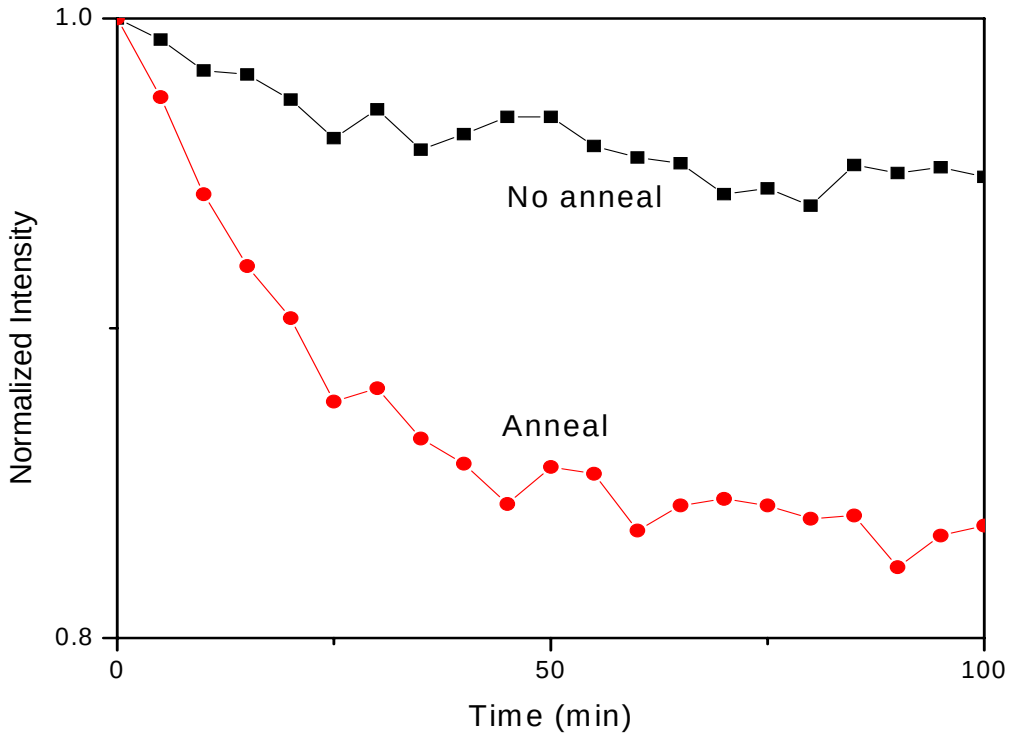

Figure 5.8: Time dependent photoluminescence of 110 nm PPV capped with 25 nm of Parylene, unannealed (■) and annealed at 250 °C (●) after Parylene deposition.

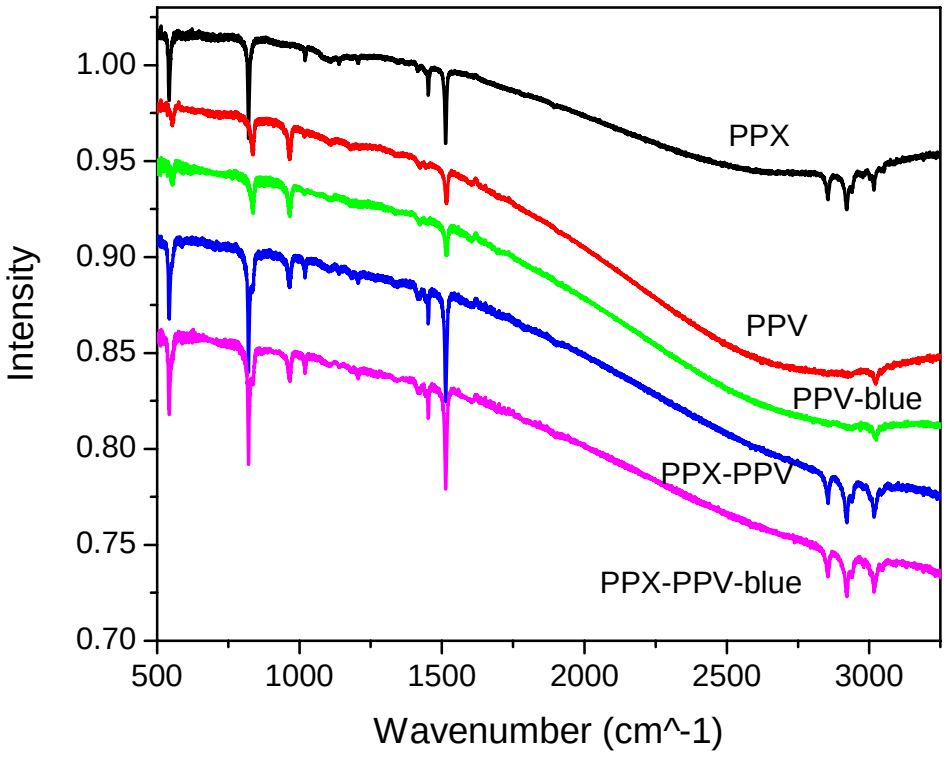

Figure 5.9: FTIR spectra of PPV and Parylene films. Spectra are shifted for clarity. From top to bottom: PPX; PPV; PPV exposed to blue light; PPX/PPV; and PPX/PPV exposed to blue light.

5.3 Conclusions

Encapsulation layers are required for devices that utilize PPV because PPV quickly degrades when exposed to oxygen in the presence of light. In this study we have used two different films as encapsulation layers and studied the photodegradation properties of the films. A ~5 nm thin film of aluminum deposited on poly(*p*-phenylene vinylene) oxidizes after exposure to atmosphere and is free of cracks and pinholes. The photoluminescence from the PPV film coated with aluminum oxide can be maintained without degradation for several hours under blue light. However, the intensity of the PL decreases to about 70 % of its original intensity after 6 hours of exposure to UV light. Since the photoluminescence of the PPV film without the coating degrades to 20 % of its

original intensity within three hours, the aluminum oxide coating still provides some protection from degradation. A thicker, more transparent aluminum oxide film is required to successfully encapsulate organic luminescent devices and prevent degradation due to oxygen contamination.

Parylene, a polymer related to PPV, was used as an alternate organic encapsulation layer. Although PPX displays excellent gas and CVD metal diffusion properties, PPX was not an effective encapsulation layer for PPV. Both thick and thin PPX layers decreased the total amount of degradation only slightly. Even after annealing the PPX/PPV structure to remove any surface oxygen the annealed sample showed a greater amount of degradation than the unannealed sample did. However, there was no significant difference in the intensity of peaks in the FTIR spectra of PPV and PPX/PPV before and after exposure to 5 hours of blue light.

6. Photoluminescence

It is well known that the properties of the photoluminescence spectra of conjugated polymers can change depending on parameters such as ambient atmosphere [79], annealing conditions [95], and substrate temperature [96]. By manipulating these conditions, researchers have been able to tune the polymer to desirable qualities such as variable luminescence colors [70] and low turn-on voltages for polymer light emitting diodes (LEDs) [97]. However, one important characteristic of a film can play a large influence on all the other properties: its morphology. Morphology of inorganic semiconductors can be influenced by factors such as substrate material and deposition methods. While these factors are important for organic materials as well, it is often the morphology of the substrate that can play an even larger role in influencing the film. When the films are very thin, substrate effects become increasingly important. Much work has been done on the influence of interfaces in devices using PPV or its derivatives and layered with other materials, such as in LEDs or for measurement of electrical properties [65, 98-103]. These interface effects often extend several nanometers into the film, so when the film itself is only a few nanometers, they influence all measurements.

6.1 Nanostructured Substrates

The study of finite size effects in quantum dots (QD) has proven to be a rich and interesting field in the past several years. By confining a semiconductor to a volume on the order of nanometers, several effects appear that give quantum dots properties of both bulk semiconductors and molecules. For example, prediction and experimentation shows that QDs possess discrete energy levels like molecules rather than the energy bands of semiconductors. Alternately, they have the large dielectric constants of semiconductors rather than the lower values of organic molecules. Recent work has combined quantum dots with polymers such as PPV and its derivatives for applications such as more efficient light emitters and photovoltaic cells [104-107]. Other efforts have begun exploring finite size effects in polymers themselves. Most efforts to document the

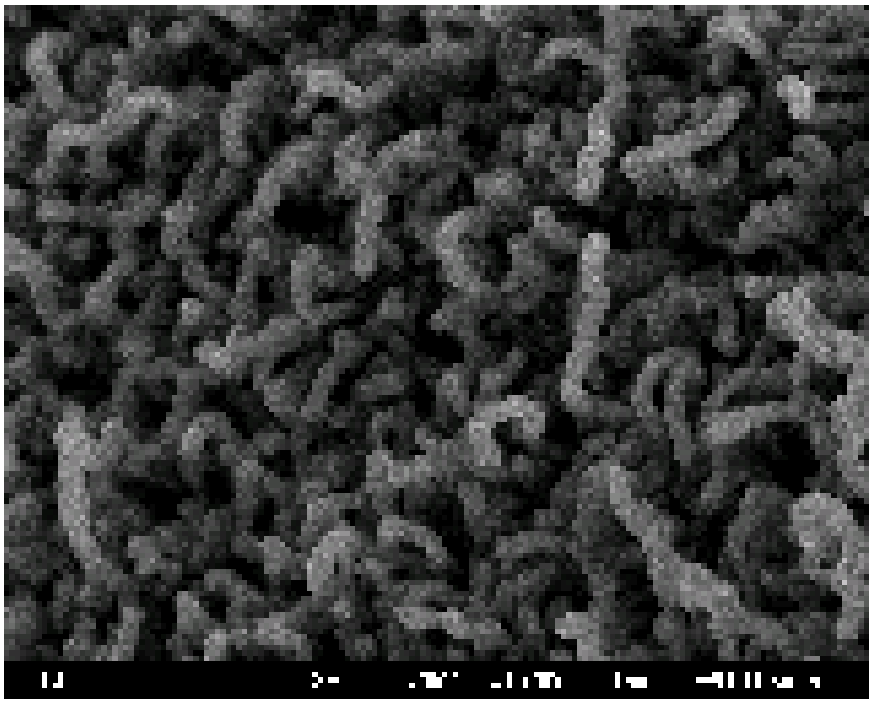

Figure 6.1: Carbon nanotubes coated with 240 nm PPV. The original diameter of the carbon nanotubes was 10 nm.

finite size effect in polymers such as PPV or in other organic materials have relied upon having a two dimensional film (i.e., very small thickness, usually a few nanometers) [108], creating copolymer films [109], introducing pores into the films [110], or filling pores with liquids instead of solids [111]. Noticeable effects arise in properties such as the glass transition temperature, which shifts from the bulk value as size is reduced [112].

Nanostructured and nanoporous substrates present a new way of manipulating the dimensions of the polymer. One advantage of using chemical vapor deposition to deposit PPV is that the polymer can be deposited conformally and pinhole-free on a variety of nanostructured substrates, including trenches, nanorods, nanotubes, and pores. Figure 6.1 shows an example of 240 nm of PPV deposited onto carbon nanotubes originally 10 nm in diameter. The structure clearly maintains individual shapes of the nanotubes while increasing their diameter with layers of polymer. Several researchers have found that the properties of oligomers [113] and polymers [114] deposited from liquid

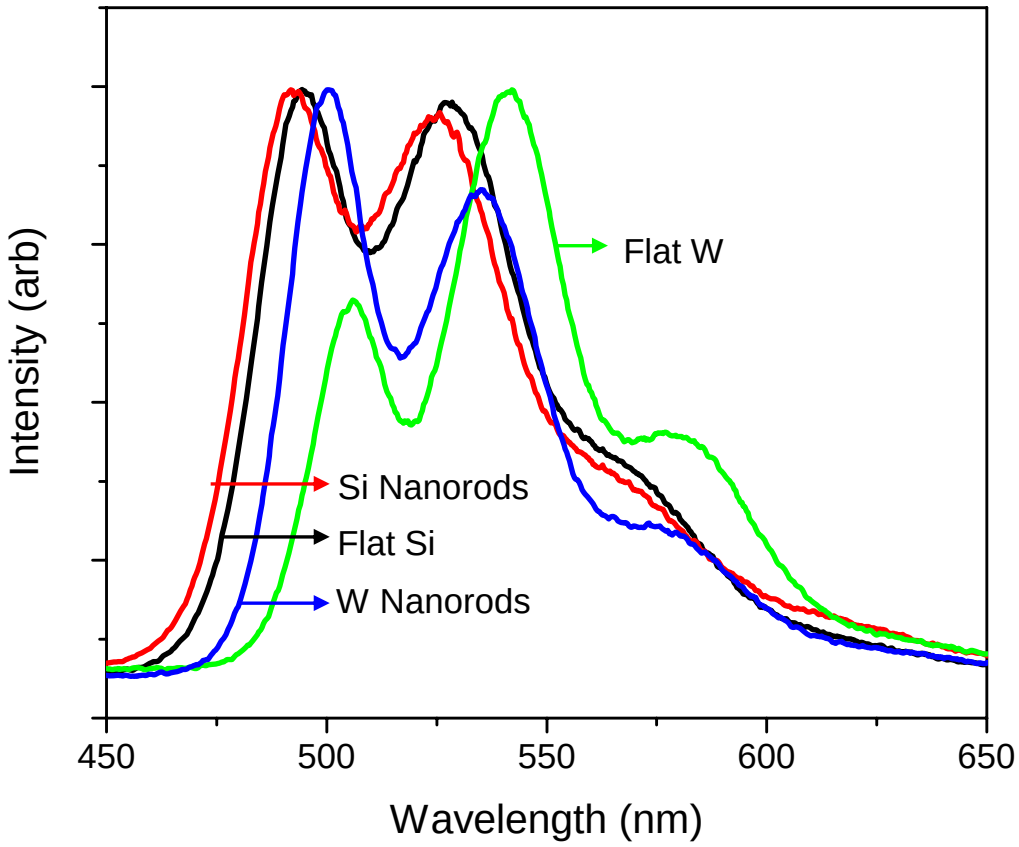

Figure 6.2: Photoluminescence spectra of PPV deposited on top of flat silicon (----) and tungsten (----) as well as silicon (----) and tungsten (----) nanorods. PPV films on both types of nanorods have a blueshifted spectra compared to the corresponding flat samples.

solution into porous materials depend on the solvent in which the oligomers and polymers are dissolved, changing traits such as chain conformation and penetration depth [115-117]. Even though liquid deposition has succeeded in limiting one polymer chain to a pore [117-119], using CVD to deposit PPV onto and into nanostructured substrates eliminates the effect of the solvent and greater control can be exerted over the penetration and conformation of PPV chains. Studying the deposition onto nanostructures of different sizes can provide insight into the origin of finite size effects in polymers and relate them to those of traditional semiconductor quantum dots.

An example of the influence of the substrate morphology on photoluminescence from PPV is shown in Figure 6.2, which compares the PL spectra from PPV deposited on both flat and nanorod substrates of both silicon and tungsten. In this figure, three main effects can be seen. First, both of the spectra from tungsten are redshifted from the silicon spectra. Second, for each material, the spectrum from the flat substrate is redshifted from that of the nanorod substrate. Finally, comparison of the flat and nanorod spectra show that in each case, the peak due to the 0 → 0 transition is the largest in the flat films, but the peak due to the 0 → 1 transition is the largest in the nanorod films. As discussed in more detail in Section 1.3.1, the interface plays a large role in the expression of the excitation in the polymer. An exciton changes the electron density in its immediate area, which changes the lengths of the carbon-carbon double and single bonds and therefore changes the shape of the polymer section. When the polymer is more confined, the shape changes less [25]. This effect will be discussed further in Section 6.2.2; here, it is enough to demonstrate the influence of substrate morphology on the characteristics of the polymer film. One additional reminder of the meaning of the redshift in photoluminescence spectra: a larger redshift indicates longer chain lengths [29, 30]. As might be expected, the flat substrates have redshifted spectra from the nanorod substrates, which have a more uneven surface and therefore are less likely to form longer fragments.

Not all nanostructures allow conformal deposition. When the feature size is too small or the structures are too close together, the polymer will deposit mostly on top of the features. An example of this is shown in Figure 6.3, where PPV is deposited on top of tungsten nanorods and leaves empty gaps in between the rods instead of completely filling in them. However, polymer units can diffuse into the structure even when the film is not entirely conformal. One example of this is from CVD into porous methyl silsesquioxane (MSQ), a low dielectric constant material ($k \sim 2.8$-3.0) that can be used for reduction of RC delay in integrated circuits [120]. Because the requirements for low dielectric constant materials exceed the actual dielectric constants of most materials, porosity is introduced into materials such as MSQ to reduce the dielectric constant further, but further processing increases the diffusion of metals into the pores. Juneja *et*

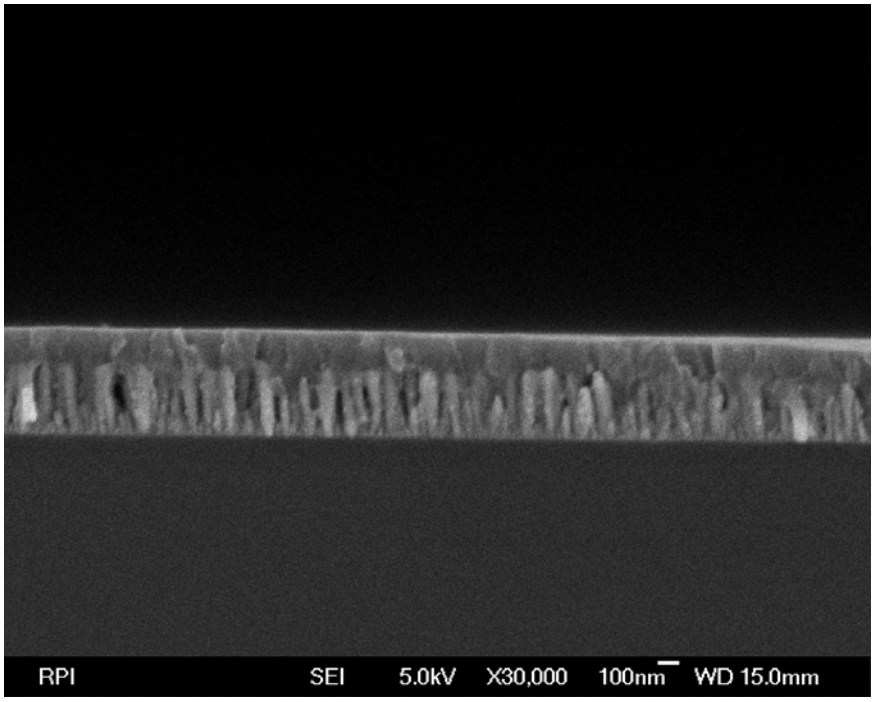

Figure 6.3: 250 nm of PPV film on top of tungsten nanorod structure.

al. used poly(p-xylylene) (PPX, or Parylene-N) deposited by CVD to cap pores approximately 4.1 nm in size and prevent metallization of the MSQ [93, 121]. During this procedure, they noticed a change in the overall dielectric constant in the films and conjectured that PPX was diffusing into the pores, with greater diffusion into MSQ with larger pores. Analysis of the carbon peak in Nuclear Resonance Analysis (NRA) of the PPX/MSQ films allowed calculation of the polymer penetration, which was found to vary with pore size as well as deposition conditions [121]. Similar results can be found for the deposition of PPV onto porous MSQ substrates. Figure 6.4 shows the depth profile of PPV deposited into MSQ calculated back calculated from NRA data of the carbon peak. In this figure, PPV penetrates at least 1500 Å into the pores, whereas a flat substrate placed in the deposition chamber at the same time would have only a 70 Å thickness. The insert shows an exaggerated image of polymer diffusion into the porous matrix, where there is a nearly continuous film on top of the pores, a thick coating on the first row of pores, and a film of decreasing thickness farther from the surface. Additionally, the flat PPV sample was too thin to have a PL spectrum detectible with our

detector, but the PPV/MSQ structure had a bright luminescence. This is most likely due to increased overall amount of polymer from deposition on the pore side walls as well as separation of polymer chains preventing interchain nonradiative excitations.

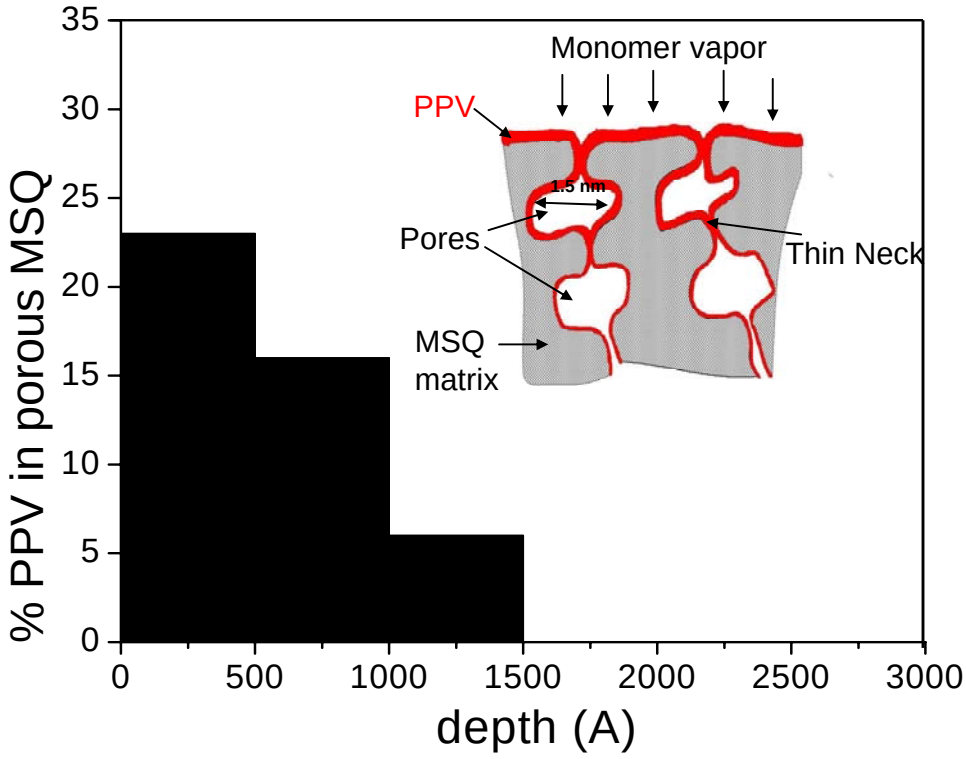

Figure 6.4: Penetration depth profile of PPV in porous MSQ. In this sample, 51 % of the material is solid MSQ. The rest is PPV or air (empty pores). Insert: Exaggerated image of diffusion of polymer into porous material.

6.2 Fluorescence Spectroscopy and Quenching

Fluorescence spectroscopy (FS) is a straightforward and sensitive tool for analyzing the photoluminescence of a variety of samples. One use of FS is in the determination of the quenching capabilities of compounds exposed to certain luminescent materials, where the interaction of the quencher with the fluorophore causes a decrease in the intensity of light emission from the sample. Applications of this method use the Stern-Volmer

equation to analyze materials ranging from biological sensors [122] to detection of environmental pollutants such as polycyclic aromatic hydrocarbons, where one of the advantages of this procedure is that the pollutants do not need to be separated from the bulk solution [123, 124]. While the Stern-Volmer equation is most commonly used with solution based reactants and expressed in terms of concentration, it is also possible to use the method with thin films. One common application of thin film fluorescence spectroscopy is in the detection of gases such as oxygen or nitroaromatic compounds, where luminescent compounds are either embedded in a matrix or deposited as a film itself and exposed to varying partial pressures of the gases [125, 126]. Other groups have modified the Stern-Volmer equation to apply to the steady-state density of hole polarons (bias voltage) or the charge injected instead of the concentration of the quencher [127, 128]. Kometani *et al*. have measured the luminescence properties of multilayer assemblies of polyelectrolytes and dyes [129]. Sharma measured the quenching capabilities of I^- in a solution of a precursor polymer of PPV [130]. The advantage of fluorescence spectroscopy for probing the layer structure of thin films over other probing systems such as neutron reflection [131], FTIR [132], or x-ray reflectivity [133] is the ease of use and inexpensive equipment.

6.2.1 The Stern-Volmer Equation

Photoluminescence spectra of PPV at varying thicknesses are given in Figure 6.5. As the thicknesses increase, the overall intensity increases and the relative intensities of the peaks change. All graphs have the characteristic shape of PPV photoluminescence spectra [9] and an additional reflection peak at 470 nm from the excitation source. Three peaks have been labeled: Peak 1 at 505 nm is assigned to the 0→0 vibronic transition, Peak 2 at 545 nm is the 0→1 transition, and Peak 3 at 590 nm is the 0→2 transition, as discussed further in the next section. For films around 200 Å, Peaks 1 and 2 are very small while Peak 3 is virtually indistinguishable from the background. As the thickness increases, so does the overall intensity of the spectrum as well as the separation between the peaks. Additionally, as the films increase in size, the second peak increases its

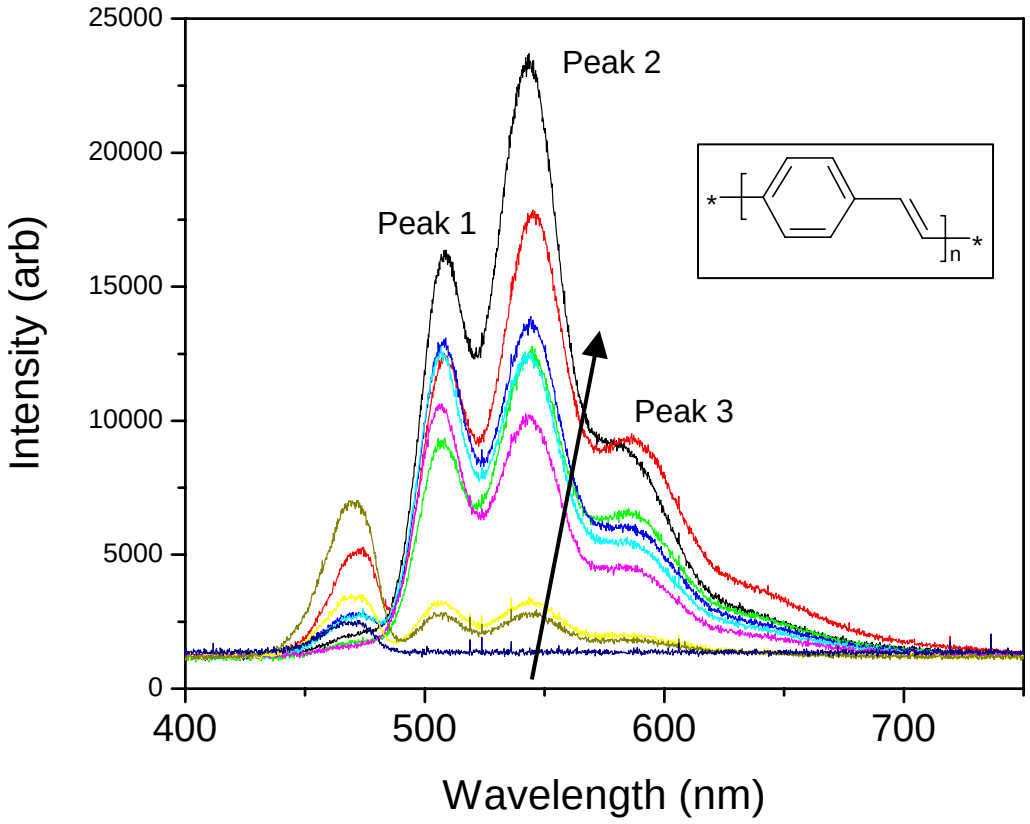

Figure 6.5: Photoluminescence spectra at increasing thicknesses. In the direction of the arrow, the thicknesses are as follows: 0 Å, 166 Å, 200 Å, 478 Å, 506 Å, 529 Å, 830 Å, 926 Å, 2000 Å. The three labeled peaks correspond to vibronic transitions 0→0, 0→1, and 0→2 for Peaks 1, 2, and 3, respectively. The remaining peak at ~470 nm is due to the reflection of the excitation source light because the thickness of the film does not exceed the penetration depth. Spectra were recorded at room temperature. Inset: PPV monomer unit.

intensity relative to the first peak to become the largest peak. This relative increase of the 0→1 transition has been attributed to a decreased contribution from interfacial excitons [98].

The methods of fluorescence spectroscopy may be useful when applied to the PPV/Si system. One of the most important equations in FS quenching studies is the Stern-Volmer equation (1),

$$I_0/I = 1 + K_{sv}[Q], \qquad (6.1)$$

which describes the behavior of a fluorescent system while it is being quenched. In equation (1), I_0 and I refer to the fluorescence intensities of the compound of interest (hereafter referred to as the fluorophore, F) in the absence and presence of quencher Q, respectively. K_{sv} is often referred to as the Stern-Volmer constant and directly relates to the binding and/or rate constants of the analyte and the quencher depending on the types of quenching involved in the samples. The Stern-Volmer equation can describe situations involving either dynamic (collisional) or static (binding) quenching. Both quenching types require contact between the F and Q molecules. In the case of dynamic quenching, contact between the excited fluorophore causes energy to transfer from F to Q, thereby preventing F from emitting radiatively. In this case the Stern-Volmer constant relates to the rate equation of the reaction. In static quenching, on the other hand, F and Q form a complex that is incapable of fluorescence in the same way that F alone was. K_{sv} is then related to the binding constant of the complex. The shape of the Stern-Volmer equation holds true for both types of quenching, but when both types of quenching are involved in the same system, or when there is more than one fluorophore emitting, the equation can become much more complex. In this case we are starting with the simplified equation, (1), which indicates that a plot of (I_0/I) versus the concentration of the quencher, [Q], would give a straight line with a slope equal to K_{sv}, with the meaning of the constant to be determined.

Although the Stern-Volmer equation has been successfully applied to many compounds, the system of a PPV film deposited onto Si presents different challenges. First, because PPV is insoluble, traditional liquid fluorescence measurements for Stern-Volmer calculations are not suitable. Instead, we have used the photoluminescence measurements from films of varying thicknesses and used those thicknesses to calculate

the amount of polymer present. Additionally, PPV acts as its own quencher through non-radiative transitions inherent in conjugated polymer systems as well as defects such as carbonyl groups or halogen groups incorporated into the film. For this reason there is no "I_0" or intensity without quenching. Instead, we use a completely quenched (nonluminescent) film as the relative intensity to calculate the ratio, similar to the procedure used by Kometani et al. [129]. We have therefore modified the Stern-Volmer equation (6.1) to take these factors into account, utilizing the ratio of intensity I_f of the films versus the intensity I_{f0} of the non-luminescent film:

$$I_f / I_{f0} = 1 + K_{svf} M_f . \qquad (6.2)$$

Here, the concentration of the quencher is given as the moles per volume of film, M_f. To calculate M_f, we used the relation $M_f = \rho \cdot t / M_w$, where t is the thickness, ρ is the density and is estimated at 1300 kg/m^3, and the molecular weight M_w is 1300 g/mol, corresponding to about 13 units of PPV, which is consistent with other measurements of the molecular weight [134]. In our calculation of the molarity, we assume that the films can be dissolved in a given volume of a solution, so M_f can be given in units of moles per cubic meter to compare to other results [129].

6.2.2 Influence of Substrates

Figure 6.6 shows the Stern-Volmer plots of thickness dependent PPV according to equation (6.2). Each of the three graphs in Fig. 2 shows two distinct areas: for M_f < ~ 60 μM, the slope is linear and steep. At higher M_f values, the slope decreases. For these graphs, the intensity used was measured at the wavelength of the maximum of each peak. This was considered acceptable because the Stern-Volmer plot of the integrated intensity for the entire spectrum (from a Gaussian multi-peak fit, not shown) has the same shape and general fit as that for a single intensity for each of the three peaks; most notably, the intersection of the two fit areas is at about 55 μM (550 Å), which is in the middle of the ranges of those for the three individual peaks. Table 6.1 summarizes the

slopes of the two trendlines for each peak (the binding constant of traditional Stern-Volmer measurements) and the location of the intersection of the two lines.

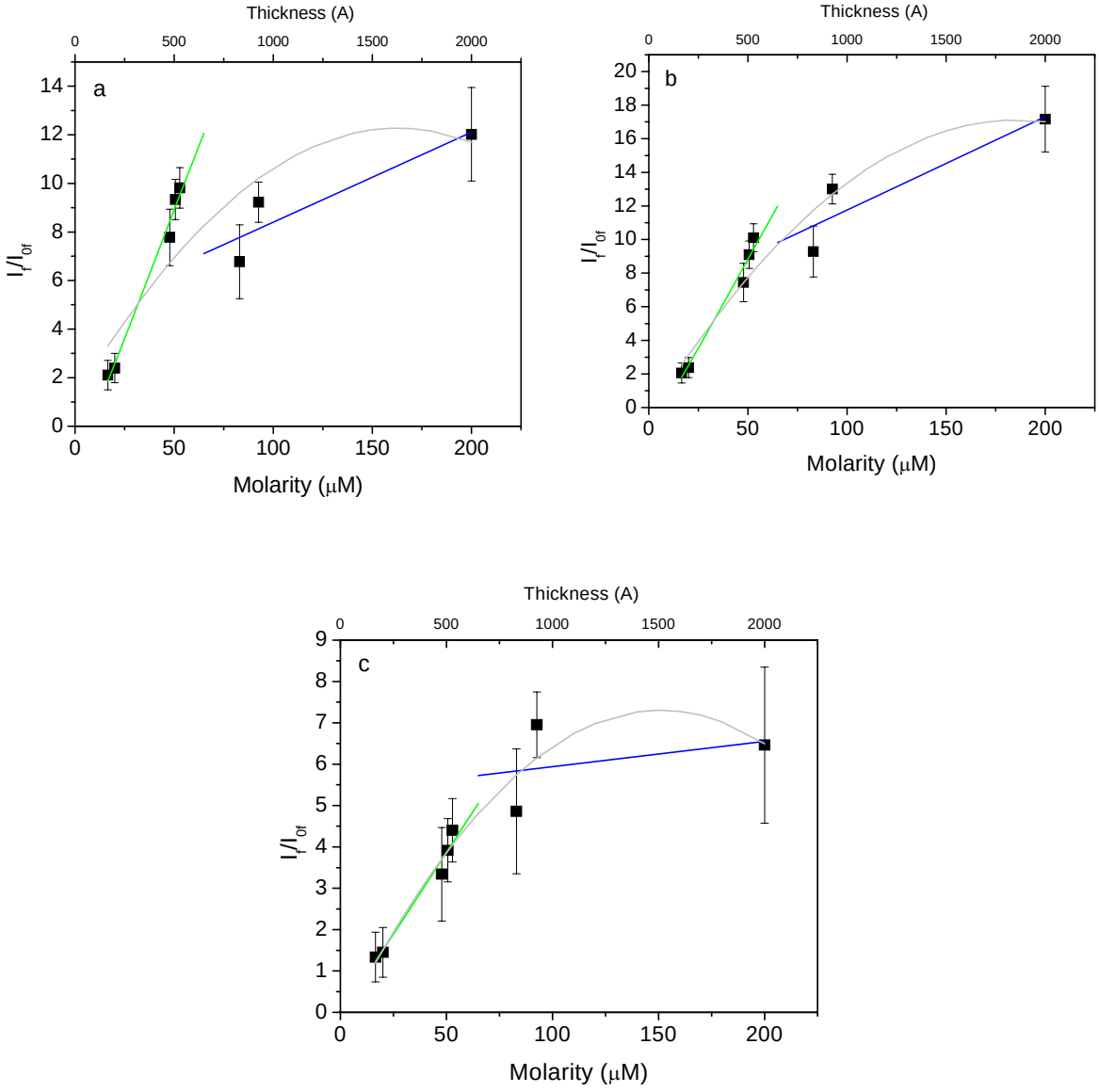

Figure 6.6: Stern-Volmer plots. A= Peak 1 at 508.7 nm, B= Peak 2 at 544.4 nm, C = Peak 3 at 587.34 nm. In all three plots, straight lines show separate trendlines for points less than 60 µM and points greater than 60 µM. Additionally, the gray line is a parabolic fit to all data points shown.

Table 6.1: Constants from application of Stern-Volmer equation.

	K_{svf-1} (1/μM)	K_{svf-2} (1/μM)	Intersection (μM)	Enthalpy (J/mol)
Peak 1	0.211	0.037	36.5	2.96
Peak 2	0.210	0.056	51.0	2.75
Peak 3	0.079	0.006	74.4	1.90

The two areas on the Stern-Volmer plots correspond roughly to a plot of the ratio of Peak 1 over Peak 2 ($I_{0\text{-}0}/I_{0\text{-}1}$) (Figure 6.7), which stays around unity until the molarity (or thickness) increases above 60 μM (600 Å). At higher thicknesses, the Peak 1 to Peak 2 ratio decreases to approximately 0.7, indicating that the 0→1 vibronic transition becomes the dominant emitter. Vibronic transitions in a spectrum are due to the coupling between the excitation (the exciton) and the geometry ("shape") of the molecule (phonon) [1]; a change in geometry allows different paths for decay instead of only the 0→0 path allowed in molecules with no shape change [25]. As mentioned in Section 1.3.1, this shape change takes a semiquinoid form, where the vinylene bonds become slightly closer to each other in length [27]. Ring rotation is hindered to a larger extent in films that have a greater quinoid character (rotation is only possible around single bonds, not double bonds, as shown in Figure 6.8). The morphology of the film plays a role in determining the degrees of quinoid character as more disordered films are more hindered in motion and so are more stable for quinoid formation.

One description of the amount of change is geometry is given by the configuration coordinate, Q. Figure 6.9 shows a configuration coordinate diagram of the transitions in PPV, including the three main transitions seen in PL spectra. Q is a relative measure of the amount of change the geometry of the molecule undergoes between the ground and excited states. The relative intensities of the vibronic peaks depend on the size of ΔQ, the change in lattice configuration between the ground and excited states; the larger the change in geometry, the larger the increase in the relaxation energy of the excited state, and the weaker the 0→0 transition becomes [25]. Hu and Karasz have previously noted

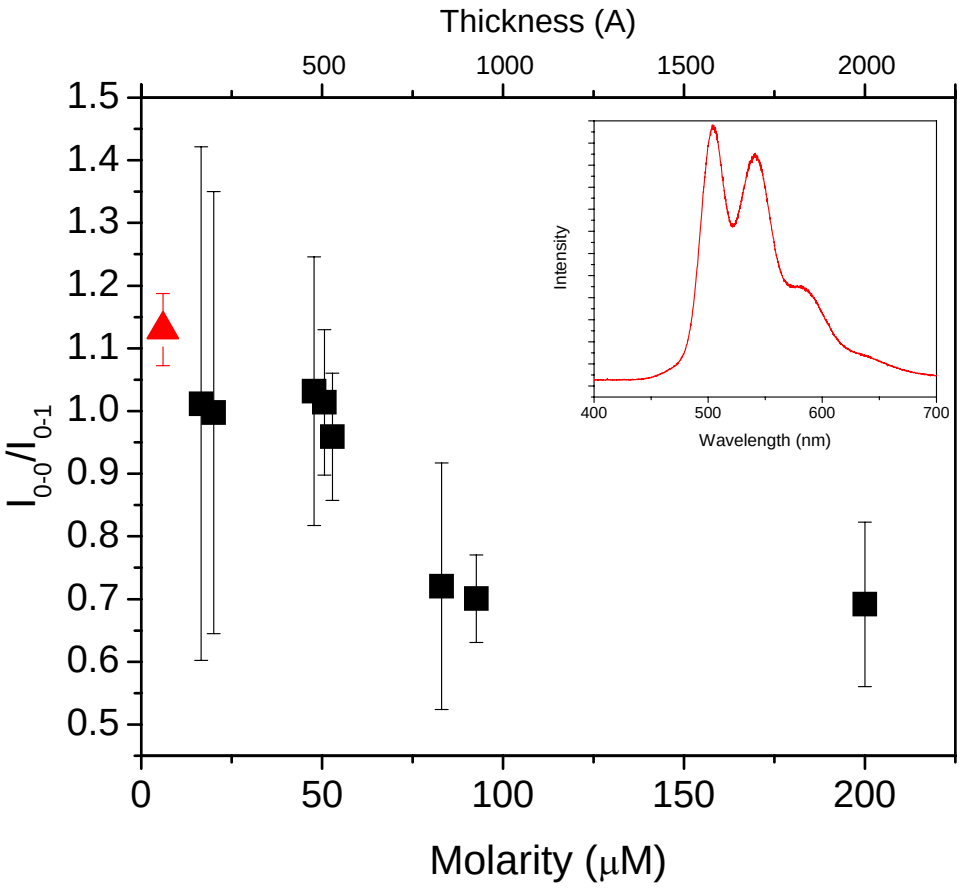

Figure 6.7: Ratio of the intensity of Peak 1 (I_{0-0}) to Peak 2 (I_{0-1}) versus Molarity. Black squares (■) are data points from 500 Å of PPV deposited on flat silicon, while the red triangle (▲) denotes the ratio for 60 Å of PPV deposited on porous MSQ. The inset shows the photoluminescence spectrum of PPV on MSQ.

that the relative intensities of the peaks also depend on the thickness of the substrate, and have attributed this effect to the influence of the substrate on the electron-phonon coupling [98]. They also show films of 60 nm and above as having "bulk" characteristics, corroborating our transition thickness. In thinner films, the 0→0 transition has the largest intensity, so the interface surface creates a polymer geometry with a smaller ΔQ between states. As the films get thicker, the interface plays a smaller role in the lattice geometry of the films and the 0→1 transition dominates the films as the polymer is goes

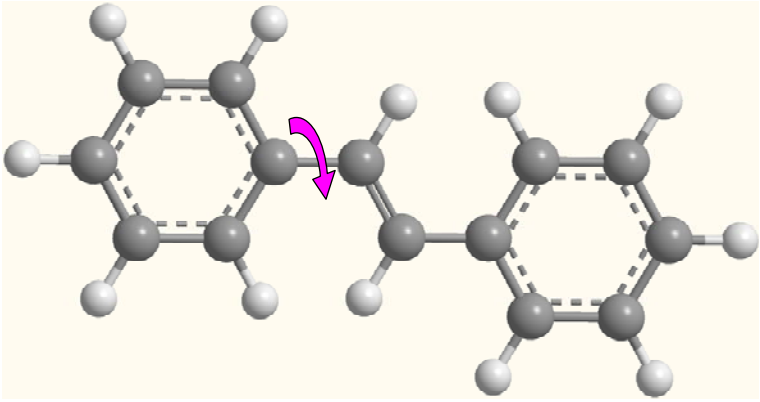

Figure 6.8: Rotation of the ring around the single bond in the vinylene unit. When an exciton is present on the chain, the single bond has more double bond character, rotation is hindered, and the overall shape of the chain is flatter. More double bond character corresponds to a larger ΔQ and a decrease in the 0-0 transition intensity. Disordered films also hinder ring rotation.

through a larger shape change. The leveling off of the Stern-Volmer plots as the thicknesses increase shows evidence of self-quenching (or PPV bound to PPV) seen in bulk films. The excitations responsible for the two areas in the Stern-Volmer plots can thus be referred to as polaron-excitons [25], where the polarons have differing values depending on proximity to the interface.

In order to show the influence of interface effects more clearly, we have also included a data point from 6 nm of PPV deposited into porous MSQ (methyl silsesquioxane), a low dielectric constant material that contains interconnected pores with an average size of 3 nm [121]. A 6 nm film of PPV on a flat surface is very faint and hard to detect without extremely sensitive equipment. By depositing into and on top of a porous material, the photoluminescence intensity (or quantum efficiency) increases due to decreased interactions between polymer chains that lead to nonradiative transitions [117]. This allows an easy measurement of the ratio of the intensity of Peaks 1 and 2, and, as expected, the ratio is greater than 1 (~1.13), indicating the predominance of interface effects in very thin films. This also indicates that the chains inside MSQ have a smaller change in structure (less of a quinoid nature).

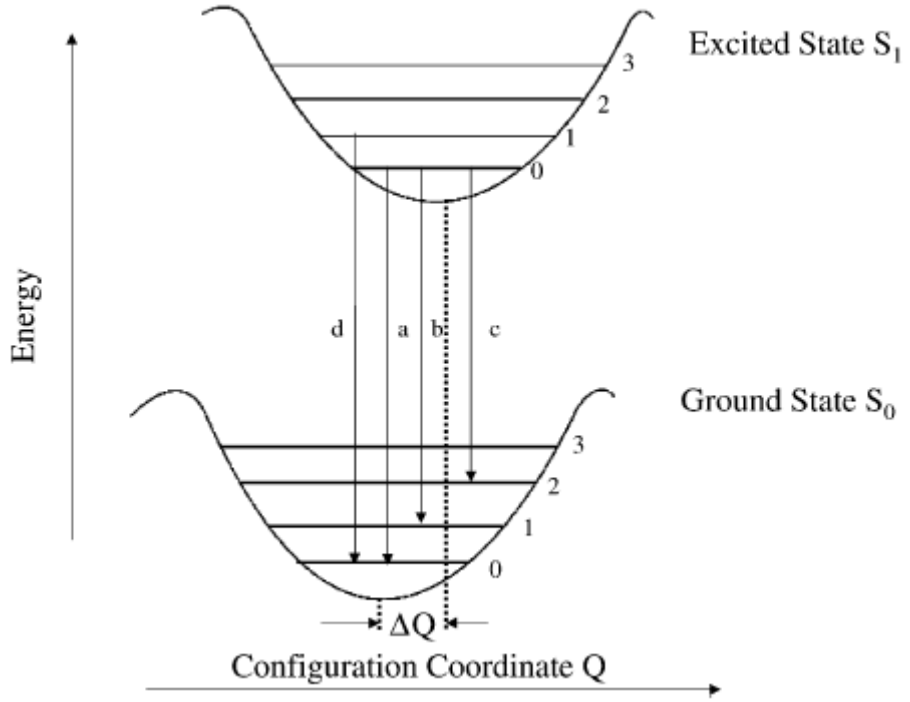

Figure 6.9: Transitions between PPV states. a: 0→0; b: 0→1; c: 0→2; d: 1→0. This figure is an expansion of the first two singlet states seen in Figure 1.6. [Image from Ref. [29]]

Other groups have also recorded downward-trending nonlinear Stern-Volmer plots [125, 135]. To contrast the straight fits, we have also included parabolic fits to the data in Figure 6.6. The parabolic fits can be described as adding a squared term to the Stern-Volmer equation in the following manner:

$$I_f / I_{f0} = 1 + (K_1 + K_2)M_f + K_1 K_2 M_f^{\,2}. \qquad (6.3)$$

In this case, K_1 and K_2 correspond to the Stern-Volmer quenching constant for two different fluorophore populations, which could include a combination of dynamic and static quenching or two different fluorophores of each type. A different explanation for

the downward trend of the slope is a saturation of the quenching. As the films get thicker, the quenching defects and the bulk film reach an equilibrium and reduce the effect of the quenching.

6.3 Temperature Dependence

The fluorescence spectra are taken as a function of the thickness of the PPV samples. The properties of the three main fluorescent transitions in the spectra can be clarified using the temperature dependent properties of the films. Temperature dependent measurements have been widely used on photoluminescent materials. Other studies commonly see results such as the intensity increase, peak sharpening, and blue shift of films with decreasing temperature [79, 96, 134, 136-139]. This work applies the methodology to the thickness study mentioned above.

6.3.1 Energy Shift

The 500 Å thick PPV sample was chosen for temperature dependence measurements because of its significant position at the border of interface effect-dominated and bulk effect-dominated films. Representative samples of these spectra are given in Figure 6.10. As the temperature decreases, all three peaks become sharper, but the effect is most noticeable in Peak 3, which only becomes well resolved below approximately 300 K. Additionally, the intensities of the individual peaks increase and the entire spectrum shifts to higher wavelengths. In order to pinpoint these changes, each of the three peaks in each spectrum was separately fit to a Gaussian curve. The calculated peak positions are shown in Figure 6.11 as a function of temperature. The overall energy shift of each peak is slightly different, but the effect is most noticeable in Peak 3, which has a shift of about 0.47 meV/K as opposed to the 0.24 meV/K and 0.29 meV/K shifts for Peaks 1 and 2, respectively. Overall, the spectrum shifts approximately 10 nm in the direction of

longer wavelengths as the temperature decreases. These results correspond to those found in similar studies [137].

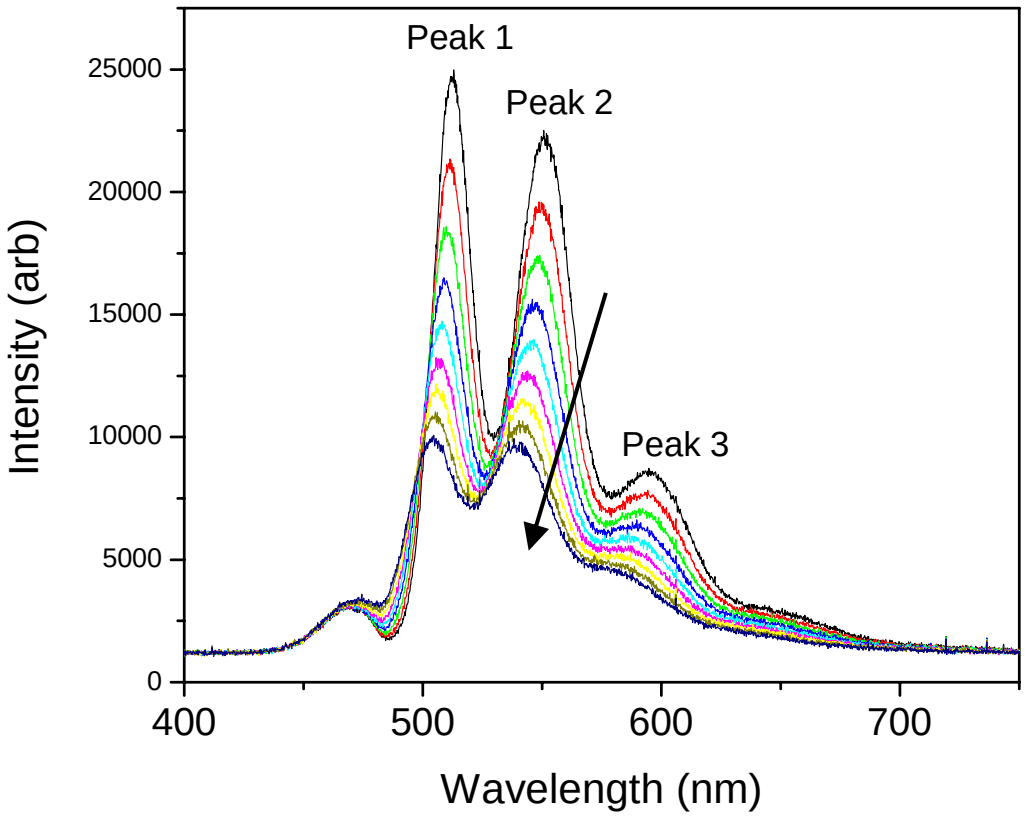

Figure 6.10: Photoluminescence spectra of a flat 500 Å PPV sample at increasing temperatures. Temperatures increase in the direction of the arrow from 180 K to 340 K in 20 K increments.

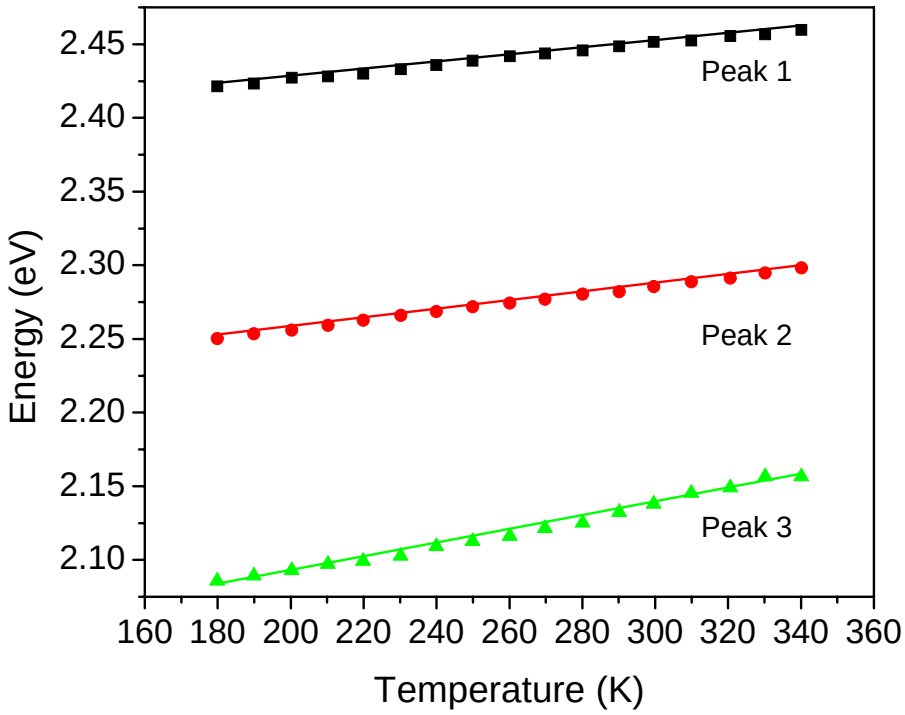

Figure 6.11: Energy shift of Peaks 1 (■), 2 (●), and 3 (▲) as a function of temperature calculated from Figure 6.10. Corresponding lines are fitted to the data.

6.3.2 Enthalpy

Figure 6.12 shows a plot of the natural log of the intensity of each peak versus the inverse of the temperature. Each peak gives a straight plot whose slope m can be used to calculate the enthalpy ΔH of the excitation, where $m = -\Delta H/R$. While peaks 1 and 2 have very similar plots both in intensity and slope, peak 3 has a much lower intensity and a smaller slope and therefore has a smaller ΔH. The enthalpies are included in Table 6.1. The differences in the enthalpies are theorized to be due to the effect of non-radiative transitions. Peak 3 is at an interesting location in the spectrum. Because of its small intensity relative to the first two peaks, it is often described as more of a "shoulder" than a separate peak.

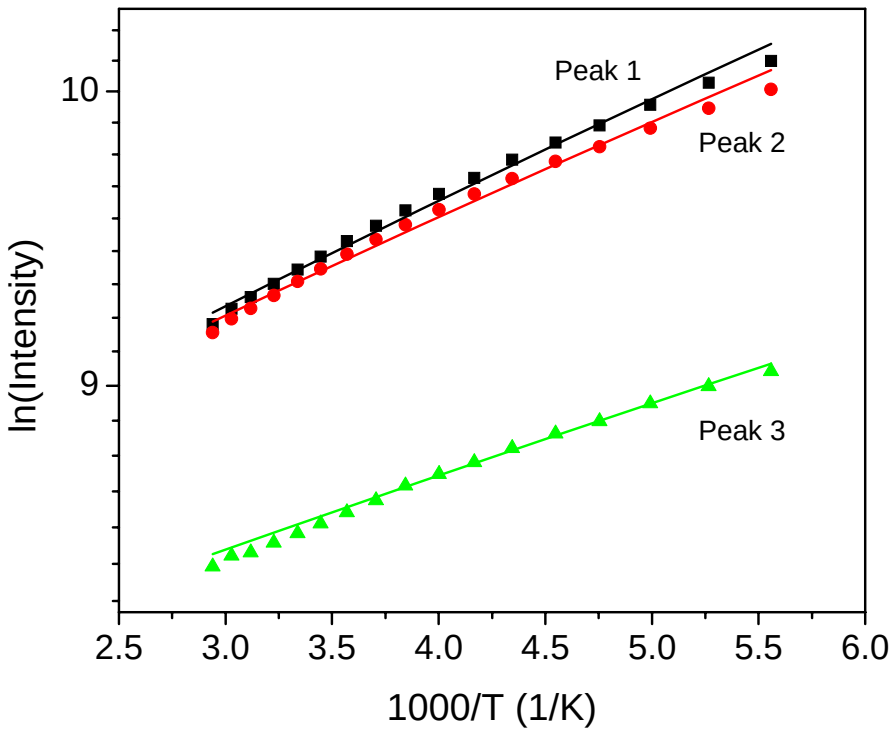

Figure 6.12: Natural log of the intensity of Peaks 1 (■), 2 (●), and 3 (▲) with increasing temperature. Corresponding lines are fitted to the data.

6.3.3 Huang-Rhys Factor

Excitations in PPV migrate along the polymer backbone until deexcitation either through a radiative pathway (photoluminescence) or a non-radiative pathway such as those provided in defect sites. In thin films, chains are close together so excitations can easily migrate from one chain to the next, which means that the excitons have shorter lifetimes before they decay [30]. Longer conjugation lengths in the polymer lead to longer decay times and redshifted spectra. The conjugation length has also been related to the Huang-Rhys factor [140], which, although technically is related to the probability of a decay from the 0 level of the excited state to the n level of the ground state, is also commonly used

as a measure of disorder in the films [141]. The disorder of the films is partially responsible for the proportion of radiative transitions vs. non-radiative transitions: the former are usually intrachain, while the latter are interchain, so isolated chains have higher fluorescence intensities, and increasing the disorder of a film increases the likelihood of excitations finding non-radiative pathways for deexcitation. As a measure of the disorder of the films, we have the Huang-Rhys factor S calculated at each temperature using the simplified relation,

$$S = (I_1 + 2I_2)/I, \qquad (6.4)$$

where I_1 and I_2 are the intensities of the 0→1 and 0→2 transitions (peaks 2 and 3, respectively) and I is the overall intensity [141]. Figure 6.13 shows S at increasing temperatures for both the 500 Å flat PPV film and a 160 Å PPV film on porous MSQ. While both films show an increase of S with temperature, the flat film shows a large, steady increase while the nanostructured film has only a slight increase. The temperature dependence of S has been attributed to the effective increase in conjugation length arising from fewer distortions in the chain at lower temperatures[134, 141]. The flat film also has a larger overall value of S: 0.76 compared with the nanostructured film at 0.66 at room temperature. Since smaller molecules tend to have larger values of S [142], nanostructured nature of the PPV deposited in porous MSQ must not have decreased the chain length of the polymer to a large extent. Instead, the decrease in S is more likely due to a smaller amount of disorder in the film because of the thinness of the film as well as the structure imposed by the porous nature of the substrate. This is consistent with the previous finding that PPV on MSQ has less of a quinoid nature than PPV on flat substrates.

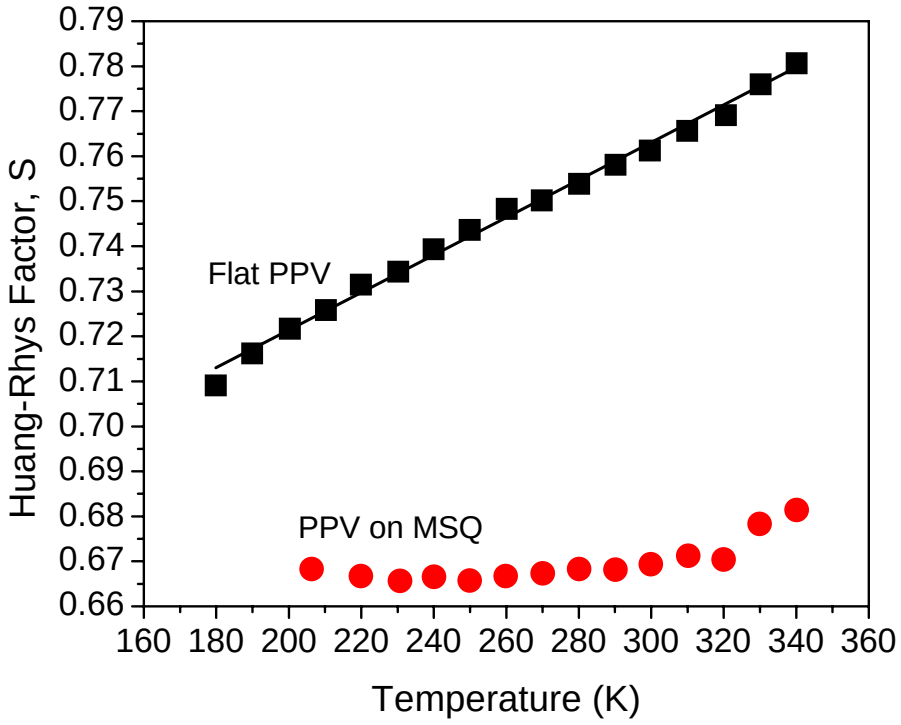

Figure 6.13: Huang-Rhys factor for PPV at increasing temperatures on flat silicon substrate (■), 500 Å, and on porous MSQ substrate (●), 10 Å. A linear trendline is shown with the data points for flat PPV in order to aid the eye.

6.4 Conclusions

The usefulness of the Stern-Volmer equation in fluorescence spectroscopy has been demonstrated in many experiments. Applying the methodology to the quenching of solid systems presents several challenges, most especially due to the self-quenching of PPV and the interface effects inherent in thin film samples. In PPV, the ratio of Peak 1 to Peak 2 vs. thickness separates the sample data into two sections: thicknesses below about 600 Å are dominated by interface effects, and those above 600 Å are dominated by bulk effects. In both ranges, Peak 1 and Peak 2 are more similar to each other than to Peak 3, which typically has not only a smaller intensity but smaller changes in intensity

with thickness. In order to clarify the differences between bulk and interface effects, fluorescence measurements were made on 100 Å of PPV deposited on porous MSQ, a sample dominated entirely by interface effects. Further comparisons were made using the temperature dependence of the photoluminescence measured on the 500 Å thick flat film. In this case, Peak 3 had a larger energy shift with temperature and an enthalpy almost half of Peaks 1 and 2. Calculation of the Huang-Rhys factor at varying temperatures for the flat film and film in porous MSQ shows a large temperature dependence for the flat film but a smaller amount of disorder in the nanostructured film.

7. Summary, Conclusions, and Remaining Challenges

This work examined the material and optical properties of poly(*p*-phenylene vinylene) deposited by chemical vapor deposition onto a variety of substrates. The conversion of the precursor polymer to PPV was explored in terms of the removal of the bromine substituent during annealing. The films were then heat treated further to high temperatures to look for structural changes. Encapsulation of the films with aluminum oxide and Parylene attempted to prevent photooxidation and degradation of the photoluminescence of the films. Finally, the Stern-Volmer equation was utilized for the thin films to explore the self-quenching and substrate effects on the film.

7.1 Conversion of Precursor to PPV

Dehydrobromination of the precursor polymer converts the deposited films into PPV at temperatures between 100-300 °C. Mass spectroscopy of the characteristic HBr ion fragment masses shows that most of the bromine is removed during the first thirty minutes of the anneal. Long time anneal at two different temperatures, 150 °C and 300 °C in vacuum, shows that the temperature of the anneal had a larger effect on the amount of bromine removed from the film than the time of the anneal did, as calculated from the bromine peak in Rutherford Backscattering Spectroscopy. A more successful procedure for reducing the amount of bromine further was to flow nitrogen gas into the chamber during the anneal.

Although the 300 °C anneal removed more bromine than the 150 °C anneal did, photoluminescence spectroscopy revealed that the 300 °C films were more completely converted but less intense than the 150 °C films. Since longer annealing times and higher temperatures both reduce the quality of the film, a median time and temperature was chosen as the standard for annealing subsequent PPV films: 2 hours at 250 °C.

The 250 °C anneal was studied further at short times. 5, 10, 15, and 30 minute anneals were monitored with mass spectroscopy for the bromine ion mass fragment peaks. The bromine lines peaked about 3 minutes after the furnace reached the annealing temperature of 250 °C, or 15 minutes total during heating. All of the films were not completely converted, as the photoluminescence spectra and thickness changes show, but as the time increased the properties reached toward a stable state for the film.

7.2 High Temperature Degradation

High temperature treatment of PPV after the initial conversion can convert the polymer to pure graphite. In order to understand the conversion process more fully, CVD PPV films were treated at temperatures of 450 °C and 500 °C while mass fragments from the film were analyzed and changes in thickness were measured. Degradation in PPV thin films has been shown to take place at 500 °C through thickness changes and mass spectra that show high molecular weight fragments eliminated from the film. Since there is no thickness change or increased intensities of mass fragments during annealing at 450 °C, this is the minimum temperature for the start of degradation. However, FTIR spectra show no significant change in bond intensity before and after heat treatment at 500 °C, so neither crosslinking nor bond breaking occur to a significant degree at this temperature. Degradation thus proceeds through densification and removal of unreacted or weakly bonded fragments.

7.3 Encapsulation and Photodegradation

Proper encapsulation materials can prevent photodegradation of PPV due to attack by oxygen radicals on the polymer chain in the presence of light. The first encapsulation layer investigated here was an ~ 10 nm layer of aluminum oxide. Typical photoluminescence of PPV film without the coating degrades to 20 % of its original intensity within three hours; photoluminescence from the PPV film coated with

aluminum oxide can be maintained without degradation for several hours under blue light. However, the intensity of the PL decreases to about 70 % of its original intensity after 6 hours of exposure to UV light. The aluminum oxide coating provides some protection from degradation but is not sufficient for extended use.

The second encapsulation material examined was Parylene, a polymer related to PPV. Although PPX displays excellent gas and CVD metal diffusion properties, PPX was not an effective encapsulation layer for PPV. Both thick and thin PPX layers decreased the total amount of degradation only slightly. Even after annealing the PPX/PPV structure to remove any surface oxygen the annealed sample showed a greater amount of degradation than the unannealed sample did. However, there was no significant difference in the intensity of peaks in the FTIR spectra of PPV and PPX/PPV before and after exposure to 5 hours of blue light.

7.4 Substrate Effects and Quenching

The morphology of the substrate can play a role in influencing the excitation properties of PPV by shifting PL spectra depending on the configuration of the layers. One useful tool is the Stern-Volmer equation. Applying the methodology to the quenching of solid systems presents several challenges, most especially due to the self-quenching of PPV and the interface effects inherent in thin film samples. In PPV, the ratio of Peak 1 to Peak 2 vs. thickness separates the sample data into two sections: thicknesses below about 600 Å are dominated by interface effects, and those above 600 Å are dominated by bulk effects. In both ranges, Peak 1 and Peak 2 are more similar to each other than to Peak 3, which typically has not only a smaller intensity but smaller changes in intensity with thickness. In order to clarify the differences between bulk and interface effects, fluorescence measurements were made on 100 Å of PPV deposited on porous MSQ, a sample dominated entirely by interface effects. Further comparisons were made using the temperature dependence of the photoluminescence measured on the 500 Å thick flat film. In this case, Peak 3 had a larger energy shift with temperature and an enthalpy

almost half of Peaks 1 and 2. Calculation of the Huang-Rhys factor at varying temperatures for the flat film and film in porous MSQ shows a large temperature dependence for the flat film but a smaller amount of disorder in the nanostructured film.

7.5 Future Work

There remain many challenges to finding ways of incorporating PPV into useful devices. Encapsulation especially is a challenge. However, new materials are being synthesized that may play a larger role in protection. One such material is a Parylene-derivative UV-resistant polymer that blocks lower-wavelength UV light while transmitting higher wavelengths as well as visible. It deposited using chemical vapor deposition, so it can be conformally deposited on nanostructured substrates as well as flat ones. Figure 7.1 shows the transmission spectrum of the UV-resistant polymer from Ossen Labs (Sunnyvale, CA) before and after exposure to 56 hours of UV light at a wavelength around 400 nm. The only difference between the films is a small dip at 300 nm.

Other devices incorporate porous matrix elements as a substrate for PPV emitting layers in order to get a larger surface area and other desirable properties [143]. Because the morphology of the film plays a large role in the emission properties of the film, device performance needs to be optimized by controlling the structure of the chains, such as by creating more ordered chains on small surface areas. Exciton dynamics need to be studied further in these materials. Additionally, porous substrates present their own challenges for encapsulation and have been studied extensively for a variety of materials [62, 92].

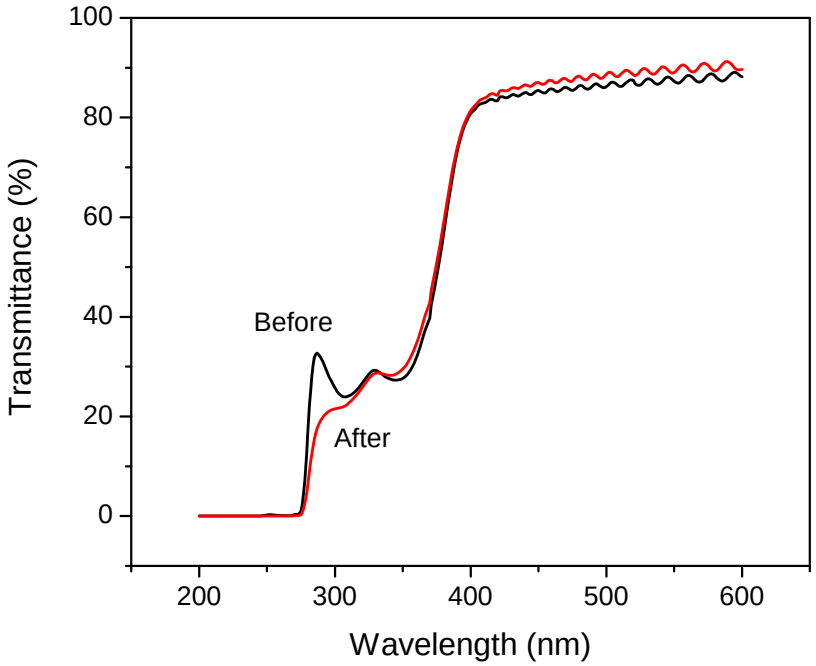

Figure 7.1: Transmittance of UV polymer before and after exposure to 56 hours of UV light at 400 nm.

8. References

1. Friend, R.H., et al., *Electroluminescence in conjugated polymers.* Nature, 1999. **397**: p. 121-128.
2. Kim, J., et al., *Fabrication and characterization of conductive polypyrrole thin film prepared by in situ vapor-phase polymerization.* Synthetic Metals, 2003. **132**(3): p. 309-313.
3. Cho, J.-H., et al., *Sensing behaviors of polypyrrole sensor under humidity condition.* Sensors and Actuators B: Chemical, 2005. **108**(1-2): p. 389-392.
4. Dodabalapur, A., et al., *Organic smart pixels.* Applied Physics Letters, 1998. **73**(2): p. 142-144.
5. Rees, I.D., et al., *Recent developments in light-emitting polymers.* MRS Bulletin, 2002. **27**(6): p. 451-5.
6. Mäkelä, T., et al., *Thin polyaniline films in EMI shielding.* Synthetic Metals, 1997. **85**(1-3): p. 1335-1336.
7. Wessling, B., *Passivation of Metals by Coating with Polyaniline: Corrosion Potential Shift and Morphological Changes.* Advanced Materials, 1994. **6**(3): p. 226-228.
8. Huh, J.W., et al., *Characteristics of organic light-emitting diodes with conducting polymer anodes on plastic substrates.* Journal of Applied Physics, 2008. **103**(4): p. 044502.
9. Burroughes, J.H., et al., *Light-emitting diodes based on conjugated polymers.* Nature, 1990. **347**: p. 539-541.
10. Talaie, A., et al., *Macromolecular architecture of new polymers via construction of new side groups within PPV chemical structure to enhance its properties for flat-panel displays.* Materials Science and Engineering B, 2001. **85**: p. 177-181.
11. Wang, M. and X. Wang, *PPV/TiO2 hybrid composites prepared from PPV precursor reaction in aqueous media and their application in solar cells.* Polymer, 2008. **49**(6): p. 1587-1593.
12. Gedelian, C.A., G.A. Ten Eyck, and T.-M. Lu, *Onset of thermal degradation in poly(p-phenylene vinylene) films deposited by chemical vapor deposition.* Synthetic Metals, 2007. **157**(1): p. 48-52.
13. Fortin, J.B. and T.-M. Lu, *Ultraviolet radiation induced degradation of poly-para-xylylene (parylene) thin films.* Thin Solid Films, 2001. **397**: p. 223-228.
14. Bernier, P., et al., *EPR study of the cis-trans isomerization process in polyacetylene films.* Journal of Physics-Paris, 1981. **42**: p. L-295 - L-299.
15. Ehlers, G.F.L., K.R. Fisch, and W.R. Powell, *Thermal degradation of polymers with phenylene units in the chain. I. Polyphenylenes and poly(phenylene oxides).* Journal of Polymer Science A1, 1969. **7**: p. 2931-2953.
16. Ou, R. and R. Samuels, *Characterization of Anisotropic Structure in Poly(Phenylene Vinylene) Films.* Polymer Engineering and Science, 2001. **41**(10): p. 1705-1713.
17. Zheng, G., et al., *First-principles studies of the structural and electronic properties of poly-para-phenylene vinylene.* Journal of Physics: Condensed Matter, 2004. **16**: p. 8609-8620.

18. Shah, H.V., J.I. Scheinbeim, and G.A. Arbuckle, *Structural Anisotropy in Unstretched and Uniaxially Stretched Poly(p-phenylene vinylene).* Journal of Polymer Science, Part B (Polymer Physics), 1999. **37**(6): p. 605-614.
19. Kim, K., et al., *Morphology of poly(p-phenylenevinylene) thin films prepared directly on the surface of silicon wafers by the chemical vapor deposition polymerization.* Synthetic Metals, 2004. **144**: p. 7-11.
20. Tessler, N., G.J. Denton, and R.H. Friend, *Lasing from conjugated-polymer microcavities.* Nature, 1996. **382**: p. 695-697.
21. Kawai, T., et al., *Secondary Battery Characteristics of Poly(p-phenylene vinylene) Derivatives.* Japanese Journal of Applied Physics, 1990. **29**(9): p. 1833-1836.
22. Papadimitrakopoulos, F., et al., *The Role of Carbonyl Groups in the Photoluminescence of Poly(p-phenylenevinylene).* Chemistry of Materials, 1994. **6**: p. 1563-1568.
23. Scholes, G.D. and G. Rumbles, *Excitons in nanoscale systems.* Nature Materials, 2006. **5**: p. 683-693.
24. Birks, J.B., *Photophysics of Aromatic Molecules*. Wiley Monographs in Chemical Physics, ed. J.B. Birks. 1970, London: Wiley-Interscience.
25. Brédas, J.-L., J. Cornil, and A.J. Heeger, *The Exciton Binding Energy in Luminescent Conjugated Polymers.* Advanced Materials, 1996. **8**(5): p. 447-452.
26. Zerbi, G., M. Gussoni, and C. Castiglioni, *Vibrational Spectroscopy of Polyconjugated Aromatic Materials with Electrical and Nonlinear Optical Properties: A Guided Tour*, in *Conjugated Polymers: The Novel Science and Technology of Highly Conducting Nonlinear Optically Active Materials*, J.L. Brédas and R. Silbey, Editors. 1991, Kluwer Academic Publishers: Dordrecht, The Netherlands. p. 435-507.
27. Beljonne, D., et al., *Theoretical investigation of the lowest singlet and triplet states in poly(paraphenylene vinylene) oligomers.* Journal of Chemical Physics, 1995. **102**(5): p. 2042-2049.
28. Cowan, D.O. and R.L. Drisko, *Elements of Organic Photochemistry*. 1976, New York: Plenum Press.
29. Bakueva, L., et al., *Luminescence of pure and iodine doped PPV: internal energetic structure revealed through spectral signatures.* Synthetic Metals, 2002. **126**: p. 207-211.
30. Heun, S., et al., *Conformational effects in poly(p-phenylene vinylene)s revealed by low-temperature site-selective fluorescence.* Journal of Physics: Condensed Matter, 1993. **5**: p. 247-260.
31. Karabunarliev, S. and E.R. Bittner, *Polaron-excitons and electron-vibrational band shapes in conjugated polymers.* Journal of Chemical Physics, 2003. **118**(9): p. 4291-4296.
32. Klessinger, M. and J. Michl, *Excited States and Photochemistry of Organic Molecules*. 1995, New York: VCH Publishers, Inc.
33. Coyle, J.D., *Introduction to Organic Photochemistry*. 1986, Chichester: John Wiley & Sons.

34. Gmeiner, J., et al., *Synthesis, electrical conductivity and electroluminescence of poly(p-phenylene vinylene) prepared by the precursor route.* Acta Polymer, 1993. **44**: p. 201-205.
35. Koch, A.T.H., et al., *Enhanced photostability of poly(1,3-phenylene diphenylvinylene)-derivatives by diphenyl-substitution.* Synthetic Metals, 1999. **100**: p. 113-122.
36. Vaeth, K.M. and K.F. Jensen, *Poly(p-phenylene vinylene) prepared by chemical vapor deposition: Influence of monomer selection and reaction conditions on film composition and luminescence properties.* Macromolecules, 1998. **31**: p. 6789-6793.
37. Yan, M., et al., *Defect Quenching of Conjugated Polymer Luminescence.* Physical Review Letters, 1994. **73**(5): p. 744-747.
38. Tran, V.H., et al., *Spectroscopic studies of the conversion of poly(p-phenylene-vinylene) precursor.* Polymer, 1996. **37**(11): p. 2061-2065.
39. Zyung, T. and J.-J. Kim, *Photodegradation of poly(p-phenylenevinylene) by laser light at the peak wavelength of electroluminescence.* Applied Phyiscs Letters, 1995. **67**(23): p. 3420-3422.
40. Harrison, N.T., et al., *Singlet Intrachain Exciton Generation and Decay in Poly(p-phenylenevinylene).* Physical Review Letters, 1996. **77**(9): p. 1881-1884.
41. Rothberg, L.J., et al., *Photophysics of phenylenevinylene polymers.* Synthetic Metals, 1996. **80**: p. 41-58.
42. Ke, L., P. Chen, and S.-J. Chua, *Photoluminescence degradation in organic light-emitting devices.* Applied Phyiscs Letters, 2002. **80**(4): p. 697-699.
43. Vaeth, K.M. and K.F. Jensen, *Chemical vapor deposition of thin polymer films used in polymer-based light emitting diodes.* Advanced Materials 1997. **9**(6): p. 490.
44. Andersson, G., et al., *Halogens as trace compounds in polymeric light-emitting diodes.* Synthetic Metals, 2000. **113**: p. 245-249.
45. Kugler, T., et al., *Buried interfaces: poly(p-phenylene-vinylene)-on-ITO.* Synthetic Metals, 1999. **100**(1): p. 163-168.
46. McDonald, R.N. and T.W. Campbell, *The Wittig Reaction as a Polymerization Method.* Journal of the American Chemical Society, 1960. **82**(17): p. 4669-4671.
47. Wessling, R.A. and R.G. Zimmerman, *Polyelectrolytes from bis sulfonium salts*, U.S.P. Office, Editor. 1968: United States.
48. Gagnon, D.R., et al., *Synthesis, doping, and electrical conductivity of high molecular weight poly(p-phenylene vinylene).* Polymer, 1987. **28**: p. 567-573.
49. Halliday, D.A., et al., *A Study on the Elimination Reaction of Sulfonium Polyelectrolyte Precursor Polymers to Poly(p-phenylenevinylene).* Journal of the Chemical Society, Chemical Communications, 1992(22): p. 1685-1687.
50. Nishikata, Y., M.-A. Kakimoto, and Y. Imai, *Preparation and properties of poly(p-phenylenevinylene) Langmuir-Blodgett film.* Thin Solid Films, 1989. **179**: p. 191-197.
51. Marletta, A., et al., *Highly Oriented Langmuir-Blodgett Films of Poly(p-phenylenevinylene) Using a Long Chain Sulfonic Counterion.* Macromolecules, 2000. **33**: p. 5886-5890.

52. Marletta, A., et al., *Self-assembly of poly(p-phenylene vinylene) using long chain counter-ion: a new process for fabrication of multilayer thin films heterostructures.* Synthetic Metals, 2001. **121**: p. 1447-1448.
53. Iwatsuki, S., M. Kubo, and T. Kumeuchi, *New method for preparation of poly(phenylene-vinylene) film.* Chemistry Letters, 1991: p. 1071-1074.
54. Gorham, W.F., *A new, general synthetic method for the preparation of linear poly-p-xylylenes.* Journal of Polymer Science: Part A-1, 1966. **4**: p. 3027-3039.
55. Staring, E.G.J., et al., *Chemical vapour deposition of poly(1,4-phenylenevinylene) films.* Synthetic Metals, 1994. **67**(1-3): p. 71-5.
56. Schäfer, O., et al., *Poly(p-phenylenevinylene) by chemical vapor deposition: synthesis, structural evaluation, glass transition, electroluminescence, and photoluminescence.* Synthetic Metals, 1996. **82**: p. 1.
57. Vaeth, K.M. and K.F. Jensen, *Selective growth of poly(p-phenylene vinylene) prepared by chemical vapor deposition.* Advanced Materials, 1999. **11**(10): p. 814.
58. Vaeth, K.M. and K.F. Jensen, *Transition metals for selective chemical vapor deposition of parylene-based polymers.* Chemistry of Materials, 2000. **12**: p. 1305-1313.
59. Vaeth, K.M., et al., *Use of microcontact printing for generating selectively grown films of poly(p-phenylene vinylene) and parylenes prepared by chemical vapor deposition.* Langmuir, 2000. **16**: p. 8495-8500.
60. Fortin, J.B. and T.-M. Lu, *Mass spectrometry study during the vapor deposition of poly-para-xylylene thin films.* Journal of Vacuum Science & Technology A (Vacuum, Surfaces, and Films), 2000. **18**(5): p. 2459-2465.
61. Kokane, S., et al., *Modified CVD deposition of poly(p-phenylene vinylene).* Synthetic Metals, 2003. **132**: p. 235-238.
62. Juneja, J.S., *CVD Parylene-N as pore sealant for porous low-k dielectrics*, in *Chemical Engineering*. 2006, Rensselaer Polytechnic Institute: Troy. p. 110.
63. Feldman, L.C. and J.W. Mayer, *Fundamentals of Surface and Thin Film Analysis*. 1986, Upper Saddle River, New Jersey: PTR Prentice Hall. 352.
64. Davies, J.A., et al., *Quantitative calibration of intense ([alpha], [alpha]) elastic scattering resonances for 12C at 5.50-5.80 MeV and for 16O at 7.30-7.65 MeV.* Nuclear Instruments and Methods in Physics Research Section B: Beam Interactions with Materials and Atoms, 1994. **85**(1-4): p. 28-32.
65. Seoul, C., et al., *Preparation of light-emitting devices with poly(p-phenylenevinylene): effects of thermal elimination conditions and polymer layer thickness on device performance.* Synthetic Metals, 1999. **99**: p. 35-43.
66. Lee, T.-W., et al., Synthetic Metals, 2001. **117**: p. 249.
67. Adriaensens, P., et al., Polymer, 2005. **46**: p. 1759.
68. Claes, L., J.-P. Francois, and M.S. Deleuze, Journal of the American Chemical Society, 2003. **125**: p. 7129.
69. Zhang, C., D. Braun, and A.J. Heeger, *Light-emitting diodes from partially conjugated poly(p-phenylene vinylene).* Journal of Applied Physics, 1993. **73**(10): p. 5177-5180.

70. Esteghamatian, M. and G. Xu, *Color changes in photoluminescence by doped, unconverted and partially converted poly(p-phenylene vinylene).* Applied Phyiscs Letters, 1994. **65**(15): p. 1877-1879.
71. Brütting, W., et al., *Doping in PPV light-emitting devices fabricated on different substrates.* Chemical Physics, 1998. **227**: p. 243.
72. Brütting, W., et al., *Control of impurities in PPV light-emitting devices.* Synthetic Metals, 1997. **91**: p. 163-168.
73. Ohnishi, T., et al., *Highly conductive graphite film prepared from pyrolysis of poly(p-phenylene vinylene).* Synthetic Metals, 1986. **14**(3): p. 207-213.
74. Mates, T., et al. in *Advanced electronic packaging materials*. 1989. Boston, MA: Materials Research Society.
75. Ueno, H. and K. Yoshino, *Electrical conductivity and thermoelectric power of highly graphitizable poly(p-phenylene vinylene) films.* Physical Review B, 1986. **34**(10): p. 7158.
76. Kim, K. and J.-I. Jin, *Preparation of PPV nanotubes and nanorods and carbonized products derived therefrom.* Nano Letters, 2001. **1**: p. 631.
77. Fortin, J.B. and T.-M. Lu, *Chemical Vapor Deposition Polymerization: The Growth and Properties of Parylene Thin Films*. 2004, Boston: Kluwer Academic Publishers.
78. Bradley, D.D.C., *Precursor-route poly(p-phenylenevinylene): polymer characterisation and control of electronic properties.* Journal of Physics D (Applied Physics), 1987. **20**(11): p. 1389-410.
79. Ghosh, D., et al., *Laser-induced degradation studies of photoluminescence of PPV and CNPPV thin films.* Thin Solid Films, 2005. **477**: p. 162-168.
80. Galvão Gobato, Y., et al., *Photoinduced photoluminescence intensity enhancement in poly(p-phenylene vinylene) films.* Applied Phyiscs Letters, 2002. **81**(5): p. 942-944.
81. Lee, K., et al., *Air-stable polymer electronic devices.* Advanced Materials, 2007. **19**(18): p. 2445-2449.
82. Riess, W., *Heterolayer Light-emitting Diodes Based on Poly-phenylene Vinylene.* Polymers for Advanced Technologies, 1997. **8**: p. 381-391.
83. Sellner, S., et al., *Mechanisms for the enhancement of the thermal stability of organic thin films by aluminum oxide capping layers.* Journal of Materials Research, 2006. **21**(2): p. 455-64.
84. Carcia, P.F., et al., *Ca test of Al₂O₃ gas diffusion barriers grown by atomic layer deposition on polymers.* Applied Physics Letters, 2006. **89**(3): p. 031915.
85. Ghosh, A.P., et al., *Thin-film encapsulation of organic light emitting devices.* Applied Phyiscs Letters, 2005. **86**: p. 223503.
86. Groner, M.D., et al., *Gas diffusion barriers on polymers using Al2O3 atomic layer deposition.* Applied Physics Letters, 2006. **88**(5): p. 051907.
87. Kobayashi, T., et al., *Reactive vacuum vapor deposition of aluminum oxide thin films by an air-to-air metallizer.* Journal of Vacuum Science & Technology A (Vacuum, Surfaces, and Films), 2006. **24**(4): p. 939-45.

88. Pang, S.W., et al., *Aluminum oxides as imaging materials for 193-nm excimer laser lithography.* Journal of Vacuum Science & Technology B, 1989. **7**(6): p. 1624-1628.
89. Ahn, H. and J.E. Whitten, *The metallicity of aluminum and gold in contact with thin films of a urethane-substituted polythiophene.* Journal of Applied Physics, 2003. **93**(6): p. 3384-3388.
90. Senkevich, J.J., et al., *Selective Deposition of Ultrathin Poly(p-xylylene) Films on Dielectrics Versus Copper Surfaces.* Chemical Vapor Deposition, 2004. **10**(5): p. 247-249.
91. Ke, L., et al., *Effect of parylene layer on the performance of OLED.* Microelectronics Journal, 2004. **35**: p. 325-328.
92. Jezewski, C., et al., *Molecular Caulking: A Pore Sealing CVD Polymer for Ultralow k Dielectrics.* Journal of the Electrochemical Society, 2004. **151**(7): p. F157-F161.
93. Juneja, J.S., et al., *Dielectric barriers, pore sealing, and metallization.* Thin Solid Films, 2006. **504**: p. 239-242.
94. Senkevich, J.J., et al., *Bias-temperature stability of ultrathin parylene-capped dielectrics: influence of surface oxygen on copper ion diffusion.* Applied Phyiscs Letters, 2004. **84**(14): p. 2617-2619.
95. Kayashima, H., et al., *Poly(p-phenylene vinylene)-based field-effect transistors with platinum source-drain electrodes.* Journal of Physics D: Applied Physics, 2007. **40**: p. 1646-1648.
96. Kishore, V.V.N.R., et al., *Time resolved photoluminescence spectra of PPV film: heterogeneity and excited state relaxation.* Chemical Physics Letters, 2004. **386**: p. 118-122.
97. Vaeth, K.M. and K.F. Jensen, *Chemical vapor deposition of poly(p-phenylene vinylene) based light emitting diodes with low turn-on voltages.* Applied Phyiscs Letters, 1997. **71**(15): p. 2091.
98. Hu, B. and F.E. Karasz, *Interfacial effects in polymer LEDs.* Chemical Physics, 1998. **227**: p. 263-270.
99. Hsieh, B.R., Y. Gao, and T.K. Park, *Characteristics of metal-poly(phenylene vinylene) interfaces.* SPIE, 1993. **1910**: p. 195-204.
100. Nguyen, T.P., et al., *A degradation study of poly(p-phenylene vinylene based light emitting diodes.* Materials Science and Engineering 1999. **B60**: p. 76-81.
101. Tu, M.-L., et al., *Effect of post annealing on performance of polymer light-emitting devices.* Japanese Journal of Applied Physics, 2005. **44**(10): p. 7482-7484.
102. Leger, J.M., et al., *Thickness-dependent changes in the optical properties of PPV- and PF-based polymer light emitting diodes.* Physical Review B, 2003. **68**: p. 054209.
103. Marletta, A., E. Piovesan, and N.O. Dantas, *Enhanced optical and electrical properties of layer-by-layer luminescent films.* Journal of Applied Physics, 2003. **94**(9): p. 5592-5598.
104. Kang, Y. and D. Kim, *Well-aligned CdS nanorod/conjugated polymer solar cells.* Solar Energy Materials & Solar Cells 2006. **90**: p. 166-174.

105. Rud, J.A., et al., *Water soluble polymer/carbon nanotube bulk heterojunction solar cells.* Journal of Materials Science, 2005. **40**: p. 1455-1458.
106. Konstantatos, G., et al., *Efficient infrared electroluminescent devices using solution-processed colloidal quantum dots.* Advanced Functional Materials, 2005. **15**: p. 1865-1869.
107. Choudhury, K.R., Y. Sahoo, and P.N. Prasad, *Hybrid quantum-dot--polymer nanocomposites for infrared photorefractivity at an optical communication wavelength.* Advanced Materials, 2005. **17**: p. 2877-2881.
108. Despotopoulou, M.M., et al., *Role of the restricted geometry on the morphology of ultrathin poly(di-n-hexylsilane) films.* Macromolecules, 1995. **28**: p. 6687-6688.
109. Jenekhe, S.A. and J.A. Osaheni, Chemistry of Materials, 1994. **6**: p. 1906.
110. Kim, T.-H., S.H. Im, and O.O. Park, *Enhanced electroluminescence and color purity in conjugated polymer with nano-porous morphology.* Applied Phyiscs Letters, 2005. **87**: p. 221114.
111. Jackson, C.L. and G.B. McKenna, *Vitrification and crystallization of organic liquids confined to nanoscale pores.* Chemistry of Materials, 1996. **8**: p. 2128-2137.
112. Jiang, Q. and X.Y. Lang, *Glass transition of low-dimensional polystyrene.* Macromolecular Rapid Communications, 2004. **25**: p. 825.
113. Nguyen, T.P., et al., *Optical properties of nanosize aggregation of phenylene vinylene oligomers.* Synthetic Metals, 2005. **151**(3): p. 269-274.
114. Nguyen, T.P., et al., *Optical properties of poly(2-methoxy-5-(2'-ethyl-hexyloxy)-phenylene vinylene) deposited on porous alumina substrates.* Composites Part A (Applied Science and Manufacturing), 2005. **36**(4): p. 515-19.
115. Nguyen, T.P., et al. *Filling porous silicon pores with poly(p phenylene vinylene)*. 2003. Puerto de la Cruz, Spain: Wiley-VCH Verlag.
116. Le Rendu, P., et al., *Formation of nanosize poly(p-phenylene vinylene) in porous silicon substrate.* Materials Science and Engineering C, 2003. **23**: p. 847-850.
117. Cadby, A.J. and S.H. Tolbert, *Controlling optical properties and interchain interactions in semiconducting polymers by encapsulation in periodic nanoporous silicas with different pore sizes.* Journal of Physical Chemistry B, 2005. **109**(38): p. 17879-86.
118. Nguyen, T.-Q., et al., *Control of Energy Transport in Conjugated Polymers Using an Ordered Mesoporous Silica Matrix.* Advanced Materials, 2001. **13**(8): p. 609-611.
119. Wu, J., A.F. Gross, and S.H. Tolbert, *Host-Guest Chemistry Using and Oriented Mesoporous Host: Alignment and Isolation of a Semiconducting Polymer in the Nanopores of an Ordered Silica Matrix.* Journal of Physical Chemistry B, 1999. **103**: p. 2374-2384.
120. Morgen, M., et al., *Low Dielectric Constant Materials for USLI Interconnects.* Annual Review of Material Science, 2000. **30**: p. 645-680.
121. Juneja, J.S., et al., *Pressure dependent Parylene-N pore sealant penetration in porous low-k dielectrics.* Journal of Vacuum Science and Technology B, 2005. **23**(5): p. 2232-2235.

122. Li, Y.-T., et al., *Gold nanoparticles for microfluidics-based biosensing of PCR products by hybridization-induced fluorescence quenching.* Electrophoresis, 2005. **26**(24): p. 4743-50.
123. Gauthier, T.D., et al., *Fluorescence Quenching Method for Determining Equilibrium Constants for Polycyclic Aromatic Hydrocarbons Binding to Dissolved Humic Materials.* Environmental Science and Technology, 1986. **20**(20): p. 1162-1166.
124. Nakashima, K., et al., *Fluorescence studies on binding of pyrene and its derivatives to humic acid.* Spectrochimica Acta Part A, 2007. **67**: p. 930-935.
125. Sacksteder, L., J.N. Demas, and B.A. DeGraff, *Design of Oxygen Sensors Based on Quenching of Luminescenct Metal Complexes: Effect of Ligand Size on Heterogeneity.* Analytical Chemistry, 1993. **65**: p. 3480-3483.
126. Le Barny, P.L., et al. *Detection of nitroaromatic compounds based on photoluminescent side chain polymers*. 2005. Bruges, Belgium: International Society for Optical Engineering, Bellingham WA, WA 98227-0010, United States.
127. Yu, J., et al., *Efficient Exciton Quenching by Hole Polarons in the Conjugated Polymer MEH-PPV.* Israel Journal of Chemistry, 2004. **44**: p. 127-132.
128. Montilla, F. and R. Mallavia, *In situ Electrochemical Fluorescence Studies of PPV.* Journal of Physical Chemistry B, 2006. **110**: p. 25791-25796.
129. Kometani, N., et al., *Luminescence properties of the mixed J-aggregate of two kinds of cyanine dyes in layer-by-layer alternate assemblies.* Journal of Physical Chemistry B, 2000. **104**(41): p. 9630-9637.
130. Sharma, S.N., *Photoinduced charge transfer mechanism in PPV [poly(p-phenylinevinylene)] polymer: Role of iodide species.* Colloid and Polymer Science, 2006. **284**(8): p. 853-861.
131. Webster, G.R., et al., *Neutron reflection study on soluble and insoluble poly[2-(2'-ethylhexyloxy)-5-methoxy-1,4-phenylenevinylene) films.* Journal of Applied Physics, 2002. **91**(11): p. 9066-9071.
132. Lu, X., I. Cheng, and Y. Mi, *Discovery of the bi-layered structure in spin-coated polyacrylamide films on the gold surface.* Polymer Communications, 2007. **48**: p. 682-686.
133. Miyazaki, T., K. Nishida, and T. Kanaya, *Thermal expansion behavior of ultrathin polymer films supported on silicon substrate.* Physical Review E, 2004. **69**(6): p. 061803.
134. Lim, S.-H., T.G. Bjorklund, and C.J. Bardeen, *Temperature-dependent exciton dynamics in poly(p-phenylene vinlene) measured by femtosecond transient spectroscopy.* Chemical Physics Letters, 2001. **342**: p. 555-562.
135. Cabarcos, E.L. and S.A. Carter, *Effect of the Molecular Weight and the Ionic Strength on the Photoluminescence Quenching of Water-Soluble Conjugated Polymer Sodium Poly[2-(3-thienyl)ethyloxy-4-butylsulfonate].* Macromolecules, 2005. **38**: p. 10537-10541.
136. Bradley, D.D.C., R.H. Friend, and W.J. Feast, *Photoexcitation in poly(arylene vinylenes).* Synthetic Metals, 1987. **17**(1-3): p. 645-650.
137. Latini, G., et al., *Investigation of heating effects in near-field experiments with luminescent organic semiconductors.* Synthetic Metals, 2004. **147**: p. 165-169.

138. Epstein, A.J., et al. *Excitons in segmented polymers for high photo- and electro-luminescence efficiency*. 2000. Boston, MA, USA: Mater. Res. Soc.
139. Quan, S., et al., *Temperature effects on photoluminescence of poly[2-methoxy-5-(20-ethyl-hexyloxy)-1,4-phenylene vinylene]*. Materials Letters, 2006. **60**: p. 1134-1136.
140. Chang, R., et al., *Experimental and theoretical investigations of absorption and emission spectra of the light-emitting polymer MEH-PPV in solution.* Chemical Physics Letters, 2000. **317**: p. 142-152.
141. Guha, S., et al., *Temperature-dependent photoluminescence of organic semiconductors with varying backbone conformation.* Physical Review B, 2003. **67**: p. 125204.
142. Hagler, T.W., et al., *Enhanced order and electronic delocalization in conjugated polymers oriented by gel processing in polyethylene.* Physical Review B, 1991. **44**(16): p. 8652-8666.
143. Wang, H., et al., *Titania bicontinuous network structures for solar cell applications.* Applied Physics Letters, 2005. **87**(2): p. 023507.